MACRO SYNTHETIC FIBER ADDITION TO CONCRETE MARINE STRUCTURES IN FREEZE THAW ENVIRONMENTS

by

Joshua J. Brown

Submitted in partial fulfilment of the requirements
for the degree of Master of Applied Science

at

Dalhousie University
Halifax, Nova Scotia
October 2012

DALHOUSIE UNIVERSITY

DEPARTMENT OF CIVIL AND RESOURCE ENGINEERING

The undersigned hereby certify that they have read and recommend to the Faculty of Graduate Studies for acceptance a thesis entitled "Macro Synthetic Fiber Addition to Concrete Marine Structures in Freeze Thaw Environments" by Joshua J. Brown in partial fulfilment of the requirements for the degree of Master of Applied Science.

Dated: October 10, 2012

Supervisor: _____

Readers: _____

_____

DALHOUSIE UNIVERSITY

DATE: October 10, 2012

AUTHOR: Joshua J. Brown

TITLE: Marco Synthetic Fiber Addition to Concrete Marine Structures in Freeze Thaw Environments

DEPARTMENT OR SCHOOL: Department of Civil and Resource Engineering

DEGREE: MASc CONVOCATION: May YEAR: 2013

_____

Signature of Author

TABLE OF CONTENTS

LIST OF TABLES

LIST OF FIGURES

ABSTRACT

Concrete marine structures are typically exposed to harsh marine environments where the ingress of chloride ions can lead to corrosion of steel reinforcing bars, reducing both strength and service life; therefore, concrete must be proportioned to resist these environments. Current recommendations for concrete mixtures and plastic shrinkage cracking both reduce the resistance to chloride ingress.

The main objective of this thesis was to understand the benefits of fiber addition to concrete exposed to chlorides and quantify those benefits, which would lead to a concrete mixture suitable for marine structures in freeze thaw environments. The research program tested two different fibers in a total of nine concrete mixtures.

The results demonstrated that fiber addition at dosages up to 0.33 % by volume resulted in significant reduction or elimination of plastic shrinkage cracking and the chloride tests determined that the ternary FRC mixtures had the best resistance to chloride diffusion.

LIST OF ABBREVIATIONS AND SYMBOLS USED

AASHTO	American Association of State Highway and Transportation Officials
ACI	American Concrete Institute
$AgNO_3$	Silver Nitrate
ASTM	American Society of Testing Materials
Ca^+	Calcium Ion
C_3A	Tricalcium Aluminate
$CaOH$	Calcium Hydroxide
Cl^-	Chloride Ion
CO_2	Carbon Dioxide
DC	Direct Current
e^-	Electron
erf	Error Function
F1	Fiber 1
F2	Fiber 2
FA	Concrete with Fly Ash
Fe^{2+}	Iron Ion
$Fe(OH)_2$	Ferrious Hydroxide
$Fe(OH)_3$	Ferric Hydroxide
$Fe_2O_3H_2O$	Hydrated Ferric Oxide
FRC	Fiber Reinforced Concrete
FRP	Fiber Reinforced Polymer
GGBFS	Ground Granulated Blast Furnace Slag
GPa	GigaPascal
GU	General Use
H_2O	Water
JSCE	Japanese Society for Civil Engineering
kg	KiloGram

kN	KiloNewton
lb	Pounds
LVDT	Linear Variable Displacement Transducer
M	Moles
m	Meter
Mg^{2+}	Magnesium Ion
mg	MilliGram
mm	MilliMeter
MPa	MegaPascal
N	Newton
N	Normality
Na^{+}	Sodium Ion
NaCl	Sodium Chloride
NaOH	Sodium Hydroxide
NC	Normal Concrete
NT	NordTest
O_2	Oxygen
OH^{-}	Hydroxide Ion
PCA	Portland Cement Association
pH	Potential of Hydrogen
RCPT	Rapid Chloride Permeability Test
RMT	Rapid Migration Test
SO_4^{2-}	Sulfate Ion
TER	Concrete with Fly Ash and Silica Fume
V	Volts
w/c	Water to Cement Ratio
WRA	Water Reducing Admixture
µm	MicroMeter

ACKNOWLEDGEMENTS

My appreciation and thanks are directed towards my supervisor, Dr. Dean Forgeron, for his guidance, support, advice and pointing me in the right direction. He allowed me to go at this project in my own way and offered his assistance when it was needed.

I would like to say thank you to my colleagues at the Centre for Innovation in Infrastructure who helped me throughout my research. A special thanks to Dr. Chris Barnes for helping me understand chloride penetration and the different test methods associated with it. I would like to thank my fellow graduate students Mr. Chris Yurchesyn, Mr. Alkailani Omer, Ms. Shannon O'Connell and Ms. Lynsey Poushay for their input and the helpful discussions during my research. I would like to thank Mr. Phil Vickers, Mr. Blair Nickerson, Mr. Jesse Keane, Mr. Brian Liekens and Mr. Brian Kennedy, the technicians that helped me with mixing, casting, testing of specimens and manufacturing of my test set-ups. I would also like to thank NSERC for granting me an IPS scholarship to pursue this research and Atlantic Fiber Technologies for contributing to my scholarship.

I cannot end without thanking my patient and loving girlfriend, who has been there for me throughout my research, and my parents, brother and extended family who have loved, supported and encouraged me throughout my life.

CHAPTER 1 INTRODUCTION

Concrete marine structures such as coastal berthing facilities, tidal barriers, breakwaters, wharfs, container terminals, dry docks, floating docks and drilling platforms are typically exposed to harsh marine environments and are usually expected to require a minimum level of repair and maintenance during their service life. The ingress of aggressive agents, such as chloride ions, can lead to corrosion of the steel reinforcing bars which can result in a reduction in strength and a subsequent reduction in the service life. To resist this type of premature deterioration, concrete must be proportioned to resist these aggressive marine environments. The most common method that is used to prevent premature deterioration of marine structures is the use of relatively impermeable concrete mixtures.

Most of the current codes and local specifications, such as the Portland Cement Association (PCA) design manual (Kosmatka et al. 2002) and the Nova Scotia Public Works specification, for concrete exposed to marine environments include recommendations of minimum cement content, maximum w/c ratio, minimum concrete cover thickness and a range of acceptable entrained air percentages for structures exposed to freezing and thawing; however, even when these specifications are met, shown in this thesis as a normal concrete (NC) mixture, the concrete has an extremely poor resistance to chloride ingress. This is the case for many concrete marine structures that are currently in service and have to be repaired far before their designed service life.

The level of impermeability that is required for a marine service life of 50 years or more can only be attained with the use of supplementary cementitious materials, such as fly ash, slag and silica fume assuming the concrete remains uncracked. However, these supplementary cementing materials can cause placement and consolidation issues and increase the potential for plastic shrinkage cracking if not proportioned properly. The consequence of cracking is an effective reduction in the thickness of the protective

concrete cover, thus it can greatly reduce the expected service life of a structure when cracks occur over reinforcement bars.

1.1 Research Motivation

Recent research has shown that the addition of self-fibrillating macro-synthetic fibers can reduce or eliminate plastic shrinkage cracking in normal concrete mixtures when added at volumes as low as 0.2 % (Trottier et al. 2002; Omer 2006; Forgeron et al. 2011). Fibers also have the added benefit of increasing concrete toughness and can be designed to replace steel reinforcing bars. There has been limited research using synthetic fibers and high performance concrete mixtures; however the combination of macro-synthetic fibers with concrete mixtures containing supplementary cementitious materials may decrease the permeability of concrete structures leading to longer service lives and a reduction in the frequency of very costly repairs.

1.2 Research Objectives and Scope

The main objective of this thesis was to understand the benefits of synthetic fiber addition to high performance concrete exposed to chlorides in a freeze thaw environment and quantify those benefits. These benefits would then be used to develop an example mixture, as well as a new fiber, that would be suitable for use in marine structures in freeze thaw environments. The author would also make some recommendations based on the test results to improve current codes and specifications. The research program was carried out to test two specific fibers in a concrete mixture with good resistance to chloride ingress and determine the fiber dosage required to eliminate plastic shrinkage cracking. The second fiber was developed after testing of the first fiber. In order to achieve the ultimate goal of this thesis, investigations were carried out in three stages: the fresh stage, plastic stage and hardened stage.

In the fresh stage, fibers are known to negatively affect the workability of normal concrete (Al Tayyib et al. 1988). Mixture optimization was required to determine the appropriate dosage of fiber to maintain a mixture that could be easily placed. Secondly, the performance of the optimized concrete mixtures in the plastic stage had to be qualified to determine the concrete resistance to plastic shrinkage cracking. The plastic stage usually covers the first 12 hours after casting. Finally, the hardened properties of concrete mixtures were evaluated including compressive strength, chloride penetration, flexural toughness and freeze thaw resistance. The plastic shrinkage resistance and hardened properties of the optimized FRC mixtures were compared to that of a typical concrete mixture used in freeze thaw marine environments. This comparison considered both the change provided by the addition of fiber to various mixtures and the potential benefit to service life provided by crack free concrete with a good resistance to chloride ingress.

The following sections will discuss the required background and information needed to follow the discussion of the test procedures and results in later sections. The background section will give an overview of marine concrete, construction factors, and materials used in conventional concrete such as supplementary materials. The literature review will go into more detail on chloride ingress and plastic shrinkage mechanisms and discuss fiber reinforced concrete in detail.

CHAPTER 2 BACKGROUND

This chapter presents background information on conventional concrete marine structures and the general causes responsible for deterioration of these structures in freeze thaw marine environments for the purpose of providing the required background needed to discuss the results of the experimental program. An overview of concrete in marine environments and the physical and chemical mechanisms that generally affect such structures are presented. The review of general causes of deterioration is focused on the corrosion of the reinforcement in concrete marine structures. The corrosion of reinforcement in marine environments is usually initiated by the penetration of chloride ions. An explanation of the influence of construction factors on the permeability of conventional concrete is also presented. These factors include improper vibration, consolidation techniques and poor curing regime. Finally, the supplementary cementitious materials and admixtures typically used in conventional concrete are presented in detail.

2.1 Concrete in the Marine Environment

Concrete structures such as wharves, jetties, breakwaters and retaining walls are widely used in the construction of harbors and docks. Such structures are exposed to harsh environments which deserve special attention and consideration. This is because coastal and offshore sea structures are exposed to simultaneous attacks by physical and chemical deterioration processes. Seawater, which is the main source of such attacks, makes up 80% of the surface of the earth, therefore, a large number of structures are exposed to seawater either directly or indirectly as seawater, via salt-ladened moisture, can be carried a few miles inland by the wind.

Seawater is fairly uniform in terms of chemical composition, which is characterized by the presence of soluble salts. The ionic concentrations of sodium (Na^+) and chloride (Cl^-)

are the highest, typically 10800 and 19400 mg/L, respectively; however, from the standpoint of aggressive action to cement hydration products, a sufficient amount of magnesium (Mg^{2+}) and sulfate (SO_4^{2-}) are present, typically 1300 and 2700 mg/L, respectively, to cause damage to the cement hydration products (Millero et al. 2008). In addition to these dissolved salts, free carbon dioxide (CO_2) can also be found in seawater, particularly in sheltered areas, where decaying organic matter is present. The CO_2 can react with cement hydration products and can lead to carbonation attack (Papadakis et al. 1992). In addition, the *pH* of seawater is approximately 8.1 (Millero et al. 2008), which in itself makes seawater an aggressive environment for Portland-cement concrete.

In addition to chemical attack, concrete exposed to marine environments may also deteriorate as a result of the corrosion of the steel reinforcement, physical erosion due to wave action, impact of floating objects, alkali-aggregate expansion, sulfate attack, and freeze thaw damage. Of all the mechanisms noted above, corrosion of the embedded steel reinforcement, which initiates as a result of the penetration of the chloride ions into the structure is by far the most severe and responsible for more capital expenses than the others. Reinforcement corrosion leads to a reduction in the strength, serviceability and subsequent reduction in the service life of many marine structures.

Chloride ions are considered the most harmful agents to reinforcing steel due to their high concentration in seawater and their unusual ability to penetrate concrete and attack the reinforcing steel (Broomfield 1997). The ability of concrete to resist the penetration of chloride ions is dependent on the material selection, concrete composition and construction factors. The first two parameters can be controlled during the mixing process; however, the construction factors are difficult to control since they are associated with the construction process, which in turn depends on the quality of the consolidation techniques and the skill of the laborers.

2.2 Corrosion of Reinforcing Steel in Concrete

Corrosion of reinforcing steel is considered the main cause of the deterioration of concrete marine structures. A description of the corrosion mechanism and corrosion damage to concrete structures is presented in the following sections.

2.2.1 Corrosion Mechanism in Concrete

The corrosion of steel in concrete is an electrochemical process. Normally, reinforcing steel in the concrete has a thin protective film on its surface caused by the alkaline environment the concrete creates when surrounding the steel, which renders the steel passive to the corrosion process. The protective film is stable in an alkaline environment, such as concrete, which has a *pH* of 12 – 13. The passivity of the thin film can be broken down when the *pH* of the concrete surrounding the reinforcement drops below 11 caused by sufficient chlorides present in the vicinity of the reinforcing steel (Broomfield 1997). In permeable concrete, carbonation can also contribute to lowering of the *pH*. The concrete in modern marine structures is essentially impermeable; therefore, the carbonation is seldom a matter of concern (Broomfield 1997). Since seawater contains a high concentration of chloride ions, the most common cause of the passive layer breaking down is the penetration of chloride ions to the level of the reinforcing steel. Chloride ions diffuse into concrete through pores or defects, which decreases the pH of the concrete, thus reducing the alkalinity of the concrete which disrupts the passive layer surrounding the reinforcing steel, more easily than other ions (ACI Committee 222 1985).It is reported that the threshold for corrosion initiation varies from 0.17 – 0.25 % by weight of cement (Glass and Buenfeld 1997).

Once the passive film is disrupted, an electrochemical or galvanic cell is established. This is similar to a flashlight battery. An anode, where electrochemical oxidation takes place, a cathode, where electrochemical reduction occurs, an electrical conductor and an aqueous

medium must be present. Both the anode and cathode occur on the surface of the steel reinforcement and are connected through the steel rebar itself, shown in Figure 2.1.

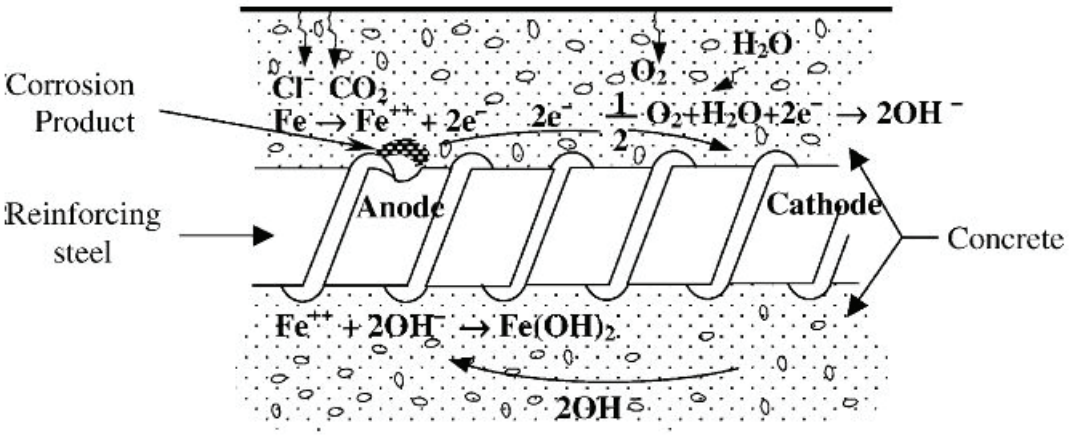

Figure 2.1 Electrochemical Process of Corrosion (after Ahmad 2003)

Chlorides are very effective in developing anodic and cathodic sites because their concentration varies in concrete, which causes variations in the passive film. These reactions are referred to as half-cell reactions. The chemical reactions that take place at the anode and cathode are described in Eq. (2.1) and Eq. (2.2), respectively (Broomfield 1997):

$$2Fe \rightarrow 2Fe^{2+} + 4e^{-} \qquad \textbf{Eq. (2.1)}$$

$$2H_2O + O_2 + 4e^{-} \rightarrow 4OH^{-} \qquad \textbf{Eq. (2.2)}$$

The flow of electrons from the anodic areas, where they are produced, to the cathodic areas, where they are used, and its counter-current ionic flow in the external concrete pore solution constitute the corrosion current, as shown in Figure 2.1. The actual loss of metal in the corrosion process occurs at the anode and is indicated by Eq. (2.1). The iron atoms (*Fe*) are ionized to ferrous (Fe^{2+}) ions, which dissolve in the water solution around

the steel. The electrons are deposited on the steel surface and raise its electric potential. The electrons then flow along the steel to lower potential (cathodic) sites. Here, the reaction in Eq. (2.2) takes place and the electrons combine with dissolved oxygen molecules (O_2) and water (H_2O) to form hydroxide (OH^-) ions. The metal removal process only occurs if there is a cathodic reaction, which acts as a sink for the electrons produced at the anode; therefore, if oxygen and water (electrolyte) are not available at cathodic sites, the corrosion process will cease. The formation of the corrosion product, rust, can be explained in several ways. Eq. (2.3) through Eq. (2.5) represents the process required for the formation of rust (Broomfield 1997):

$$Fe^{2+} + 2(OH)^- \rightarrow Fe(OH)_2\ (Ferrious\ Hydroxide) \qquad \textbf{Eq. (2.3)}$$

$$4Fe(OH)_2 + O_2 + 2H_2O \rightarrow 4Fe(OH)_3\ (Ferric\ Hydroxide) \qquad \textbf{Eq. (2.4)}$$

$$2Fe(OH)_3 \rightarrow 2Fe_2O_3H_2O\ (Hydrated\ Ferric\ Oxide) + 4H_2O \qquad \textbf{Eq. (2.5)}$$

$Fe(OH)_2$ is a weak base formed during the reaction and is unstable. In the presence of oxygen, another reaction occurs and $Fe(OH)_2$ is converted into $Fe(OH)_3$, or rust, which precipitates out of the solution. Rust can occupy up to ten times the volume of the steel and leads to significant pressure on the concrete surrounding the bar, which eventually cracks and spalls.

Since seawater contains high concentrations of chloride ions, which are responsible for initiating corrosion, steel reinforced concrete structures exposed to seawater are highly susceptible to reinforcement corrosion and shortened lives due to premature deterioration. Due to the mechanisms noted above, the tidal and splash zones of a marine structure are the most susceptible to chloride ingress and corrosion; however, chloride ingress and corrosion can occur several kilometers inland at a highly reduced rate. Submerged

concrete is also exposed to a high concentration of chlorides; however there is limited free oxygen present in the seawater which is needed for corrosion to occur.

2.2.2 Effect of Corrosion on Concrete Material

Deterioration of concrete due to corrosion is a progressive process. Rust occupies a much larger volume than the original reinforcing steel. This increase in volume results in an increase in pressure on the concrete surrounding the bar, which leads to cracking and delamination of the concrete cover. Staining can occur on the surface around these cracks. As the corrosion continues, the concrete cover may begin to spall or "pop off". The corrosion process is somewhat self-accelerating; once cracking and spalling begin, the concrete cover is compromised and higher corrosion rates may be expected. This loss of concrete and corrosion of steel may eventually result in structural distress. The corrosion and spalling process is shown schematically in Figure 2.2.

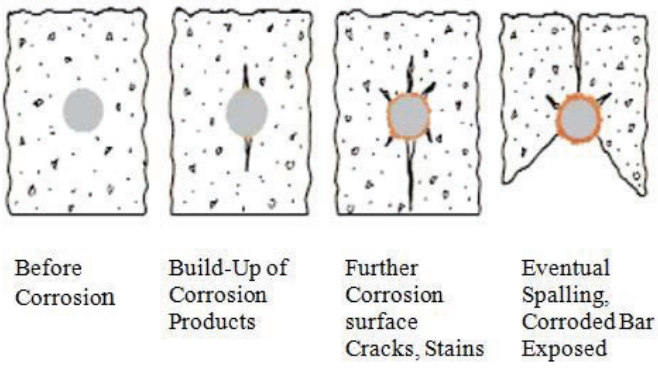

Figure 2.2 Effect of Corroded Rebar on Surrounding Concrete (after Ahmad 2003)

The corrosion damage is usually first observed as rust stains and minute cracks on the concrete surface. These cracks tend to run in straight lines above the underlying reinforcement, as shown in Figure 2.3. If repair is not undertaken at this early stage, the steel corrosion will cause severe damage through delamination and spalling of the

concrete cover, shown in Figure 2.4. This can lead to safety hazards and even the loss of structural integrity.

Figure 2.3 Corrosion Damage Exhibiting Rust and Cracking Parallel to Main Reinforcement

Figure 2.4 Damage in Marine Structure Showing Concrete Spalling and Corrosion of Reinforcing Steel

2.3 Effect of Vibration and Consolidation Techniques on Concrete Permeability

The vibration and consolidation techniques used when placing concrete can adversely affect the mechanical properties and cause plastic shrinkage problems which can lead poor resistance to chloride ingress when performed improperly. This can lead to inhomogeneous distribution of solids, liquid and air. Over-vibration can lead to bleeding and segregation, both of which will be discussed in the following sections.

2.3.1 Bleeding

Bleeding is the development of a layer of water at the surface of freshly placed concrete. Bleeding is caused by the settlement of heavy solid particles and the upward migration of water. Some bleeding is normal, but excessive bleeding caused by over-vibration can be a problem. Excessive bleeding increases the w/c ratio near the surface, which can result in poor durability. After the bleed water has evaporated, the hardened surface will have settled slightly and be lower than intended. This is called settlement shrinkage and can result in cracks above reinforcing bars as the bars will not let the concrete settle at that location (Kosmatka et al. 2002). Bleeding can also cause fine bleed water channels in the concrete, which can be especially harmful because most pathways have a capillary nature that allow the absorption of harmful agents (chlorides, oxygen, moisture, etc.) into the concrete cover, which can accelerate the deterioration of the reinforcing bars (Aldred 1988).

2.3.2 Segregation

Segregation, which is usually coupled with bleeding, is also a result of over-vibration. Segregation is the tendency for coarse aggregate to separate from the mortar; this results in part of the mixture having too much coarse and the remainder having too little. The lack of coarse aggregate can lead to shrinkage cracking, which facilitates the ingress of

chloride ions. On the other hand, the lack of fine aggregate results in gaps in the concrete that significantly impair the permeability of the structure (Weyers et al. 1982; Kosmatka et al. 2002; Sansone and Brown 2007). An example of segregation can be seen in Figure 2.5.

Figure 2.5 Segregation Due to Poor Compaction

2.4 Supplementary Cementitious Materials

When added to Portland cement, supplementary cementitious materials are materials that contribute to the properties of hardened concrete through hydraulic activity, pozzolanic activity or both. Examples of supplementary materials are fly ash, silica fume and ground granulated blast furnace slag (GGBFS).

2.4.1 Fly Ash

Fly ash is a byproduct of burning pulverized coal at electric power generating plants. It's a fine-grained material consisting of spherical, glassy particles comprised of silicate glass containing silica, alumina, iron and calcium with diameters ranging from 1 μm up to 100 μm and a surface area from 300 m^2/kg to 500 m^2/kg. Due to its chemical composition, fly ash exhibits both pozzolanic and hydraulic activities (Kosmatka et al. 2002).

These properties allow it to be added to Portland cement as a mineral additive at the time of batching, or it can be interground with the cement clinker during the production of the cement. Fly ash is typically used to replace 15% to 25% by mass of cementing material, depending on required properties and workability (Kosmatka et al. 2002). In the hardened state, the addition of fly ash greatly reduces the permeability of concrete which provides great resistance to chloride ion ingress (Thomas and Bamforth 1999). The reduction is primarily due to the fineness of fly ash compared to cement. The smaller particles aid in particle packing and result in a more compact concrete mix which reduces pore sizes in the cement paste which reduces the space available for chlorides to penetrate into the concrete.

2.4.2 Silica Fume

Silica fume is the byproduct of the reduction of high-purity quartz with coal in the manufacture of silicon or ferrosilicon. Silica fume has a spherical shape with a diameter of 1 μm or less and an average diameter of 0.1 μm. Silica fume has a surface area of about 20000 m^2/kg.

Silica fume is used in dosages between 5% and 10% by mass of cementitious material. It is used when a high degree of impermeability is desired and in high strength concrete. Silica fume accelerates the hydration process and leads to an increase in the early compressive strength and greatly reduces the permeability of concrete providing improved resistance to chloride ion ingress; however, due to its low bleeding characteristics and possible self-desiccation, silica fume concrete may exhibit an increase in plastic shrinkage cracking if the concrete is not properly protected against drying during curing, such as curing compounds or additional curing water (Kosmatka et al. 2002).

2.4.3 Ground Granulated Blast Furnace Slag (GGBFS)

Ground Granulated Blast Furnace Slag (GGBFS) is a glassy sand like granulated material consisting essentially of silicates and aluminosilicates of calcium developed in a molten condition simultaneously with iron in a blast furnace. The sizes of the particles vary, but all are less than 45 μm in diameter and have a surface area of 400 m^2/kg to 600 m^2/kg. GGBFS hydrates and sets in a similar manner to that of cement when exposed to water and an activator, *NaOH* or *CaOH*, both of which are provided by Portland cement (Kosmatka et al. 2002).

GGBFS is typically added in dosages of 30% to 45% by mass of cementitious material, but can be added in dosages of 70% or more in some cases. The addition of GGBFS reduces the permeability of concrete, which improves its resistance to chloride ion ingress; however, concrete containing GGBFS is more susceptible to plastic and drying shrinkage (Kosmatka et al. 2002).

2.5 Chemical Admixtures

Chemical admixtures are those ingredients which can be added to a concrete mixture just before or during mixing to improve workability or other concrete properties. The use of chemical admixtures, such as water reducing and air entrainment admixtures are essential in freeze-thaw marine environments where certain strength is required, but the concrete mixture must also be workable and able to resist the freezing and thawing cycles present in a northern climate.

2.5.1 Water Reducing Admixtures (WRA)

Water Reducing Admixtures (WRA) allow a reduction in the water content in a mixture while maintaining slump and workability (Hover 1998). The use of water reducers decreases the interparticle friction, which in turn reduces the water required by the

mixture (Aldred 1988). WRA's allow a concrete mixture to have a high slump while maintaining a low water to cement ratio required when considering protection against chloride ingress. The high slump allows placement to be much easier especially when fiber is added to a mixture.

2.5.2 Air Entraining Admixtures

Air Entraining Admixtures are used to introduce and stabilize microscopic air bubbles in concrete. Air entrainment increases durability of concrete exposed to freeze thaw cycles and also improves concrete resistance to surface scaling caused by deicers. Air entrainment can also improve workability and reduces segregation and bleeding (Kosmatka et al. 2002).

CHAPTER 3 LITERATURE REVIEW

The ability of a concrete structure to resist aggressive environments is directly related to the continuity and permeability of the concrete cover layer protecting the steel reinforcing bars. The cover should limit the ingress of aggressive agents, such as chlorides, that can cause damage to the structure while remaining crack free. In practice, permeability depends on material selection, concrete composition and construction factors as discussed in Chapter 2. Typically when low permeability is desired, supplementary cementitious materials are added to the concrete mixture; however, this can result in an increase in plastic, drying and autogenious shrinkage cracking (Cohen et al. 1990; Bloom and Bentur 1995; Almussalam et al. 1999). The addition of fiber reinforcement in these cases may be a solution while still maintaining low permeability.

This chapter presents an overview of the relevant literature on chloride penetration, plastic shrinkage cracking and fiber reinforced concrete (FRC). Initially, an overview of the chloride penetration mechanisms is presented, followed by typical preventative measures for chloride penetration, service life prediction of marine structures and some testing methods for chloride diffusion in concrete. This is followed by the mechanisms of plastic shrinkage cracking and the test methods associated with quantifying the plastic shrinkage of a concrete mixture. Finally, literature on the synthetic fiber reinforcement and its effects on concrete fresh and hardened properties are presented.

3.1 Chloride Penetration Mechanisms

There are four fundamental mechanisms in which chlorides can penetrate into uncracked concrete. They are capillary absorption, evaporative transport, hydrostatic pressure and diffusion; each mechanism is described below: (Thomas et al. 1995, Hamilton III et al. 2007).

- Capillary absorption is caused by moisture gradients. A dry surface is exposed to moisture and the solution is drawn into the pore structure of the concrete by capillary channels. The shallow depth of capillary action will rarely cause chloride ions to reach the level of the reinforcing bars; however it can reduce the distance the ions have to travel by other mechanisms.

- Evaporative transport, also called the wicking effect, is the mechanism in which water vapor condenses from a wet surface to a drier atmosphere. This evaporation can leave deposits of chlorides in the concrete increasing the local concentration. For this mechanism to occur, one surface of the concrete has to be exposed to the air.

- Hydrostatic pressure gradients can cause another mechanism for chloride ingress known as permeation. This mechanism occurs when one face of the concrete is exposed to a hydraulic head or pressure generated by constant wave action or a retained body of water. Permeation usually occurs in the submerged portion of the structure.

- The final mechanism, diffusion, is the movement of chloride ions under a concentration gradient. It occurs when the concentration of chloride ions on the surface is greater than the concentration in the concrete. The chloride ions will naturally migrate to the area of lower concentration as long as there is sufficient moisture along the path of migration.

The presence of cracks in the concrete cover, due to shrinkage or structural cracking, provides direct access for chlorides to penetrate into the concrete. This may mean that the chloride ions will not follow the transport mechanisms described previously if the crack extends to the level of the steel reinforcement; however, the transport mechanisms may partially occur if the crack does not extend to the level of the reinforcement.

Of the four transport mechanisms described, diffusion is the most important in marine structures (Thomas et al. 1995, Hamilton III et al. 2007). It is rare for a significant hydraulic head to be placed on one side of a concrete structure where the structure is not constantly submerged, and the effect of absorption is limited to a region very close to the surface. In the bulk concrete, the pores remain saturated in the tidal and splash zones and the movement of chloride ions is controlled by concentration gradients. A review of the relevant theory behind diffusion is presented in the following section.

3.2 Chloride Diffusion Theory

In bulk concrete, the diffusion of chloride ions is controlled by Fick's First Law, shown in Eq. (3.1) (Poulsen and Mejlbro 2006):

$$J = -D_{eff}\left(\frac{dC}{dx}\right) \qquad \textbf{Eq. (3.1)}$$

Where:

J : the flux of chloride ions (mol/m^2·s)

D_{eff} : the effective diffusion coefficient (m^2/s)

C : the concentration of chloride ions (kg/m^3)

x : a position variable (m)

In practical terms, Eq. (3.1) is only useful when steady state conditions have been reached as it assumes that the diffusion coefficient, temperature and chloride concentration are all constant with time. Fick's First Law can be used to derive the equation for non-steady state conditions, where the chloride concentration changes with time. This is referred to as Fick's Second Law, shown in Eq. (3.2):

$$\frac{\partial C}{\partial t} = D_{eff} \frac{\partial^2 C}{\partial x^2} \qquad \textbf{Eq. (3.2)}$$

Fick's Second Law includes the effect of concentration changing over time (*t*). This equation has been solved using the boundary condition $C_{(x = 0,\, t > 0)} = C_s$ (the surface concentration is constant (C_0)), the initial condition $C_{(x > 0,\, t = 0)} = 0$ (the initial concentration in the concrete is 0) and the infinite point condition $c_{(x = \infty,\, t > 0)} = 0$ (far enough away from the surface, the concentration will always be 0). This equation still assumes that the diffusion coefficient and temperature are constant with time.

The solution is Eq. (3.3) (Stanish et al. 1997):

$$C_t = C_s \left(1 - erf \left(\frac{x}{2\sqrt{D_{eff} t}} \right) \right) \qquad \textbf{Eq. (3.3)}$$

Where:

C_t : the chloride concentration (kg/m^3) at time t (days)

C_s : the chloride concentration at the surface (kg/m^3)

erf : the error function, mathematical constant

The effective diffusion coefficient, which can be calculated by rearranging Eq. (3.3), is used to quantify and indicate the ability of concrete to resist the ingress of chloride ions due to diffusion.

3.3 Concrete Properties that Affect the Rate of Chloride Penetration

Several parameters affect the penetration of chloride ions into concrete. They include porosity of concrete cover, the type of cement, cement content and temperature. It is important to note these parameters have a significant impact on the diffusion coefficient and thus determining an appropriate concrete mixture for marine environments.

3.3.1 Concrete Porosity and W/C Ratio

When chloride ions are diffused into concrete from the surrounding environment, the rate of diffusion is a function of the pore structure of the concrete as well as the chloride concentration on the surface. The porosity, a measure of the density of the pores in the concrete is significantly affected by degree of curing and w/c ratio. The porosity of concrete increases as the w/c ratio increases; therefore, concrete with higher w/c ratios have a higher rate of penetration of chloride ions compared to concrete with a low w/c ratio (Bader 2003). The degree of curing also affects the porosity of concrete where longer curing time decreases the porosity. Hence, the rate of chloride ion penetration decreases as curing time increases (Bader 2003). It can therefore be concluded that in order to limit the chloride penetration rate, a well cured concrete with a low w/c ratio is ideal for concrete placed over steel reinforcement. This means that careful control and measurement of mixtures constituents and curing conditions are critical to an accurate testing program.

3.3.2 Type of Cement and Cement Content

The type of cement and content in concrete play an important role in controlling the rate of chloride diffusion. Portland cement containing a higher amount of tricalcium aluminates (C_3A) has less corrosion damage due to chlorides because C_3A reacts chemically and bonds with a portion of the free chlorides in the concrete. This binding slows the overall rate of chloride diffusion (Page et al. 1986, Hansson et al. 1990).

Cement content is also important when considering the rate of chloride penetration. The higher the cement content in a concrete mixture, the greater number of chloride ions that can be bonded with C_3A and the slower the rate of chloride penetration (Bader 2003).

The use of blended cement containing supplementary cementitious materials, such as fly ash, silica fume and GGBFS, as a replacement for a percentage of Portland cement is more effective than normal Portland cement in reducing the rate of chloride diffusion when properly cured. It was found that the addition of fly ash greatly reduced the chloride diffusion rate compared to normal Portland cement in concrete over a long term(Hansson et al. 1985, Thomas et al. 1999; Thomas et al. 2011). These researchers also found that the addition of silica fume dramatically reduced the chloride diffusion rate of concrete at an early age. Also, the use of GGBFS was found to reduce to chloride diffusion rate over a long term similar to fly ash(Thomas et al. 1999); therefore, the use of blended cement is recommended when concrete will be exposed to a marine environment where chloride induced corrosion may take place in order to increase the chloride ingress resistance both during the early age with silica fume and over the long term with either fly ash or GGBFS.

3.3.3 Temperature

Temperature has a significant effect on the rate of diffusion of chlorides in concrete. Since diffusion is thermally activated, the rate of diffusion increases as the concrete temperature rises as described by Eq. (3.4) (Xi and Bazant 1999):

$$D_T = D_0 \exp\left[\frac{U}{R}\left(\frac{1}{T_0} - \frac{1}{T}\right)\right] \qquad \textbf{Eq. (3.4)}$$

Where:

D_T : diffusion coefficient at temperature T (x10^{-12} m^2/s)

D_0 : diffusion coefficient at temperature T_0 (x10^{-12} m^2/s)

T_0 : reference temperature (°K)

T : current temperature (°K)

R : gas constant (J/mol·°K)

U : activation energy (kJ/mol)

The activation energy of the diffusion process (U) has been found to depend on the w/c ratio and cement type used in the concrete mixture (Page et al. 1981; Collepardi et al. 1972).

3.4 Chloride Penetration Preventative Measures

Several methods have been developed to try and prevent the penetration of chloride ions into concrete, or to stop them from causing corrosion of the steel reinforcing once in the concrete. In addition to the use of supplementary cementing materials as described above, several of the commonly used preventative measures are outlined below as well as the possible problems that can arise when using such measures.

3.4.1 Reinforcement Bars

Using resin to coat the outside of the reinforcing bars or on the concrete surface has been used to prevent corrosion. Epoxy coated rebar are typically cut and bent to shape then coated with a thermoset epoxy that will not melt after bonding is complete. This coating protects the steel rebar from corroding as long as the epoxy remains intact on the surface of the bar (Dante et al. 2009). Some of the problems with using epoxy coated rebar are that the process is more expensive than traditional rebar and it must be handled and placed with care as damage to the coating can cause corrosion to occur at the damaged location, nullifying any positive effects of the epoxy coating. Corrosion at the damaged

area can also lead to debonding of the epoxy adjacent to the damage resulting in a larger exposed area of steel, thus increasing the corrosion affected area (Clear 1996). Stainless steel is also available; however this method is very expensive compared to traditional steel reinforcement.

Another option for corrosion resistant reinforcement is the use of fiber reinforced polymer (FRP) bars. These bars come in similar sizes to steel reinforcement, but are made of fibers, usually glass, that are bonded together to form a bar. These bars are lighter than steel and can be placed in the same manner; however they are more costly than steel and do not have the same properties. Due to these differences in properties, mainly a lack of ductility and bond strength, FRP bars have to be designed using different codes (Nanni 2005). FRP bars have been used a lot in bridge decks to eliminate the costly repairs associated with bridge decks exposed to salt water or deicer salts.

It is also possible for the concrete surface to be coated in epoxy or wrapped using a fiber reinforced polymer sheet to protect the concrete against chloride penetration (Caijun and Mo 2008). Although this can be effective, it can be very expensive and labor intensive, especially for cope walls and slabs that have a very large area to cover. These coatings could also be damaged if impacted, thus eliminating the protection, allowing chlorides to diffuse into the concrete.

3.4.2 Corrosion Inhibiting Admixtures

Corrosion inhibiting admixtures are added to the concrete mixture as an additive during the mixing process. These admixtures are chemical compounds such as calcium nitrite or sodium nitrite that help reduce the potential for steel corrosion. Corrosion inhibitors work by chemically reinforcing the passive layer on the steel rebar preventing the chloride ions contacting the steel rebar (Kosmatka et al. 2002). Most corrosion inhibitors will not protect against corrosion forever, but they will increase the threshold value required for

corrosion to occur, thus delaying the start of corrosion based on the dosage used (Goodwin et al. 2000).

3.4.3 Cathodic Protection

Cathodic protection is another measure that can be used to prevent or slow the corrosion process. Cathodic protection works by attaching an artificial anode, usually made of zinc, magnesium or aluminum and may be connected to a DC power source, to the reinforcing bars to force the corrosion to occur on the device instead of on the rebar (Baeckmann et al. 1997). These devices are usually used when repairing concrete structures that have problems with corrosion (Neville 1995). The issue with using cathodic protection is that a device needs to be attached to each bar that is experiencing corrosion, or the bars need to be in contact with each other so that the device can draw the electrons from the bar. This can be very difficult to accomplish and also be very expensive.

3.5 Service Life Based on Chloride Penetration Theory

The steel corrosion process in concrete can be divided into two phases, initiation and propagation. In the initiation phase, chloride ions penetrate the concrete cover layer and reach the level of reinforcement. When chloride concentration at the reinforcement level reaches a threshold value, depassivation of the passive layer on the surface of the reinforcement occurs, as described in previous sections, and active corrosion begins (Bloomfield 1997). In the propagation phase, active corrosion has already been initiated; however, the rate of corrosion is hard to predict in this phase as it can be governed by many factors, such as temperature, humidity and availability of oxygen (Ahmad 2003). Therefore, the service life is often specified as the initiation time only.

The service life for reinforced concrete can be predicted based on the chloride diffusion coefficient value (D), using Fick's Second Law, Eq. (3.3) with several simplifying assumptions. Corrosion will initiate when C_t reaches the threshold value at the

reinforcement level. The threshold value required to initiate corrosion ranges from 0.17% to 0.25% by weight of cement (Glass and Buenfeld 1997). Chloride content at the surface (C_s) in marine environments can have a large range based on the time a sample is exposed and the location of the sample. The surface concentration ranges from 0.2 % to 2 % by weight of cement based on research by several researchers (Bamforth 1994; Mangat and Molloy 1994; Thomas and Bamforth 1999; Stanish and Thomas 2003). By assuming a concrete cover thickness (x), typical chloride threshold (C_t) and surface concentration (C_s), the service life (t) can be calculated using the diffusion coefficient (D) and Eq. (3.3).

Calculating the service life as described above, as noted, assumes that the chloride diffusion coefficient remains constant throughout the exposure life, which is not the case. The diffusion coefficient decreases with time with a significant reduction expected if fly ash or slag are present (Thomas and Bamforth 1999). Thomas and Bamforth (1999) developed a model, based on research by Mangat and Molloy (1994), that can be used to predict the diffusion coefficient (D) at any age (t) using the diffusion coefficient determined after 28 days of curing. This model is presented in Eq. (3.5):

$$D_t = D_{28}\left(\frac{t_{28}}{t}\right)^m \qquad \textbf{Eq. (3.5)}$$

Where:

D_t : diffusion coefficient at time t

D_{28} : diffusion coefficient at 28 days

t_{28} : 28 days

m : constant

The value of m varies depending on the supplementary materials used in the concrete mixture as well as the water to cement ratio. Thomas and Bamforth (1999) used a best fit

model with samples from six different ages to produce a value of *m* for both ordinary concrete and concrete with fly ash added at 25% - 30%. The *m* values produced were 0.1 for ordinary concrete and 0.7 for concrete containing fly ash.

More recent research has shown that the value of *m* can vary quite a bit. Nokken et al. (2006) found that the value of *m* for plain concrete could be as high as 0.6 with the value for concrete containing fly ash being as high as 0.9 with w/c ratios of 0.4 and 0.35, respectively. They also showed that the addition of silica fume does not have much of an effect on the value of *m*; however, it does decrease the initial value of the diffusion coefficient. Audenaert et al. (2010) found that the value of *m* for plain concrete could be as low as 0.2 with a w/c ratio of 0.41. Some of this variation may be attributed to the time frame used in the tests. Thomas and Bamforth (1999) used 8 years as the end of the longest test, and Audenaert et al. (2010) used 5 years. The values presented in these two papers seem to agree with each other, whereas the high values presented by Nokken et al. (2006) used only 3 years for their longest test.

Nokken et al. (2006) also presented three different methods of determining the value of *m* based on the total time, the average time and the effective time. The total time method used the time from casting until the end of chloride exposure. This method produced the lowest values of *m* and thus the most conservative. This method is the most commonly used by researchers and the *m* values presented above use this method. The average time method used the curing period plus the average of the time exposed to chlorides. This method produced *m* values higher than that of the total time method. The effective time method was developed by Stanish and Thomas (2003) and is a little more complicated than the other two. The effective time is determined by first determining the average diffusion coefficient from a bulk diffusion test, which assumes the age of the concrete to be the average time between the start and end of the test, then determining the time during the test that average occurs instantaneously, as the decrease is exponential and that

time is the effective time. This method results in the largest *m* value, thus the least conservative.

In order to calculate service life properly, the diffusion coefficient should be varied over time according to Eq. (3.5) to give an accurate service life as the rate of diffusion will decrease over time. There are computer programs, such as Life 365 (Bentz et al. 2010) that use the equations provided above and use a finite difference model to calculate the service life whilst taking temperature variation, concrete mixture, surface chloride concentration and decreasing diffusion coefficients into account.

Life 365 is the software program used by the author to determine the service lives of the concrete mixtures used in this thesis. The program uses location specific data, such as surface chloride concentration, yearly temperature variation and concrete mixture proportions to predict the service life. The program either chooses an *m* value or the user can dictate a value to use to predict the diffusion coefficient over time. With the inherent variability caused by the assumptions the service life and diffusion equations make, it is hard to accurately predict the service life. The program also underwent an update during the course of this research which greatly increased the service life of all the mixtures in this thesis. The author attempted to determine the change in the program that caused the increase in the predicted service lives; however, he was unable to determine the cause.

3.6 Chloride Penetration Testing Methods

To assess chloride penetration as a quality control parameter, the slow chloride penetration process must be accelerated. There have been several methods suggested to allow the determination of chloride ingress in a reasonable timeframe. Two of these methods are presented in the following sections along with the method used to determine the chloride penetration in real time.

3.6.1 Electrical Indication of Concrete's Ability to Resist Chloride Ion Penetration (ASTM C1202)

The ASTM C1202 test provides a rapid indication of the concrete resistance to the penetration of ions. In the test, a water saturated, 50 mm thick, 100 mm diameter concrete specimen is subjected to a 60 V applied DC voltage for a period of 6 hours using an apparatus shown in Figure 3.1.

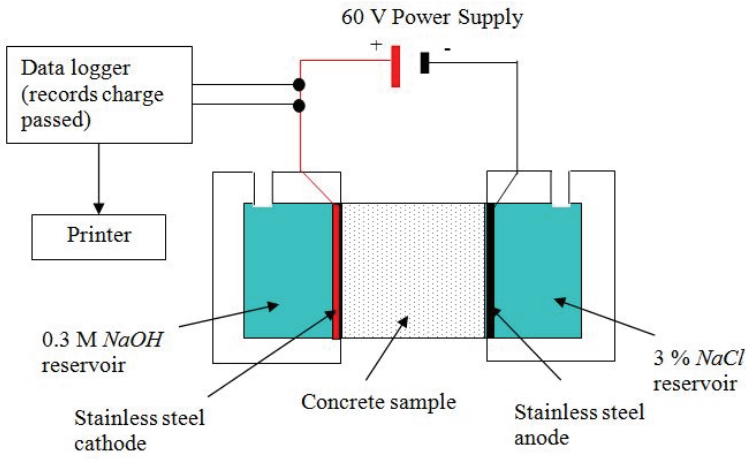

Figure 3.1 ASTM C1202 Test Set-Up (after Stanish et al. 1997)

In one reservoir is a 3.0 % *NaCl* solution and in the other reservoir is a 0.3 M *NaOH* solution. The total charge passed through the specimen is measured and this is used to rate the concrete according to the criteria tabulated in the standard, shown in Table 3.1. This test is commonly referred to as the Rapid Chloride Permeability Test (RCPT) and was first developed by Whiting (1981).

Table 3.1 RCPT Ratings (per ASTM C1202)

Charge Passed (coulombs)	Chloride Ion Penetrability
> 4000	High
2000 - 4000	Moderate
1000 - 2000	Low
100 - 1000	Very Low
< 100	Negligible

Although this test has been adopted as a standard, a number of criticisms have arisen regarding its mechanism. The main criticisms are (Andrade 1993; Zhang and Gjorv 1991; Malek and Roy 1996; Roy 1989; Geiker et al. 1990):

- The current passed is related to all ions in the pore solution and not just the chloride ions.
- The high voltage applied leads to an increase in temperature, especially in lower quality concretes, which further increases the charge passed. This causes poor concrete to look even worse than it would otherwise.

These criticisms lead to a loss in confidence in this test for measuring chloride ion penetrability. In addition, they also lead to a loss of precision. ASTM C1202 states that the single operator coefficient of variation of a single test is 12.3 % and that two properly conducted tests should not differ by more than 42 %. The multilabratory coefficient of variation is naturally less precise at 18.0 %, so two properly conducted tests between two labs should not vary by more than 51 %. To reduce this variation, three samples are normally tested and averaged; however, this only reduces the variation to 42 % between two separate laboratories.

Another difficulty with the RCPT is that it depends upon the conductivity of the concrete being in some way related to the chloride ion penetrability (Stanish et al. 1997); therefore, any conductive material present in the sample will bias the results, causing them to be too high. This would be the case if any reinforcing steel, conductive fibers or ionic conductive pore solution, such as corrosion inhibiting admixtures, are present in the concrete sample. All of these cases would result in a higher coulomb rating than would otherwise be recorded; therefore, the test method can be used as a quality control measure to qualify a mixture, but not necessarily disqualify it (Ozyildirim 1994). If an acceptable rating is achieved, it is known that the concrete cannot be any worse than that within the precision of the test method.

Despite these drawbacks, this test method still remains common and attempts have been made to correlate RCPT values with diffusion coefficients from other tests (Stanish et al. 2000).

3.6.2 Rapid Migration Test (NordTest Standard NT Build 492)

This technique was first developed by Tang and Nilsson (1992) and is known as the NordTest Standard Rapid Migration Test (RMT). The test consists of a migration cell set-up, shown in Figure 3.2, with a 50 mm thick, 100 mm diameter sample. The bottom side is subjected to a 10 % *NaCl* solution while the upper surface is subjected to a 0.3 M *NaOH* solution. A voltage potential of 30 V is applied to the specimen, which drives the chloride ions to migrate into the specimen.

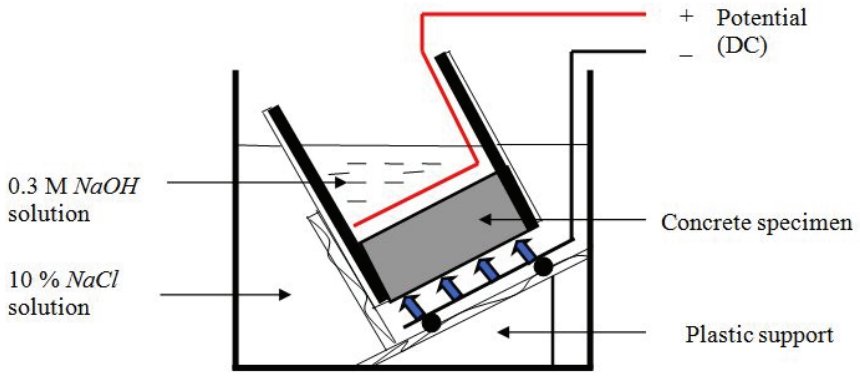

Figure 3.2 Chloride Migration Cell Set-Up

After a specified duration, based on the current through the sample, the specimens are removed from the test and axially split. The chloride penetration is then determined on half of the split sample using a colorimetric technique in which silver nitrate ($AgNO_3$) solution is used as a colorimetric indicator. The silver nitrate solution reacts with chloride ions present in the concrete causing silver chloride to be produced, a whitish substance. In the absence of chloride ions, the silver reacts with the hydroxides present in the concrete to produce silver hydroxide, a brownish substance. Otsuki et al. (1992) determined that a 0.1 N silver nitrate solution was the optimum concentration and that the color change border corresponds to the location of a soluble chloride concentration of 0.15 % by weight of cement. To measure the penetration depth accurately, seven depths are measured in intervals of approximately 10 mm, as shown in Figure 3.3. The depths are averaged and can be used in Eq. (3.6) (NT Build 492) to determine a diffusion coefficient.

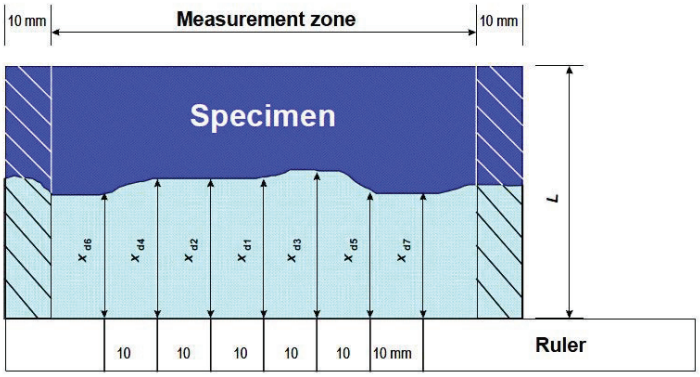

Figure 3.3 Illustration for Measurement of Chloride Penetration Depths

$$D_{nssm} = \frac{0.0239(273+T)L}{(U-2)t}\left(X_d 0.0238\sqrt{\frac{(273+T)LX_d}{U-2}}\right) \qquad \textbf{Eq. (3.6)}$$

Where:

D_{nssm} : diffusion coefficient (x10^{-12} m^2/s)

U : applied voltage (V)

T : average temperature of *NaOH* solution (°C)

L : specimen thickness (mm)

X_d : average penetration depth (mm)

t : test duration (hrs)

The RMT is capable of addressing the criticisms of the RCPT related to examination of actual chloride ion movement and temperature rise. The test measures the penetration distance of chloride ions only and uses a lower voltage potential compared to the RCPT. The voltage applied is varied according to the current through the sample; therefore, a lower current is maintained in the sample reducing the temperature rise in the sample (Stanish et al. 2000); however, the inclusion of conductive materials can short circuit the cell, or affect the chloride ion movement by reducing the penetration distance (Stanish et

al. 1997). Therefore care should be taken to avoid including conductive materials in the sample.

In the standard, no acceptance criteria is given for the chloride diffusion coefficient, however, Tang and Nilsson (1992) gave the following guidelines:

- $D < 2 \times 10^{-12}$ m^2/s : very good resistance
- $D < 8 \times 10^{-12}$ m^2/s : good resistance
- $D < 16 \times 10^{-12}$ m^2/s : moderate resistance
- $D > 16 \times 10^{-12}$ m^2/s : no suitable for marine environments

According to NordTest NT Build 492, the coefficient of variation for a single operator is 9 % while the multilabratory coefficient of variation is 13 %. The RMT shows better repeatability and reproducibility than the RCPT, meaning it will give more precise results when considering multiple samples. One drawback to the test is that is the concrete is of poor quality, the chlorides may penetrate the entire sample before the end of the test; however this would indicate a very poor concrete mixture not suitable for a marine environment.

It should be noted that the diffusion coefficients determined from the RMT are not the same diffusion coefficients determined by the bulk diffusion test. Stanish et al. (2000) compared the results of the tests, including the RCPT; however they did not establish an equation between the methods. They showed that all three test methods showed that an increase in one method resulted in an increase in the other two methods when comparing various samples with different diffusion coefficients.

3.6.3 Bulk Diffusion Test (ASTM C1556)

This test was developed to overcome the deficiencies of the salt ponding test, where a salt solution was placed on top of a dry concrete sample while the bottom was exposed to air (Stanish et al. 2000). The bulk diffusion test uses a concrete sample that has been moist cured for 28 days and conditioned in lime water prior to the start of the test to eliminate any sorption effects. The sample is sealed on all sides with an impermeable membrane except the surface which is to be exposed to the 2.8 M *NaCl* solution. The sample is submerged in the solution as seen in Figure 3.4 and left for a minimum of 35 days, longer for high quality concrete.

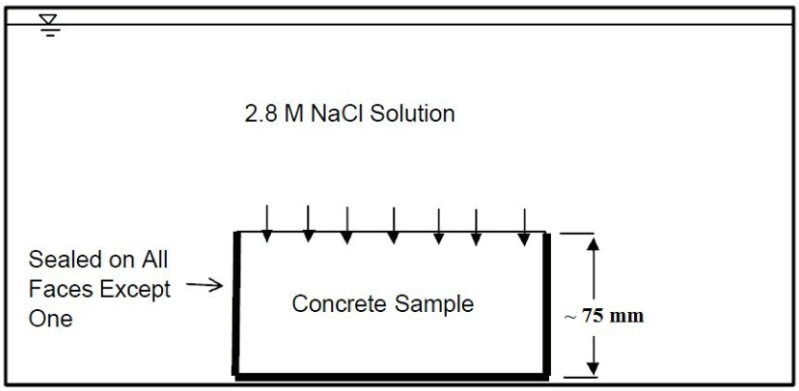

Figure 3.4 Bulk Diffusion Test Set-up

Prior to submerging the sample, a slice is cut from the sample to determine the initial chloride content. After the required time has passed, the sample is removed from the solution and evaluated by mounting the sample in a mill or lathe with a diamond tipped bit. The mill is used to gather concrete dust samples at various depths for chloride content determination. The water soluble chloride content is determined according to ASTM C1218. The error function solution of Fick's Second Law is then fit to the curve and the diffusion value is determined.

While this test is capable of modelling the chloride diffusion into concrete, it is a long term test requiring 35 days for low quality concrete, while high quality can require 90 days or more.

When predicting service life, all programs and calculations use the diffusion coefficient determined from the bulk diffusion test. Recommendations have been given regarding the RMT and RCPT on whether or not a mixture has good chloride ingress resistance, but to predict the service life of a structure, the bulk diffusion coefficient is needed.

The three tests described above all assume that the samples are uncracked, as do the service life calculations; however concrete cracks and this needs to be considered if a mixture is to have a long service life.

3.7 Mechanisms of Plastic Cracking in Fresh Concrete

Plastic cracking occurs on the surface of fresh concrete within the first few hours after placement, while the concrete is still in the plastic state, which is while the concrete is still fluid or semi-fluid. Plastic shrinkage cracks occur before sufficient tensile strength has been attained (Cabrera et al. 1992). Two mechanisms have been recognized as being responsible for shrinkage cracking. The most common mechanism is the development of capillary stress near the surface of concrete, which is caused by the imbalance between the evaporation rate and the bleeding rate (Powers 1968; Wittmann 1976; Radocea 1990). The other common mechanism is plastic settlement (Weyers et al. 1982). Both mechanisms are described in the following sections.

3.7.1 Capillary Stress

Bleeding and evaporation occur in fresh concrete in three separate stages, and these stages are related to the volume contraction of fresh concrete (Ravina and Shalon 1968).

In the first stage, the bleeding exceeds evaporation and the concrete surface remains wet. During the first stage there is no volumetric contraction and even some expansion may be observed. During the second stage, the rate of evaporation exceeds the bleeding rate. This causes a volume contraction that is proportional to the water that is removed from the fresh concrete and a linear relationship is normally observed between time and shrinkage. Water channels may also collapse during this stage due to the low strength of the concrete, forming a more dense structure. For the third stage, the concrete gains rigidity due to the hydration process resulting in a considerable decrease in volumetric contraction. If the concrete surface has developed sufficient tensile strength, cracks do not form; however, if the surface dries rapidly before sufficient tensile strength develops, shrinkage cracking will occur.

Wittmann (1976) presented a theoretical analysis of capillary pressure to explain the mechanism of plastic cracking. He stated that when rapid moisture loss occurs on the surface of fresh concrete, it cannot be compensated by bleeding water rising to the surface; therefore, water between particles near the surface dries and a curved liquid surface is formed, introducing a surface meniscus. As drying continues the radius of the capillary meniscus changes over time. The magnitude of capillary tension developed is described by Eq. (3.7).

$$P_c = -\frac{2\gamma_L}{r} \qquad \textbf{Eq. (3.7)}$$

Where:

P_c : capillary pressure (MPa)

γ_L : liquid surface tension (N/mm)

r : liquid surface radius (mm)

Several researchers conducted tests to verify the capillary pressure theory. It was concluded that a breakthrough pressure exists where an abrupt change in capillary pressure can be measured. The breakthrough pressure is reached when the critical conditions are established that are responsible for plastic shrinkage cracking (Wittmann 1976). It was also found that the measured capillary pressure was a time dependent function of mixture proportions, which is the space between the solid particles, and the location of the sensor from the top surface. The time corresponding to the development of a breakthrough pressure was thought to be related to the creation of a self-supporting body (Radocea 1990; Johansen et al. 1993; Radocea 1994; Hammer 1998; Radocea 1998).

3.7.2 Plastic Settlement

Subsidence of the fresh concrete surface can cause plastic shrinkage cracking. Differential settlement can be observed to occur over reinforcing bars or at changes in section height, which frequently corresponds to the location of cracking (Weyers et al. 1982; Sansone and Brown 2007).

As concrete settles, water bleeds to the top surface resulting in volumetric contraction or settlement. Settlement may be prevented locally by rigid inclusions, such as reinforcing bars. The concrete above the inclusion settles at a reduced rate compared to the bulk concrete. This difference in settlement causes a tensile stress to develop above the inclusion which can result in plastic shrinkage cracking, as seen in Figure 3.5. The amount of settlement is a function of sample thickness, water to cement ratio (W/C) and slump (Powers 1968). The magnitude of the tensile stress caused by the plastic settlement is related to the cover thickness, bar size and the mixture properties (Weyers et al. 1982). Qi (2003) also showed that the crack width is very dependent on the cover thickness. As the cover thickness increases, the crack width decreases. Kayir and Weiss (2002) have also determined that the use of high range water reducer can increase the settlement of concrete.

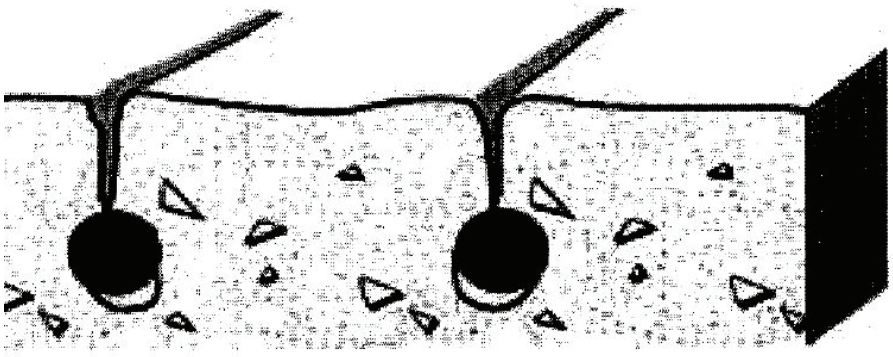

Figure 3.5 Plastic Settlement around Reinforcing Bars (after Qi 2003)

3.8 Factors Contributing to Plastic Shrinkage Cracking

The extent of plastic shrinkage cracking can be affected by the mixture composition and environmental factors. The following section describes the main factors that influence the potential for plastic shrinkage cracking.

3.8.1 Mixture Composition

It is generally accepted that low water to cement ratios (w/c), increased cement content and increased cement fineness tend to increase the potential for plastic shrinkage cracking. The addition of very fine cementitious materials, such as silica fume, also increase the potential of shrinkage cracking. Fine cementitious materials reduce the rate and amount of bleeding water that reaches the surface, therefore, water loss due to evaporation cannot be replenished resulting in shrinkage cracking (Cohen et al. 1990; Bloom and Bentur 1995; Almussalam et al. 1999).

Chemical admixtures are frequently used in concrete to achieve the desired properties in both the fresh and hardened states. Admixtures with prolonged set-retarding provide a longer time period for water to bleed to the surface, at the same time admixtures may delay the early-age strength development which is required to tolerate environmental

loading; therefore, the possibility of shrinkage cracking can increase with the use of admixtures (Cabrera et al. 1992; Soroka and Ravina 1998).

3.8.2 Environmental Conditions

Plastic shrinkage cracking is increased by high ambient temperature, high wind velocity, and low relative humidity, all of which accelerate water evaporation, resulting in a higher shrinkage rate. ACI 305R (2010) describes how the evaporation rate can be used to determine if a high potential for cracking exists. Plastic shrinkage cracking is thought to occur as the evaporation rate exceeds one kilogram of water from one square meter in one hour (ACI 305R 2010). Figure 3.6 can be used to approximate the evaporation rate; however, in construction practice evaporation rates below one cannot be accepted as safe. This is especially true if plastic shrinkage cracking occurs due to settlement.

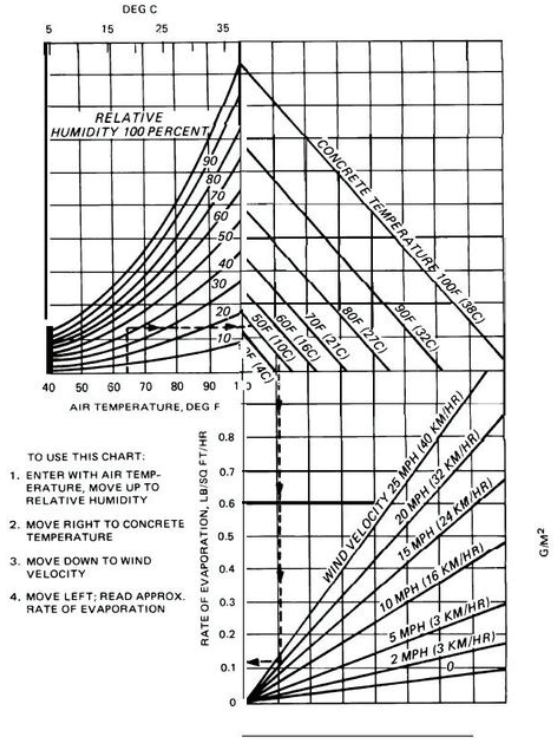

Figure 3.6 Evaporation Rate Estimation (after ACI 305R-10)

3.8.3 Geometry and Construction

Geometry of a structure is an important factor to consider in assessing the susceptibility to plastic shrinkage cracking of a mixture. Plastic shrinkage cracking is usually observed in large flat structures such as bridge decks or wharfs. In these structures the area that is exposed to evaporation is large and the sub-base beneath provides a high degree of restraint (Banthia et al. 1996).

Improper construction practices and curing can significantly increase the potential for plastic shrinkage cracking. This can be minimized by reducing the evaporation of water, which include the use of wind breaks and sun shades, sub-grade dampening prior to concrete placement and the use of a curing compound or covering during early curing. It should be noted that there is no consensus on a single procedure to prevent cracking.

3.9 Plastic Shrinkage Testing Methods

Several test methods have been proposed and utilized by researchers in an attempt to qualify plastic shrinkage cracking. Most test methods focus on parameters that describe crack width, length and area. Since fiber addition is considered as a solution to reduce or eliminate plastic cracking, most tests focus on testing fiber reinforced concrete (FRC) and comparing it to a similar mixture without fiber addition. Two of these methods have been adopted as standards; however, these methods are mainly used to compare a non-fiber mix to one with fiber addition at a specific volume.

There are test methods for both restrained and unrestrained shrinkage; however, unrestrained shrinkage tests provide little useful information as most concrete structures have restraint present either externally from sub-grade or internally from steel reinforcement (Soroushian et al. 1995); therefore, unrestrained shrinkage tests were not investigated by the author.

3.9.1 Restrained Plastic Shrinkage Test

Restrained plastic shrinkage tests can be classified by specimen geometry as ring type tests, linear beam specimens and slab type specimens. The difference between these specimens is the geometry, type and degree of restraint.

The ring type method was used by Johansen et al. (1993) in which concrete is cast between inner and outer steel rings. The outer ring is furnished with ribs to provide restraint, as seen in Figure 3.7. After casting, the sample is put under an air funnel with high wind velocity. The ring type test provides sufficient end restraint and avoids eccentricity in applying end restraint. A specially designed hood is required to maintain the air circulation around the specimen at constant speed, temperature and humidity. This ring type test has been adopted as the NordTest Standard NT Build 433.

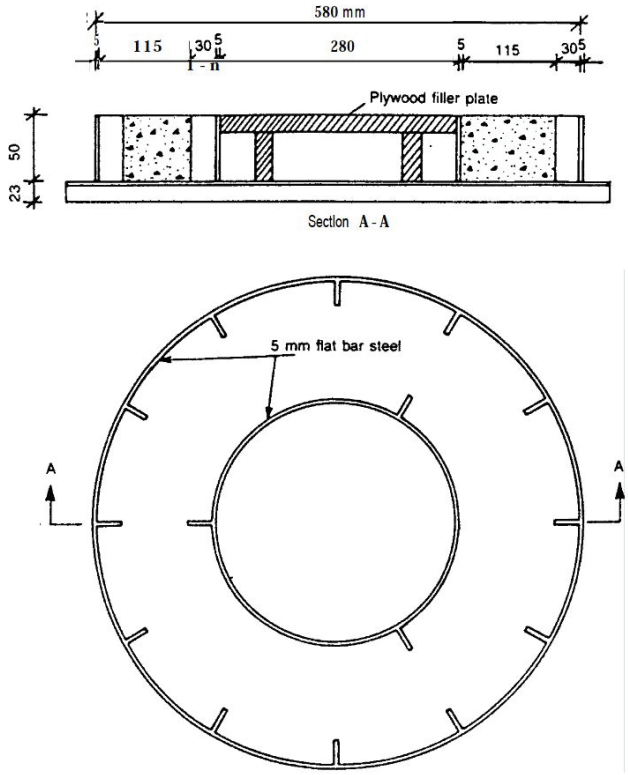

Figure 3.7 Shrinkage Ring Test Specimen (after NordTest NT Build 433)

A linear beam specimen was used by Banthia et al. (1993; 1994), with restraint provided by triple-bar anchors at the ends of the beam. However, sufficient and constant end restraint in this geometry is difficult to achieve while the concrete is still in the plastic state.

Slab specimens of various sizes and restraint have been tested by several researchers. Kraai (1985) tested the influences of mixture proportions and environmental conditions using a slab with wire mesh as the restraint mechanism. Other researchers have used a similar set-up (Cohen et al. 1990; Wang et al. 2001). Banthia et al. (1996; 2000) used slab specimens cast directly on a concrete sub-base with exposed aggregates to simulate restraint in real structures; however, due to the complex stress field and random crack patterns, quantitative analysis was difficult.

While these test methods can give an approximate susceptibility of a concrete mixture to plastic cracking, the results vary widely and no consensus exists regarding data interpretation. Several researchers agree that there is a need for a standard test that effectively evaluates the efficiency of fiber reinforcement in plastic cracking (Naani et al. 1993; Banthia et al. 1996).

Berke and Dalliare (1994) designed a restrained slab test to characterize the efficiency of low fiber volumes on plastic cracking. The specimen is cast in a mold with a stress riser on the bottom to reduce the slab thickness, as seen in Figure 3.8. The cast specimens are placed in an environmental chamber with a fan to blow air across the top of the sample. Cracking is expected to occur above the stress riser and across the width of the specimen. This test method has been adopted as standard ASTM C1579.

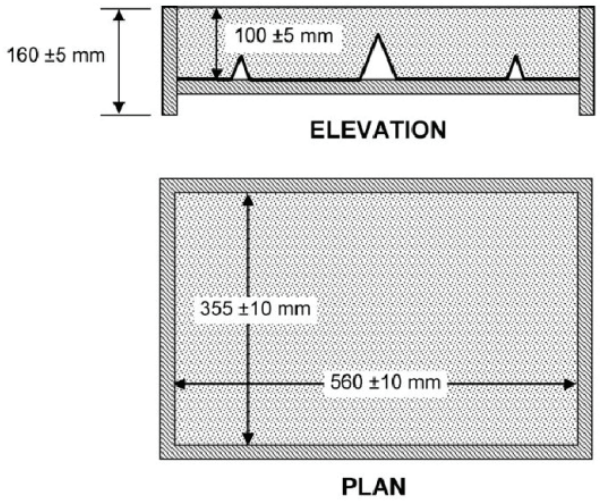

Figure 3.8 Shrinkage Slab Test Specimen (after ASTM C1579)

3.10 Effects of Shrinkage Cracking on Chloride Penetration

When service life is calculated based on a diffusion coefficient, the concrete is assumed to be in the perfect state, which is well cured and uncracked. This best case scenario overestimates the performance of the structure (Qi 2003). This best case scenario is rarely the case and shrinkage cracks commonly occur. These shrinkage cracks commonly occur over reinforcement which can significantly reduce the effective cover to the steel reinforcing bar thus reducing the distance the chlorides have to travel to reach the bar. This effectively reduces the service life of the concrete structure as corrosion will occur much earlier than predicted.

Research has shown that as the crack width increases, the penetrability of aggressive agents increases by several orders of magnitude for structural cracking (Wang et al. 1997), as shown in Figure 3.9.

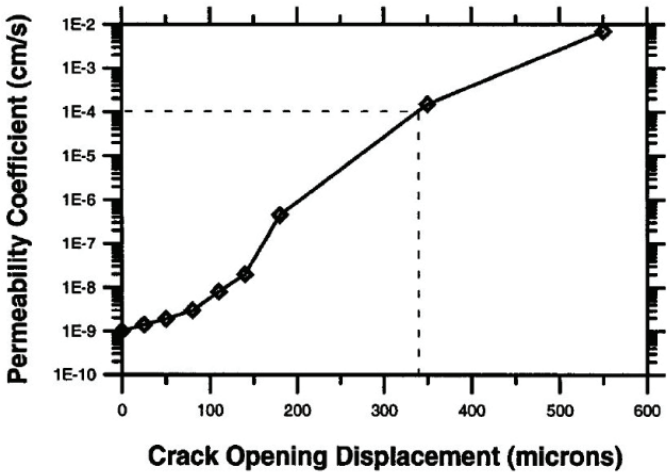

Figure 3.9 Crack Opening vs. Permeability in Concrete (after Wang et al. 1997)

Qi (2003) showed that increasing crack width greatly reduced the time to corrosion initiation in samples with shrinkage cracking above a steel reinforcing bar. This was more profound in samples with larger cover thicknesses. Omer (2006) also showed that a crack caused by plastic shrinkage can increase the depth of chloride penetration around the crack effectively reducing the cover by the depth of the crack.

Limiting crack width is important when considering the possibility of self-healing (Jacobsen et al. 1996). Self-healing of small cracks can occur due to further hydration in a moist environment or a reaction where calcite crystals are deposited in the crack. Sanjuan and Toledo Filho (1998) found that the reduction in crack size caused by self-healing significantly lowers the potential for corrosion.

3.11 Freezing and Thawing Damage

Freezing and thawing damage occurs when a concrete structure is exposed to temperatures below the freezing point of water. The concrete freezes from the surface inwards causing damage to the exterior of the structure. Bakharev and Struble (1995) identified that this damage is caused by micro-cracking on the surface. This initial cracking is in the form of vertical cracks. These cracks propagate inwards from the

surface several millimeters. Additional freezing and thawing causes these vertical cracks to be connected by horizontal cracks, which can cause spalling of the concrete surface. These cracks are caused by the expansion of water within cement paste and aggregates when frozen.

Freeze-thaw damage is mitigated through the use of air-entraining admixtures that cause small air bubbles to form in the concrete; however, even properly proportioned concrete mixtures with good quality air voids are subject to damage caused by freezing and thawing (Forgeron 2005).

The effect of freezing and thawing on the mechanical properties of concrete, such as permeability, compressive strength and flexural strength depend on the severity of the freezing and thawing damage which depends on the availability of water, quality of the air-void system, rate of freezing, permeability of the concrete, presence of shrinkage cracking and fatigue cracking (Forgeron 2005).

It should be noted that there is a size effect in freeze-thaw damage as the damage only affects the surface; therefore, this loss of surface material has a much larger impact on thin or small elements than those that are much larger. Also, members subjected to flexural loads are affected differently compared to those subjected to compressive loads. The tension zone in a flexural member can experience more damage than the compressive zone as the tensile stresses may cause cracking to occur, thus allowing water to penetrate further into the sample causing more damage when it freezes. This reduction can cause an overall reduction in flexural strength and stiffness. This is not the case with compressive forces as they tend to decrease the tendency of surface cracking.

3.12 Fiber Reinforced Concrete (FRC)

Different types of discontinuous fibrous materials (steel, glass, polymeric, etc.) have been added to concrete to improve plastic and hardened properties, as well as durability. Fibers have been added as the primary reinforcement in bridge decks, concrete pavements, industrial slabs and many precast concrete structures. They have also been used as secondary reinforcement along with steel rebar to reduce cracks caused by plastic shrinkage and settlement. In the hardened stage, fibers have been shown to improve cracking resistance, impact resistance, abrasion resistance, ductility and toughness, and the overall durability of concrete structures. Since fiber addition in concrete can significantly improve its resistance to cracking, they are recommended to be used in marine structures (Al-Tayyib et al. 1990).

Fibers used in concrete are usually steel or synthetic and are available in a variety of lengths, sizes, shapes and thicknesses. They are added to fresh concrete during the mixing process. The main differences between steel reinforcing bars and fibers are that fibers are much smaller and are randomly distributed in concrete, whereas steel rebar are placed at specific locations.

The following discussion will focus on monofilament self-fibrillating macro-synthetic fibers as they were chosen for the purpose of this thesis, due to their resistance to corrosion compared to steel fibers. They were also chosen because of their ability to mitigate the effect of plastic shrinkage cracking as well as improve the durability of concrete. It should also be noted that the fiber addition in this thesis is not intended to replace steel reinforcing bars, but as a secondary reinforcement in addition to steel rebar.

3.12.1 Synthetic Fiber Characteristics

Synthetic fibers, usually a blend of polypropylene and other polymers, are widely used in the concrete industry and are available as either macro or micro fibers. The difference

between the two types are that micro fibers have a much smaller diameter and are shorter in length than macro fibers and are generally used to only control plastic shrinkage cracking. The diameter is generally less than 0.1 mm and they are used in small dosages of 0.03% to 0.1% by volume. Macro fibers are larger and have a diameter between 0.2 to 1.5 mm and have been used at addition rates up to 2% by volume, however common dosages are between 0.2% and 0.5% by volume. Research by Trottier and Mahoney (2001) has shown that macro synthetic fibers can be produced as a monofilament self-fibrillating fiber. These fibers have the ability to fibrillate during the mixing process where each fiber frays causing a number of thin fibrils (micro fibers) at the ends which improve the anchorage of the fibers with the concrete. This can significantly increase the plastic shrinkage resistance of the concrete as well as other properties such as impact resistance and toughness. These fibers have an effective diameter of 1.1 mm and can range in length; however, 50 mm is the most common. These fibers have been used both as the main reinforcement in slab on grade and pavement applications, and as secondary reinforcement in conjunction with steel reinforcing bars to control shrinkage and temperature cracks in parking and bridge structures (Euclid Chemical 2010).

Macro and micro fibers are known to adversely affect the workability of conventional concrete. These effects on workability as well as the plastic and hardened properties will be discussed in the following sections.

3.12.2 Effect of Synthetic Fibers on the Workability of Conventional Concrete

FRC appears stiffer (lower slump) when compared to conventional concrete without fibers but under vibration the workability of the two mixtures are approximately the same (Johnston 2001). Workability tests have shown that the slump of FRC decreases as the volume fraction of fiber is increased. Al Tayyib et al. (1988) found that the addition of 0.5% by volume of synthetic macro fiber reduced the slump of a conventional concrete mixture (w/c of 0.5) from 89 mm to 13 mm even though the mixture flowed satisfactorily and responded well to vibration.

According to ACI Committee 544 (1993), a well-adjusted FRC mixture can be pumpable despite its stiff appearance. It is recommended to reduce the coarse aggregate content by 5% to 10% compared with plain concrete to facilitate pumping. When proportioning FRC mixtures, the slump of the plain concrete should be 50 – 75 mm more than the desired final slump, or a superplasticizer can be used rather than excess water (Johnston 2001). The use of the superplasticizer is the better option when the addition of excess water cannot be facilitated due to strength or permeability restraints.

The size and length of the fibers relative to that of the coarse aggregate will determine their distribution. This distribution is important because good fresh and hardened properties depend upon a proper distribution. In order for the fibers to be effective in the hardened state, Johnston (1996) recommends that fibers not be shorter than the maximum aggregate size. Normally fibers range from 2 – 4 times the size of the maximum aggregate. Another factor to consider when determining fiber length is the aspect ratio, which is the ratio between the diameter of the fiber and its length. An aspect ratio less than 100 should be maintained to avoid fiber balling which leads to poor distribution (Trottier et al. 2002)

3.12.3 Effect of Fibers on Conventional Concrete in Plastic and Hardened State

The primary use of synthetic fibers in conventional reinforced concrete structures is to enhance its properties in both the plastic and hardened state. In the plastic state, micro fibers can significantly reduce the cracking caused by plastic shrinkage and settlement. This reduction in cracking prior to setting improves the long-term durability of the concrete. In the hardened state, several improvements can occur when macro synthetic fibers are added. The first improvement is an increase in the flexural toughness by providing post-crack load resistance similar to that of conventional steel reinforcement; however the fiber is uniformly distributed (Trottier et al. 1997). The second is the effect of fibers on the freeze thaw resistance of concrete mixtures. The final potential improvement is a reduction of bleeding and thus the number of bleed channels, resulting

in less water migration to the concrete surface. This helps to maintain the w/c ratio throughout the depth of the concrete and produces concrete with less permeability. These improvements can also be of significant benefit to concrete marine structures. In the following sections, an overview of the role of macro synthetic fibers in controlling cracking, effect on freeze thaw resistance and decreasing the permeability, are presented.

3.12.4 Resistance and Control of Plastic Shrinkage Cracking

The method that is commonly used to quantify and evaluate concrete plastic shrinkage cracking potential involves drying the surface of a freshly placed restrained concrete slab. After drying the cracking is measured and quantified as the product of crack length and width, per unit area, of tested surface. Comparing the crack area with that of a control sample containing no fiber allows the improvement in plastic shrinkage cracking caused by the fiber addition to be quantified (Kraii 1985).

Typically, the results of plastic shrinkage testing demonstrate that micro synthetic fibers are very effective at reducing and controlling plastic shrinkage cracking (Balaguru 1994; Banthia et al. 1996; Banthia and Yan 2000; Trottier and Mahoney 2001). Research has also shown the self-fibrillating macro fibers are also effective in reducing and controlling plastic shrinkage cracking (Trottier and Mahoney 2001; Omer 2006; Forgeron et al. 2011). The ability of fibers to reduce plastic shrinkage cracking was found to be dependent on the fiber type, length and volume fraction (Trottier et al. 2002). Naaman et al. (2005) and Qi (2003) found that when different fiber types, lengths and volume fractions were tested, the volume fraction was the most influential parameter. The addition of 0.1% by volume of synthetic fibrillated micro fiber reduced the total crack area by 30 to 40% and the crack width by 20% compared to normal concrete (Wang et al. 2001). By using a higher dosage of 0.4% by volume, Naaman et al. (2005) found that plastic shrinkage cracking could be eliminated. Omer (2006) showed that synthetic macro self-fibrillating fibers added at a dosage of 0.4% by volume can also reduce the total crack area by 70% and reduce the average crack width by 50%. Furthermore, fibers have

also been found to be effective at reducing other types of cracking such as thermal, settlement and drying shrinkage cracks (Zollo et al. 1986).

3.12.5 Effect on Freeze Thaw Resistance

The addition of fiber to concrete exposed to freezing and thawing has been shown to have little effect on the resistance of a concrete mixture when compared to the same mixture without the addition of fiber with the same entrained air content (Balaguru and Ramakrishnan 1986; Forgeron 2005). This is attributed to the fact that freeze thaw damage only affects the outer 5 – 6 mm of a sample, where few if any macro fibers would be present.

3.12.6 Effect on Permeability

Permeability is a very important when considering the long-term durability of marine concrete structures. Permeability generally refers to the rate at which particular aggressive substances such as water, chloride ions, sulfates, etc. can flow through the concrete under pressure. It is thought that since the inclusion of fibers significantly stiffen the concrete in the fresh state, it may reduce the settlement of the aggregate particles, thus reducing bleeding and the formation of bleed channels and intern reduces the permeability (Zollo et al. 1986). Qi (2003) showed that the addition of fibers does significantly reduce the settlement of aggregate particles; however, there was no evidence of any resulting decrease in permeability. Other studies using macro fibers up to 0.20% by volume have shown no significant improvement in permeability (Al-Tayyib and Al Zahrani 1990; Soroushian et al. 1995). This agrees with a later study by Omer (2006), which indicated the inclusion of macro self-fibrillating fiber up to 0.40% by volume had no noticeable effect on the chloride ingress using the RMT which can give an indication of the permeability Accordingly, fibers do not seem to have a negative effect on permeability or chloride ingress and may reduce the permeability and chloride ingress of

concrete by reducing or eliminating plastic or drying shrinkage cracks or cracks caused by loading conditions.

It should be noted that that both permeability and chloride ingress using small cylinders in the laboratory is not the same as the permeability of large concrete structures. The lab samples are in ideal conditions and do not take into account the effect of real conditions such as improper placement and consolidation. These defects can have a significant effect on the permeability and serviceability of concrete structures.

One can now see the benefits that synthetic fibers add to concrete mixtures without hindering the performance of the concrete; therefore, the incorporation of synthetic macro fibers should be considered when the shrinkage cracking potential of a mixture is high for a marine concrete structure.

CHAPTER 4 EXPERIMENTAL PROGRAM

A comprehensive experimental program was carried out to achieve the purpose of this thesis. The main objective of this thesis was to determine if the addition of a macro-synthetic fiber was beneficial to the chloride diffusion and plastic cracking resistance of concrete typically used in a freeze thaw environment. Previous research has not covered the fibers used in this thesis added to air-entrained marine concrete mixtures subjected to plastic shrinkage cracking and chloride diffusion.

Most codes and specifications for marine concrete built in a freeze thaw environment specify a maximum water to cement ratio (w/c) of 0.40, minimum cement content of 390 kg/m^3, a minimum compressive strength, at 28 days, of 35 MPa and an air content of 5 – 8 %. All concrete mixes in this study were designed to meet these specified requirements. It is also recommended by the Nova Scotia Department of Public Works that the specified slump without the addition of admixtures be 20 – 80 mm, and that admixtures be used to increase the slump for workability requirements.

In this study, a total of 9 air-entrained concrete mixtures were investigated with a w/c ratio of 0.4. The NC mixture in this thesis, which had no supplementary materials, is a typical mixture used by the Nova Scotia Department of Public Works in marine applications, and the other mixtures were designed by the author to have similar properties to the mixture by Public Works, but have better chloride resistance. The FA mixture, which had fly ash added, was designed to make use of the abundant supply of fly ash in the region as well as mitigate any alkali aggregate reactivity which is characteristic of the aggregates in the area. The four TER 50-1 mixtures had both fly ash and silica fume added and were designed to have a service life of 50 years according to the Life 365 software. The three TER 50-2 mixtures also had both fly ash and silica fume added, but used a different coarse to fine aggregate ratio to try and achieve better plastic shrinkage resistance. It should be noted that the 50 year design life was using an old version of Life 365 and the updated design life is 132 years.

Two different macro synthetic fibers, F1 and F2, were added at different dosage rates to optimize the FRC mixtures that would typically be used in Marine structural applications, while maintaining a high cracking resistance and low permeability. The proportions for each mixture used in this study are presented in Table 4.1.

Table 4.1 Concrete Mixture Compositions

Mixture No.	**NC**	**FA**	**TER 50-1**	**TER 50-1 F1**	**TER 50-1 F1**	**TER 50-1 F2**	**TER 50-2**	**TER 50-2 F1**	**TER 50-2 F2**
Fiber Vol. (%)	-	-	-	0.20	0.33	0.20	-	0.20	0.16
W/C	0.40	0.40	0.40	0.40	0.40	0.40	0.40	0.40	0.40
Cement (kg/m^3)	390	315	285.6	285.6	285.6	285.6	265.2	265.2	265.2
Fly Ash (kg/m^3)	-	105	105	105	105	105	97.5	97.5	97.5
Silica Fume (kg/m^3)	-	-	29.4	29.4	29.4	29.4	27.3	27.3	27.3
Fine Aggregate (kg/m^3)	780	722.8	702.6	702.6	702.6	702.6	903.6	903.6	903.6
Coarse Aggregate (kg/m^3)	1011	1040	1040	1040	1040	1040	910	910	910
Water (kg/m^3)	156	168	168	168	168	168	156	156	156
Plastol 341 (L/m^3)	0.440	0.440	0.324	1.117	1.117	0.824	0.588	0.882	0.882
Airex-L (L/m^3)	0.053	0.200	0.259	0.259	0.259	0.259	0.294	0.294	0.294

In this project, commercially available Type GU cement from Holcim, Joliette, Quebec, Canada, were used in all mixtures. The fly ash used in the mixtures was provided by Shaw Resources Nova Scotia, Canada, and was added at 25 % by weight to Type GU cement. The silica fume used in the mixtures was provided by Euclid Chemical,

Cleveland, Ohio, United States and was added at 7 % by weight to Type GU cement and fly ash.

The mixtures were proportioned with coarse aggregate having a maximum size of 19 mm and a natural fine aggregate with a fineness modulus of 3.12. The coarse aggregates were from Rocky Lake Quarry and the fine aggregates were from Shaw Resources, both located in Nova Scotia, Canada. The aggregates were sampled and tested to determine their specific gravity, absorption and gradation. The specific gravity and absorption values of the coarse aggregate and fine aggregate were 2.68 and 2.60, and 0.7 % and 1.5 %, respectively. All the aggregate testing was performed in accordance with ASTM C127 and C128. The grain size distributions of the coarse and fine aggregates are shown in Figure 4.1 and Figure 4.2 respectively. In addition to the grading curves, the minimum and maximum threshold values for each aggregate, as stated in ASTM C33, are shown as dashed lines in Figure 4.1 and Figure 4.2. The results show that the grading of the 19 mm coarse aggregate and the fine aggregate, used in this study, are both within ASTM C33 requirements.

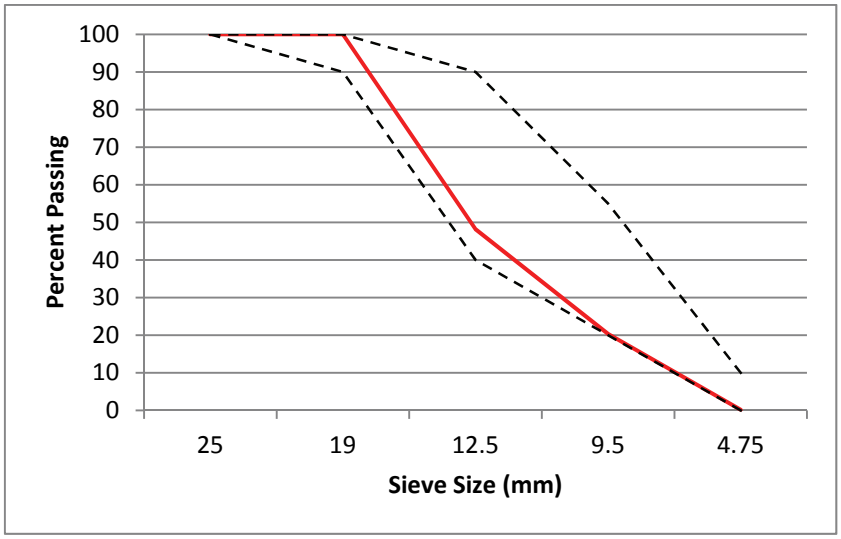

Figure 4.1 Coarse Aggregate Gradation Curve

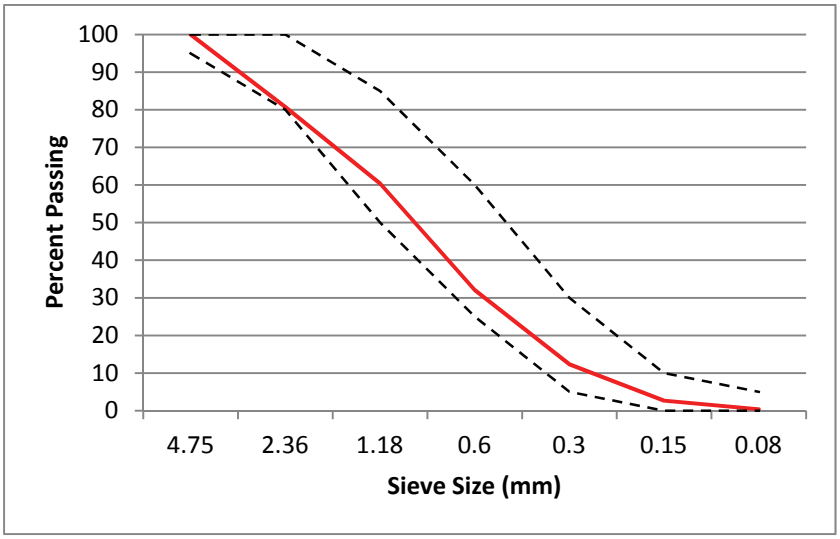

Figure 4.2 Fine Aggregate Gradation Curve

Plastol 341, a polycarboxylate based mid-range/high-range water reducing and plasticizing admixture, supplied by Euclid Chemical Company, was used in this project. The data sheet for Plastol 341 can be seen in Appendix A. The dosages of Plastol were adjusted in each mixture to provide a slump similar to what would be seen in practice.

Airex-L, a liquid solution of hydrocarbons used as an air-entraining agent, supplied by Euclid Chemical Company, was used in this project. The data sheet for Airex-L can be seen in Appendix A. The dosages of Airex were adjusted in each mixture to provide the required percentage of entrained air.

Two fibers were selected for this study. Fiber 1 (F1) is a monofilament macro-synthetic self-fibrillating fiber. This fiber type was chosen because it provides concrete with a high cracking resistance and improved mechanical properties, such as increased abrasion resistance and flexural resistance. These fibers are unique in that they are self-fibrillating when mixed in concrete, meaning the fibers break apart when mixed, as seen in Figure 4.3. Fiber 2 (F2), seen in Figure 4.4, is also a monofilament macro-synthetic fiber, however it is not self-fibrillating, and was specifically designed for this thesis by the

author to allow for more individual fibers to be added while maintaining the same volume percentage by changing the geometry. The length, specific gravity, tensile strength, modulus of elasticity and color of the fibers are given in Table 4.2.

Table 4.2 Fiber Geometry and Properties

Fiber	Specific Gravity (kg/m^3)	Tensile Strength (MPa)	Modulus of Elasticity (GPa)	Length (mm)	Color
F1	920	600 – 650	9.5	51	White
F2	920	800 – 850	8.8	51	White

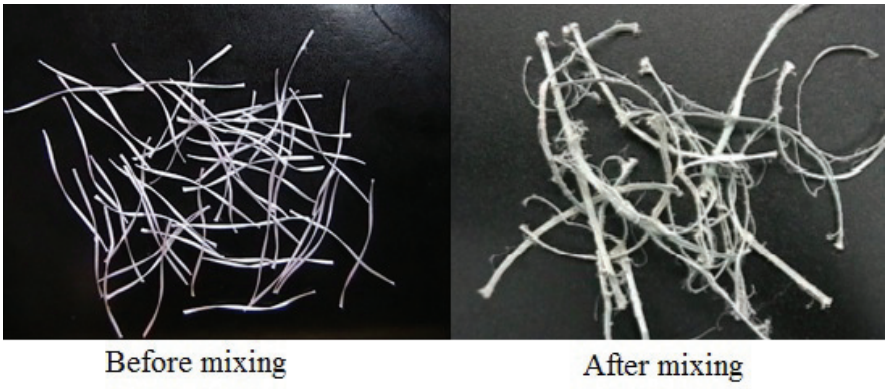

Figure 4.3 Fiber 1 Before and After Mixing

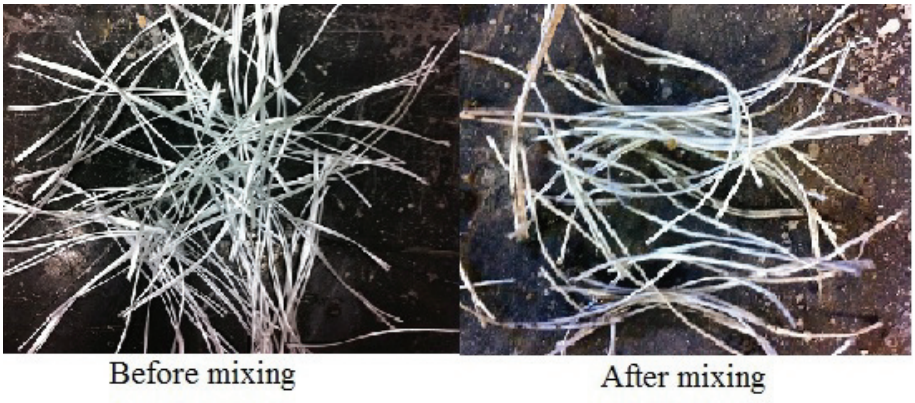

Figure 4.4 Fiber 2 Before and After Mixing

All the mixtures were prepared in the concrete mixing laboratory at Dalhousie University. The batching of all mixtures took place over a period of 5 months in the fall/winter.

All mixtures were prepared in a 0.252 m^3 capacity lab concrete drum mixer. The size of the mixer was selected to mix a batch size of 0.17 m^3. The size of the batch was determined based on the volume required to perform all fresh concrete tests plus the volume of the concrete required for the preparation of the test specimens. The Laboratory concrete mixer is shown in Figure 4.5.

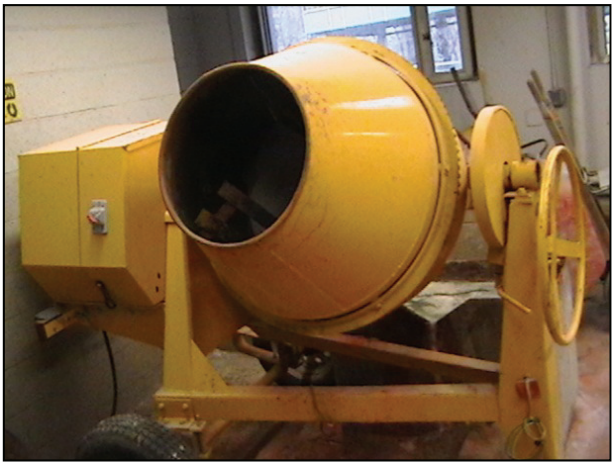

Figure 4.5 Laboratory Concrete Mixer

The mixing procedure used for all mixtures is shown below:

- The moisture content of the fine and coarse aggregate is calculated and the appropriate aggregate and mixing water contents are adjusted
- All fine and coarse aggregate are added and mixed together for 30 seconds.
- The cement, fly ash and silica fume (if applicable) are added and mixed with the rest of the ingredients for 30 seconds
- The mixing water and air entrainment are added and mixed for 3 minutes
- The air entrainment is adjusted until the desired properties are achieved
- Fibers are added (if applicable) and mixed for 10 minutes
- The water reducer is added and mixing continues for 3 minutes
- The water reducer and air entrainment are adjusted until the desired properties are achieved
- The mixture is mixed for an additional 2 minutes

The total mixing time was 9 minutes, with the exception of the FRC mixtures, which had a total mixing time of 19 minutes.

After batching and mixing, the fresh properties, including slump (ASTM C143), air content (ASTM C231) and unit weight (ASTM C138) were recorded. In addition to the fresh properties, test specimens were cast for the hardened property evaluation. The following tests were performed to characterize the plastic and hardened properties of each mixture:

- Plastic shrinkage cracking test (ASTM C1579)
- Compressive strength test (ASTM C39)
- Rapid chloride permeability test (ASTM C1202)
- Rapid migration test (NordTest Build 492)
- Bulk diffusion test (ASTM C1556)

- Flexural strength and toughness test (ASTM C1609 or ASTM C78)
- Freeze thaw test (ASTM C666)

4.1 Specimen Preparation for Plastic Shrinkage and Hardened Property Evaluation

After the fresh properties were tested, specimens for plastic shrinkage cracking and hardened property evaluation were cast. The number of samples for each test was that recommended by the standard for each test method. The following specimens were cast from each mixture:

- 2 slabs (560 mm x 355 mm x 140 mm) for plastic shrinkage cracking evaluation (ASTM C1579)
- 3 cylinders (100 mm x 200 mm) for compression test (ASTM C39)
- 3 cylinders (100 mm x 200 mm) for chloride penetration test (ASTM C1202)
- 2 cylinders (100 mm x 200 mm) for chloride penetration test (ASTM C1556)
- 3 cylinders (100 mm x 200 mm) for chloride penetration test (NordTest Build 492)
- 3 beams (150 mm x 150 mm x 500 mm) for flexural toughness tests (ASTM C1609 or ASTM C78)
- 2 beams (100 mm x 100 mm x 350 mm) for freeze thaw tests (ASTM C666)

All NC and FRC specimens were cast using a vibrating table to achieve proper consolidation. With the exception of the plastic shrinkage slabs, all specimens were demolded at 24 hours and stored in a moist room at 23 °C and 100 % humidity for curing, as specified in ASTM C511, until the day of testing. All of the non-FRC mixtures were batched twice as two additional samples were required to determine the effect of cover depth in the plastic shrinkage test. These mixtures had the same proportions and the same

admixture volumes as the first batch. The fresh properties were measured and were the same as the first set of batches.

The cylinders and beams were cast in two layers, while the slabs were cast in one layer. All specimens were consolidated on a vibrating table. In addition, 100 mm x 50 mm thick cores were drilled from each plastic shrinkage slab after 24 hours for chloride penetration testing if cracking was present. The samples were drilled from locations with plastic shrinkage cracking to evaluate the effect of plastic shrinkage cracking on the ingress of chlorides. All specimens were cured in accordance with ASTM C511.

In addition to the samples prepared from the laboratory mixtures, 4 cores were taken from a local container terminal at two locations on the cope wall and two locations on the supporting cribs. Two cores were taken from the section cast 25 years ago and two cores were taken from the section cast 30 years ago. A chloride profile was established using the profile grinding procedure described in the bulk diffusion test procedure described below. These samples were taken to determine if the NC mixture in the lab is comparable to concrete that is in a real structure that has been exposed to chlorides for many years. The samples were also used to show the influence of the *m* value on the prediction of the service life of a structure.

4.2 Plastic Shrinkage Cracking Test

The plastic shrinkage cracking test was conducted immediately after the fresh properties were evaluated. The test specimens were prepared in accordance with ASTM C1579; however the mold was changed to better simulate in situ cracking caused by settlement by using three FRP reinforcing bars as the restraint instead of the stress risers used in the standard. FRP bars were used so that the cracked samples could be cored and then exposed to one of the rapid chloride tests. Steel bars could not be used as there is an electrical current running through the sample during testing. The mold used can be seen

in Figure 4.6. Two specimens were cast for each non-FRC mixture with all three bars at a cover depth of 65 mm. After no cracking presented, the center bar was moved to a cover depth of 50 mm in one sample and 35 mm in the other to determine the effect of bar depth. The FRC samples only had samples cast with 50 mm and 35 mm cover depths. The bar depths were chosen based on work by Barnes and Trottier (2008) showing that rebar cover depth can vary greatly even when 75 mm is specified. All samples were finished with five trowel passes.

Figure 4.6 Shrinkage Mold (50 mm center bar)

The specimens were placed in an environmental chamber and exposed to uniform drying using a fan moving air across the top of the samples at a rate of 5.5 m/s^2 until final setting occurred according to ASTM C403. The temperature during testing ranged from 36 °C to 38 °C and the relative humidity ranged from 25 % to 35 %. The moisture loss of the samples was measured directly from the sample using a load cell weighing system, instead of using a water tray as specified in ASTM C1579. After final setting occurred, the plastic shrinkage cracks were evaluated. The total area of cracking, total number of cracks and the average crack widths were measured. The plastic shrinkage test set-up can be seen in Figure 4.7.

Figure 4.7 Shrinkage Chambers

4.3 Compressive Strength

Compressive strength testing was performed after 28 days of curing in accordance with ASTM C39. Prior to testing, the specimens were capped according to ASTM C617. The testing machine used for compressive testing was a Forney Testing Machine Model F-40 with a capacity of 250 000 lb, shown in Figure 4.8. The compressive strength of each specimen was calculated according to ASTM C39.

Figure 4.8 Compression Machine

4.4 Chloride Penetration Tests

The ability of concrete to resist the penetration of chloride ions was evaluated using 3 different tests. The 3 tests were chosen to compare the differences between each and determine which rapid test produces more accurate results when compared to the bulk diffusion test. The 3 tests are described below.

4.4.1 Rapid Chloride Permeability Test

The rapid chloride permeability test determines the resistance of concrete to the penetration of chloride ions by measuring the electrical conductance of the concrete sample. This test was conducted in accordance to ASTM C1202. Cylinders are cut with a water-cooled diamond saw to a thickness of 50 ± 2 mm. Prior to testing, the sides of the specimens are sealed, pretreated in a vacuum chamber in air for 3 hours and then placed in de-aerated water under vacuum for an additional hour. The vacuum is then removed, and the samples remain in the water for 18 ± 2 hours. The vacuum chamber is shown in Figure 4.9.

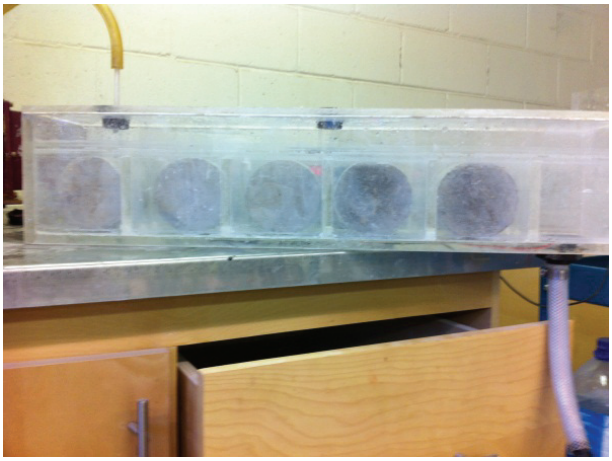

Figure 4.9 Vacuum Chamber

The specimens are removed from the water and placed in the test apparatus, shown in Figure 4.10, and an electrical current is passed through the sample for a 6 hour period. A potential difference of 60 V is maintained across the specimen, with one side immersed in a sodium chloride solution and the other immersed in a sodium hydroxide solution. The total charge passed is measured during the test and is used to determine the chloride penetration resistance.

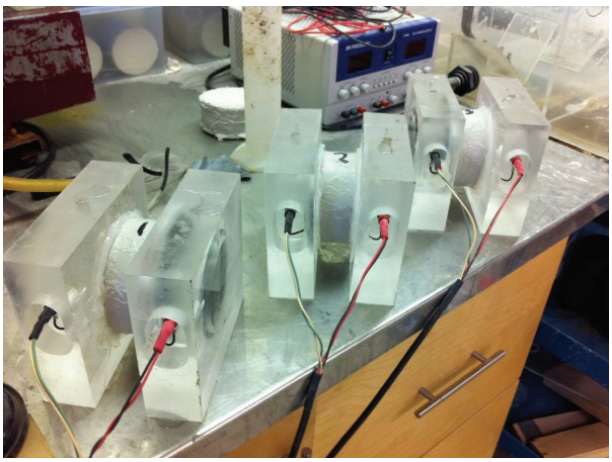

Figure 4.10 Rapid Chloride Permeability Test

4.4.2 Rapid Migration Test

The rapid migration test determines the chloride penetration resistance of concrete by measuring the penetration depth of chloride ions in a concrete sample. This test was conducted in accordance with NordTest Build 492. Cylinders are cut using a water-cooled diamond saw to a thickness of 50 ± 2 mm. Prior to testing, the specimens are pretreated in the same vacuum chamber shown in Figure 4.9. The samples are vacuumed in air for 3 hours and then placed in a calcium hydroxide solution under vacuum for an additional hour. The vacuum is removed and the samples remain in the solution for 18 ± 2 hours.

The samples are removed from the calcium hydroxide solution, and placed in a rubber sleeve. The bottom of the sample is placed in the test chamber containing sodium chloride solution and the top of the sleeve is filled with a sodium hydroxide solution (anolyte). The testing chamber can be seen in Figure 4.11. A potential of 25 – 30 volts DC is applied across the sample for 24 ± 0.5 hours. During testing, the temperature of the anolyte and electrical current are monitored.

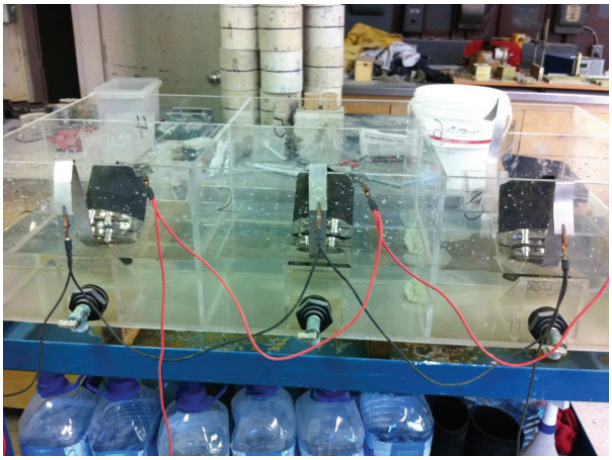

Figure 4.11 Rapid Migration Test

After testing, the samples are split axially into 2 halves. A silver nitrate solution is then sprayed on the split sample to identify the depth of chloride penetration. The penetration depth is identified by the white/purple color of the silver chloride, as seen in Figure 4.12 and is measured using a slide caliper. Seven depths are measured from each specimen, averaged and then used to calculate the chloride coefficient.

Figure 4.12 Rapid Migration Test Sample

4.4.3 Bulk Diffusion Test

The bulk diffusion test determines the chloride penetration resistance of concrete by allowing chloride ions to penetrate into the sample without forcing them using an electrical current. This test was conducted in accordance with ASTM C1556. Cylinders were cut using a water-cooled diamond saw to a thickness of 75 ± 2 mm. The samples are sealed are all sides except the top and then pretreated in the same manner as the samples in the rapid migration test.

After pretreatment, the samples are immersed in a sodium chloride solution for 60 days at a temperature of 23 ± 2 °C, as seen in Figure 4.13. After 60 days, the samples are removed from the sodium chloride solution and dried in air for 24 hours. The samples are then ground using a profile grinder, shown in Figure 4.14, to collect 8 samples at varying depths depending on the chloride penetration depth. An initial sample is also collected from a 20 mm thick sample cut from the same cylinder the immersed sample is taken from. The water soluble chloride ion content of the powder samples was determined by chemical testing by an outside laboratory according to ASTM C1218, which determines the percent chloride by mass of concrete, allowing a chloride profile to be plotted.

Figure 4.13 Bulk Diffusion Test

Figure 4.14 Profile Grinding

4.5 Flexural Strength and Toughness Test

After 28 days of curing, the flexural strength and toughness was evaluated in accordance with ASTM C1609 for FRC samples and ASTM C78 for non-FRC samples. The two methods are similar except the C1609 test also evaluates post crack strength, while C78 stops when the beam cracks. The specimens were tested under third-point loading using a servo-hydraulic 150 kN Instron testing machine controlled by an 8501+ Instron control

panel. The specimens were tested on a span of 450 mm, as shown in Figure 4.15. To eliminate any extraneous deformations, a yoke device was placed around the beam specimen and secured at its mid-height. The extraneous deformation may occur as a result of the concrete crushing at the supports, specimen twisting, specimen seating or deflections due to inadequate stiffness of the test set-up from the measured specimen deflections. Two linear variable displacement transducers (LVDTs) were mounted directly to the yoke device, at the center of the beam on both sides of the specimen, as shown in Figure 4.16. The LVDTs were arranged to measure the center-point deflection of the sample. To ensure uniform contact between the specimen and the loading set-up, beams were tested on their side with the finished face towards the front of the test machine.

Figure 4.15 ASTM C1609 Test Set-Up

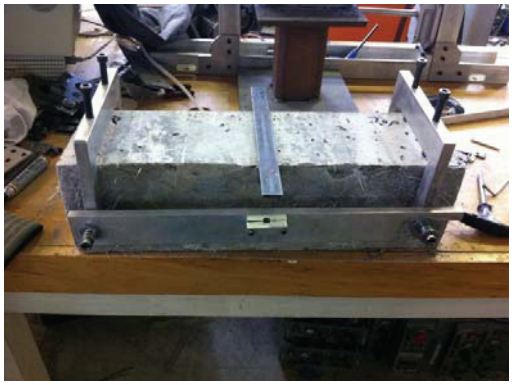

Figure 4.16 ASTM C1609 Yoke Device

4.6 Freeze Thaw Test

After 56 days of curing, the freeze thaw resistance was evaluated in accordance with ASTM C666 Procedure A. The specimens were exposed to freeze thaw cycles in a freeze thaw chamber, as shown in Figure 4.17. The specimens are cycled between 4 °C and -18 °C in a span of 5 hours. The specimens are removed after every 33 cycles, tested for fundamental transverse and longitudinal frequency according to ASTM C215, as seen in Figure 4.18 and Figure 4.19 respectively, and then returned to the freeze thaw chamber. The test is considered complete after 300 cycles or the relative dynamic modulus of elasticity reaches 60 % of the initial modulus.

Figure 4.17 Freeze Thaw Chamber

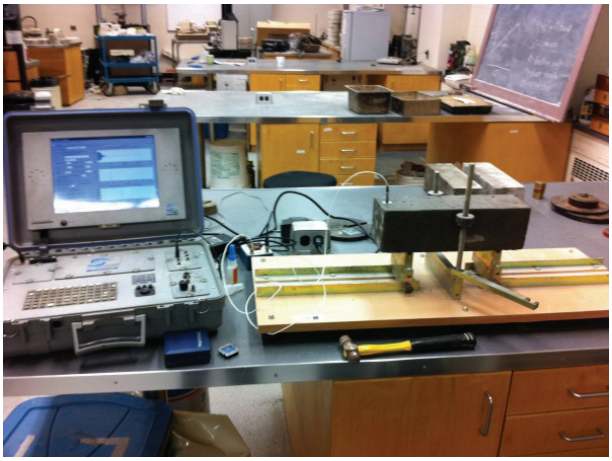

Figure 4.18 Fundamental Transverse Frequency Setup

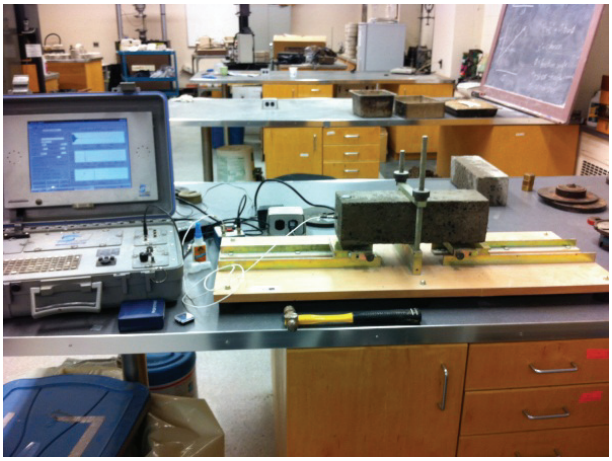

Figure 4.19 Fundamental Longitudinal Frequency Setup

The next chapter presents the results of the test program along with the discussion of the results.

CHAPTER 5 TEST RESULTS AND DISCUSSION

This chapter is split into three main sections: Section I covers the results and discussion of the fresh properties of the concrete mixtures. Section II covers the results and discussion of the plastic shrinkage cracking resistance of each concrete mixture. Section III covers the results and discussion of the hardened properties, which include compression strength, chloride penetration, freeze thaw resistance and flexural toughness.

5.1 Fresh Concrete Properties

The fresh properties of the concrete mixtures, including concrete density, air content and slump, were measured prior to sample casting. These measurements are presented in Table 5.1.

Table 5.1 Fresh Properties of Concrete Mixtures

Mixture No.	Fiber Volume Fraction (%)	Concrete Density (kg/m^3)	Air Content (%)	Slump (mm)	Plastol 341 (L/m^3)
NC	-	2340.8	5.0	150	0.440
FA	-	2374.3	3.0	135	0.440
TER 50-1	-	2332.9	5.2	160	0.324
TER 50-1 F1	0.20	2335.7	5.0	105	1.117
TER 50-1 F1	0.33	2342.9	5.0	95	1.117
TER 50-1 F2	0.20	2341.4	5.1	145	0.824
TER 50-2	-	2331.4	5.0	130	0.588
TER 50-2 F1	0.20	2304.3	5.8	185	0.882
TER 50-2 F2	0.16	2307.1	5.8	170	0.882

All concrete mixtures had densities within the normal range of 2300 kg/m^3 and 2400 kg/m^3. The air content of all mixtures was to be between 5 % and 8 % to ensure adequate freeze thaw resistance; however, due to an error during the air content test, the air content for the FA mixture was only 3 %. This error was discovered after testing was complete through theoretical density comparison and only affected the freeze thaw resistance based on the results presented later in this chapter.

A slump of 150 mm was targeted for concrete mixtures without fiber addition as this would be a common slump in industry when using admixtures. The Plastol 341 was added after a w/c ratio of 0.4 was achieved using water. A slump of 100 mm was targeted for the mixtures with fiber addition in an attempt to keep the amount of Plastol 341 used comparable with that of the non-fiber mixtures. Fiber 2 mixtures and TER 50-2 mixtures showed better flow characteristics resulting in slumps higher than what was targeted, but this did not have any adverse effects on the samples.

5.2 Plastic Concrete Properties

A summary of the plastic shrinkage cracking test results of all the mixtures that presented shrinkage cracking can be seen in Table 5.2. The test results are graphically compared in Figure 5.1 and Figure 5.2. The results represent the average of the total cracking area, average crack width and the maximum crack width in each sample. The reduction in total crack area, due to the addition of fibers, was calculated as a percentage of the total crack area in the same mixture without fiber addition. All samples included in Table 5.2 had a center bar depth of 35 mm and the mixtures that did not present cracking were not included. It should be noted that all mixtures did have a rate of water loss greater than 1.0 kg/m^2/hr as required in the standard. It should also be noted that cracks only occurred above the center bar, which had a total length of 355 mm. The full table of results can be found in Appendix B.

Table 5.2 Summary of Plastic Shrinkage Test Results

Mixture No.	Fiber Volume Fraction (%)	Average Crack Width (mm)	Maximum Crack Width (mm)	Total Crack Length (mm)	Total Crack Area (mm^2)	Reduction in Total Crack Area (%)
TER 50-1	-	0.34	0.88	256.8	87.3	-
TER 50-1 F1	0.2	0.15	0.39	154.0	23.1	73.5
TER 50-1 F1	0.33	0	0	0	0	100
TER 50-1 F2	0.2	0	0	0	0	100
TER 50-2	-	0.19	0.33	149.1	28.3	-
TER 50-2 F1	0.2	0	0	0	0	100
TER 50-2 F2	0.16	0	0	0	0	100

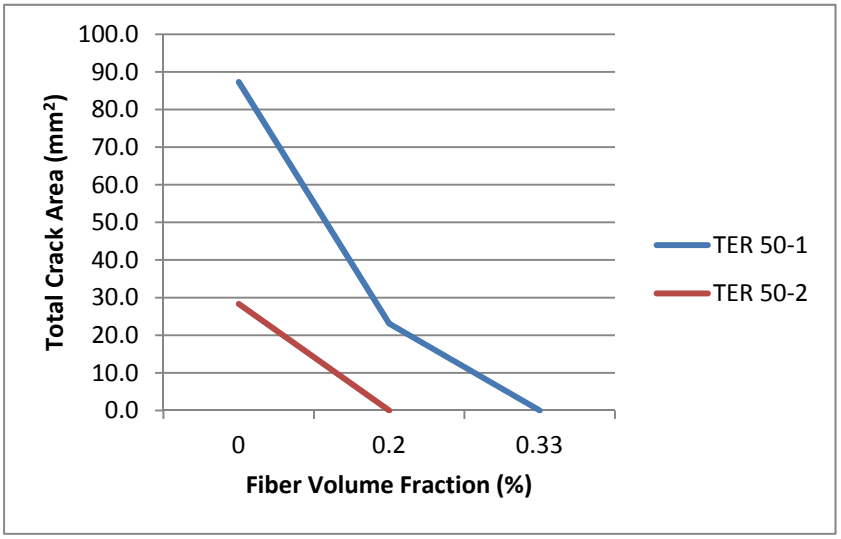

Figure 5.1 Effect of Fiber Volume Fraction on Total Plastic Shrinkage Cracking Area

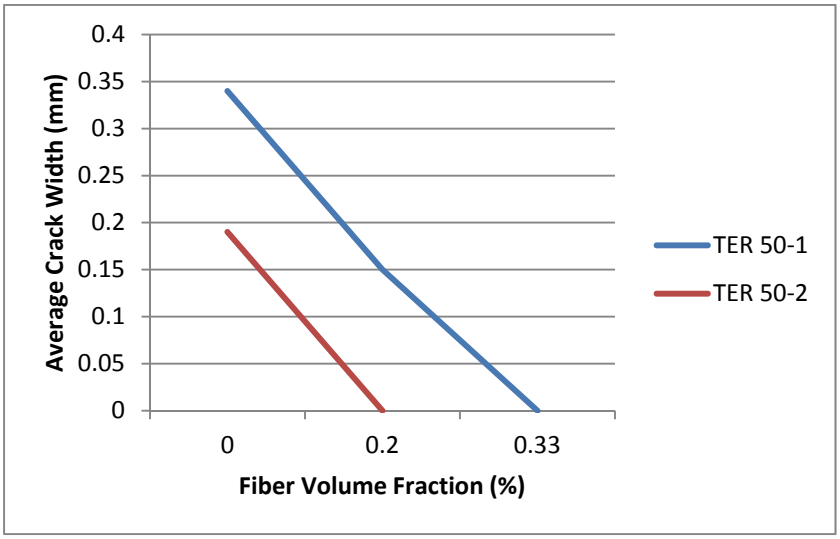

Figure 5.2 Effect of Fiber Volume Fraction on the Average Plastic Shrinkage Crack Width

For specimens in TER 50-1 mixtures, the addition of 0.20 % by volume of fiber F1 reduced the total crack area, the average crack width and maximum crack width by 73.5 %, 55.9 % and 55.7 %, respectively, when compared with the TER 50-1 mixtures without fiber addition. This resulted in the maximum crack width being reduced from 0.88 mm to 0.39 mm as shown in Figure 5.3 and Figure 5.4. The fiber addition also resulted in discontinuous cracking, as shown in Figure 5.4, whereas the sample without fiber addition had one long crack across the sample, shown in Figure 5.3. An increase in fiber volume to 0.33 % led to no cracking in the sample. The addition of fiber F2 at a volume fraction of 0.20 % also led to no cracking in the sample.

This fiber addition (F1) most importantly reduced the percentage of crack length compared to the overall length of the center bar from 72.3 % to 43.4 %. The addition of another 0.13 % of fiber decreased that percentage to zero. The addition of only 0.20 % of fiber F2 also reduced that percentage from 72.3 % to zero. These reductions can be of major importance when considering structures that have very long pieces of rebar, which could have very long cracks above them if shrinkage cracking occurs.

Figure 5.3 Maximum Plastic Shrinkage Crack Width in TER 50 Mixture

Figure 5.4 Maximum Plastic Shrinkage Crack Width in TER 50 with 0.20 % Fiber Volume Fraction

For specimens in the TER 50-2 mixtures series, the addition of fiber F1 at a fiber volume fraction of 0.20 % resulted in the elimination of cracking and a volume fraction of 0.16 % of fiber F2 was enough to eliminate cracking as well. The fiber addition lead to a reduction in the crack length percentage of the center bar length from 42 % to zero with a small dosage of fiber.

The TER 50-2 mixture required a lower fiber volume fraction to eliminate cracking, compared to the TER 50-1 mixture, due to a reduced paste content resulting from a ratio of coarse to fine aggregates of nearly 50/50 as seen in Table 4.1. This reduced paste content leads to a faster initial set, thus a shorter time for plastic shrinkage to occur. This

paste reduction resulted in a 67.5 % reduction in total cracking area when comparing the two non-fiber samples.

The effect of silica fume addition on plastic shrinkage was clearly observed. The mixtures without silica fume presented no cracking at any of the varying center bar heights, whereas mixtures with silica fume and a center bar height of 35 mm presented considerable cracking. This increase in plastic shrinkage cracking is due to a reduced bleed rate caused by a combination of surface drying and the self-desiccation caused by the silica fume.

Overall, the addition of fiber F1 and F2 to air-entrained marine concrete mixtures with silica fume greatly reduce or completely eliminate shrinkage cracking caused by slumping around the reinforcing bars close to the surface. This can be of great benefit to concrete structures in marine environments where a high degree of impermeability is desired since the reduction in crack length, width and total area will lead to less ingress of chlorides to the reinforcement, thus increasing the durability of the structure significantly. In addition to the fiber addition, ensuring the proper cover depth is achieved during construction can greatly reduce the potential of shrinkage cracking caused by slumping around the reinforcing bars.

5.3 Hardened Properties

The compressive strength, chloride penetration, flexural toughness and freeze thaw resistance of all mixtures were evaluated and are presented in the following sections.

5.3.1 Compressive Strength

A summary of the compressive strength test results of all mixtures is presented in Table 5.3. The results are the calculated average 28 day compressive strength of three

specimens taken from each mixture. Additional details and complete tables of the individual compressive strength results, for all mixtures are shown in Appendix C.

In general, the addition of fiber had little effect on the compressive strength of each FRC mixture when compared to the companion non fiber mixture.

Table 5.3 Summary of Compressive Strength Test Results

Mixture No.	Fiber Volume Fraction (%)	Avg. Compressive Strength (MPa)	Std. Deviation Strength (MPa)
NC	-	39.6	0.68
FA	-	39.8	0.56
TER 50-1	-	36.2	0.72
TER 50-1 F1	0.20	35.0	0.87
TER 50-1 F1	0.33	35.2	1.13
TER50-1 F2	0.20	39.0	0.41
TER 50-2	-	36.8	1.99
TER 50-2 F1	0.20	37.9	1.92
TER 50-2 F2	0.16	36.4	1.22

The results indicate that all mixtures have reached the minimum specified compressive strength value of 35 MPa at 28 days, which is required for most marine applications.

5.3.2 Chloride Penetration

The results of the three different chloride penetration test methods used are presented in the following sections including a comparison of the results from each method.

5.3.2.1 Rapid Chloride Permeability

The results of the RCPT are presented in Table 5.4. The results include the average 28 day values of charge passed from three samples; however, some samples experienced leaks due to improper sealing around the sample and were not included in the results. Figure 5.5 graphically shows the average charge passed over the entire test. Additional details and complete tables of the individual RCPT measurements are shown in Appendix D.

Table 5.4 Summary of RCPT Results

Mixture No.	Fiber Volume Fraction (%)	Avg. Total Charge Passed (C)	Std. Deviation Charge Passed (C)
NC	-	4364	224.9
FA	-	3279	129.4
TER 50-1	-	1627	62.9
TER 50-1 F1	0.20	1257	54.4
TER 50-1 F1	0.33	1225	41.9
TER 50-1 F2	0.20	1383	33.2
TER 50-2	-	1287	14.2
TER 50-2 F1	0.20	1162	-
TER 50-2 F2	0.16	1251	70.6

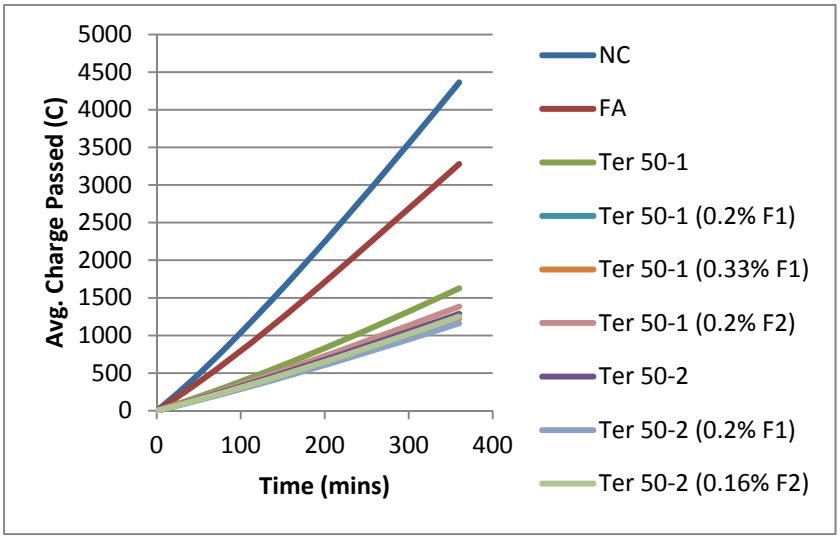

Figure 5.5 RCPT Avg. Charge Passed Over Time

The results clearly show that the NC mixture is by far the worst in terms of charge passed, while the addition of supplementary materials drastically reduces that charge, especially when silica fume is added. Despite the high water to cement ratios, the TER 50-1 and TER 50-2 mixtures both had low values of charge passed; however, they were not below the recommended value of 1000 coulombs passed. The researcher believes that if the water to cement ratios were slightly lower than 0.4, which would result in a less permeable mixture, then the values of charge passed would be well below 1000.

The results also show that fibers have no significant effect on the charge passed. It should be noted that the value of the TER 50-1 mixture without fiber is quite a bit higher than that of the TER 50-1 mixtures with fiber addition; however, the test has a high level of variability between tests, and this difference is within that level of variability.

Finally, it is clear that there is little difference between the TER 50-1 and TER 50-2 mixtures. This is not a surprise as the two mixtures have the same water to cement ratios and the difference in mixture proportions is a different ratio of aggregates to reduce the overall cementitious content.

5.3.2.2 Rapid Migration

The chloride diffusion coefficients obtained from the RMT are presented in Table 5.5. The results include the average 28 day values of chloride diffusion coefficient, D, of three samples from each mixture. The mixtures with plastic shrinkage cracking are also presented in Table 5.5; these samples show the effect of drying on the diffusion coefficient. Additional details and complete tables of the individual RMT measurements are shown in Appendix E.

Table 5.5 Summary of RMT Results

Mixture No.	Fiber Volume Fraction (%)	Avg. Chloride Coefficient (D) at 28 days (x 10^{-12} m^2/s)	Std. Deviation Chloride Coefficient (D) (x10^{-12} m^2/s)
NC	-	13.01	0.48
FA	-	11.90	0.41
TER 50-1	-	7.79	1.61
TER 50-1 dry	-	6.07	-
TER 50-1 F1	0.20	7.91	2.91
TER 50-1 F1 dry	0.20	8.25	-
TER 50-1 F1	0.33	7.49	0.33
TER 50-1 F2	0.20	6.17	0.54
TER 50-2	-	5.13	0.81
TER 50-2 dry	-	9.16	-
TER 50-2 F1	0.20	6.11	0.72
TER 50-2 F2	0.16	6.23	0.45

The results clearly show that the TER mixtures are better than the FA and NC mixtures. The results also indicate that the inclusion of fiber has no significant effect on the diffusion coefficient. The results vary in both directions when compared to the non-fiber samples.

The diffusion coefficients for the surface dry samples appear to be slightly higher than the other samples which indicate that drying can cause an increase in chloride ingress. The researcher believes that this increase is caused by micro cracking near the surface caused by drying. Figure 5.6 and Figure 5.7 show chloride ingress in cracked samples using the RMT. Figure 5.6 shows that the chloride ingress follows the crack, shown by the red line, thus reducing the effective cover over the reinforcing bar. Figure 5.7 shows multiple cracks interconnected resulting in a lot of chloride ingress all the way to the depth of the rebar.

Figure 5.6 TER 50-1 Cracked Sample

Figure 5.7 TER 50-2 Cracked Sample

Both these samples have shrinkage cracks directly above the FRP reinforcing bar, but have two different patterns below the surface. This indicates that the direction of the plastic shrinkage crack is not always vertical. The crack can propagate diagonally depending on where aggregates are located in the crack path. The cracking appears to only affect the area around the crack, effectively reducing the concrete cover in that area and allowing chlorides to penetrate deeper into the concrete. Figure 5.8 shows that the chlorides also penetrate from the sides of the crack as well as the tip and it appears the penetration distance is approximately the same laterally as it is from the surface.

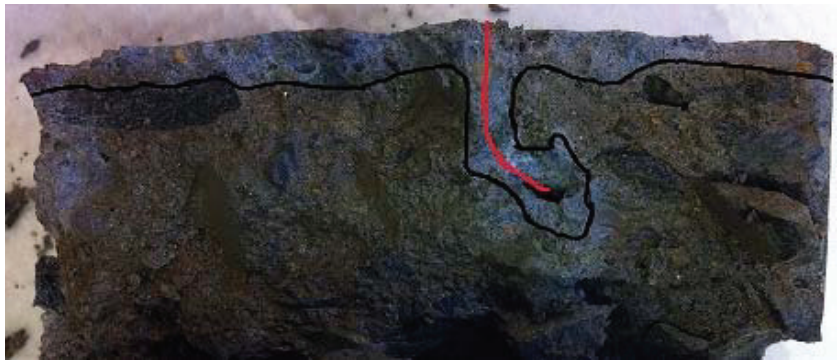

Figure 5.8 TER 50-1 Crack Close-up

5.3.2.3 Bulk Diffusion

The results from the bulk diffusion test are shown in Table 5.6. Two samples for each mixture are presented, except for the mixtures containing fiber F2. No samples for these mixtures were tested due to time constraints; however, judging from the results of the other chloride tests, the difference in fiber has no direct effect on chloride penetration. Figure 5.9 shows the chloride profile with depth of each sample. Additional details and complete tables of each sample are shown in Appendix F.

Table 5.6 Summary of Bulk Diffusion Test Results

Mixture No.	Fiber Volume Fraction (%)	m Value	Avg. Diffusion Coefficient (D) at 28 days (x 10^{-12} m^2/s)	Std. Dev. Diffusion Coefficient (D) (x10^{-12} m^2/s)
NC	-	0.2	30.17	5.49
FA	-	0.6	18.97	1.27
TER 50-1	-	0.6	5.96	0.37
TER 50-1 F1	0.20	0.6	6.82	1.52
TER 50-1 F1	0.33	0.6	4.08	1.50
TER 50-2	-	0.6	3.72	0.61
TER 50-2 F1	0.20	0.6	5.84	1.41

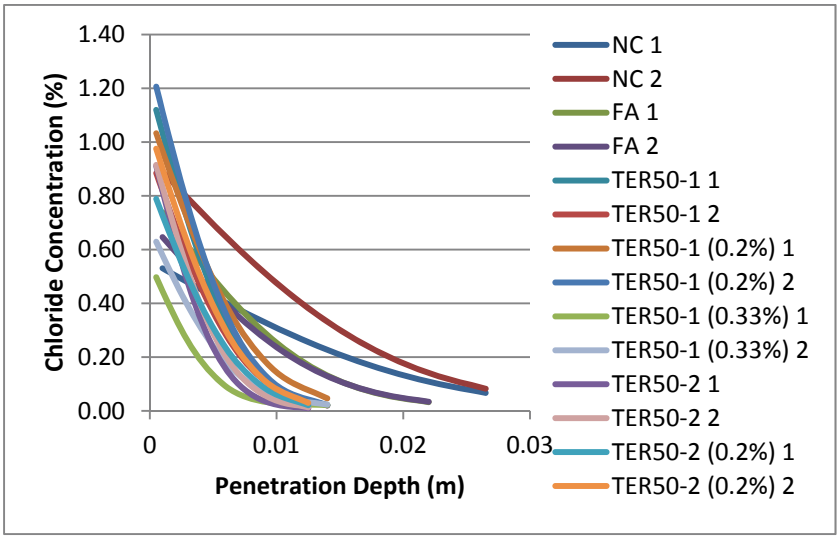

Figure 5.9 Chloride Profile with Depth from Bulk Diffusion Test

The results of the bulk diffusion test, similar to the other chloride tests, indicate that the use of supplementary materials greatly decreases the chloride diffusion at 28 days, especially the use of silica fume. Table 5.6 shows that the TER samples all have low diffusion coefficients, while the NC samples have very high coefficients, with the FA samples being in the middle, but still quite high. The *m* values are higher for those mixtures containing fly ash, as fly ash reduces the diffusion coefficient over time faster than cement alone. Figure 5.9 shows that the TER samples all have a penetration depth of less than 15 mm after 60 days of exposure to chlorides, while the FA samples have penetration depths around 22 mm and the NC samples have almost twice as much penetration at 26 mm compared to the TER samples.

Again the results show that the addition of fiber has no significant effect on the value of the diffusion coefficient or the penetration depth. There is some variation among the samples but this is due to the test and not the inclusion of fibers, as some fiber samples are higher than the non fiber counterparts and some are lower.

The results also indicate that there is little difference between the TER 50-1 and TER 50-2 samples as seen in previous tests. In this case the TER 50-2 samples appear to have

performed slightly better, but overall the two mixtures performed equally for the most part.

Testing was also carried out on cores taken from two sections of a cope wall located at a container terminal in Halifax, NS to determine the chloride profile of a NC mixture exposed to chlorides for many years. Section one has been in use for 30 years while section two has been in use for 25 years. Two cores were taken from each section and tested for chloride penetration depth and that was used to determine the diffusion coefficient. Sample 1 from each section was taken from the crib supporting the cope wall and the container terminal and sample 2 was taken from the cope wall itself. A normal concrete mix was used in both sections of the cope wall, that is, no supplementary materials were added. This diffusion coefficient was used with an assumed *m* value to determine the diffusion coefficient at 28 days. Table 5.7 summarizes the results of this testing using two different *m* values. The first *m* value is 0.2 as is recommended by some researchers. The second *m* value is 0.5 and this value gives similar diffusion coefficients to that of the NC samples tested in the lab. Additional details and complete tables can be found in Appendix G.

Table 5.7 Summary of Cope Wall Diffusion Coefficients

Sample No.	Diffusion Coefficient (D) at 28 days (x 10^{-12} m^2/s)	Diffusion Coefficient (D) at 28 days (x 10^{-12} m^2/s)
	m value = 0.2	m value = 0.5
Section 1 Sample 1	1.392	8.347
Section 1 Sample 2	4.032	24.17
Section 2 Sample 1	4.840	27.49
Section 2 Sample 2	4.843	27.49

The results show how drastic the effect of changing the *m* value is on the projected diffusion coefficient, which ultimately affects the service life of the structure; therefore it is difficult to accurately predict the service life of a structure.

5.3.2.4 Chloride Test Comparison

Three different chloride penetration test methods were used in this thesis and it is important to compare these test methods, specifically the two rapid methods with the much longer bulk diffusion method. If a correlation can be made between either of the rapid methods and the bulk method then the results from the rapid tests could be used to better estimate the service life of a structure and assess the resistivity of a concrete mixture to chloride penetration without having to wait several months for testing to be completed.

Figure 5.10 and Figure 5.11 graphically show the relationship between the RMT and the bulk diffusion test and the RCPT and bulk diffusion test, respectively. The squared correlation coefficient (R^2) values show that the fit when considering all samples is reasonable, but there are samples that deviate from the linear line, especially when considering the RMT and bulk diffusion relationship. A 2^{nd} order polynomial line is also shown on the RMT vs bulk diffusion graph, which has a very good R^2 value, but there is only a limited number of samples.

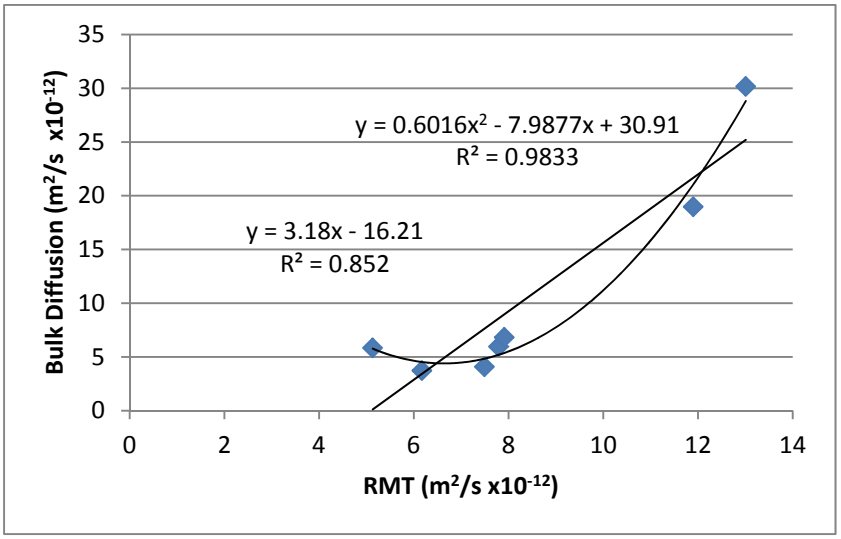

Figure 5.10 RMT vs. Bulk Diffusion Comparison

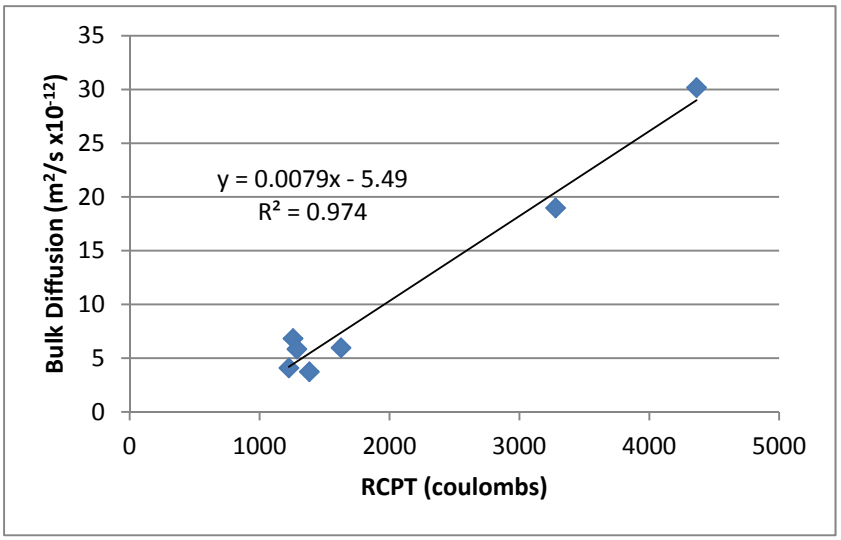

Figure 5.11 RCPT vs. Bulk Diffusion Comparison

Another comparison that can be made when just considering the TER 50-1 mixtures is just a multiplicative factor or considering the bulk diffusion value as a percentage of either the RMT or RCPT. When correlating the RMT and the bulk diffusion, the bulk diffusion is an average of 69.4 % of the RMT, but this value varies between 54 % and 86 % in the four mixtures with a standard deviation of 14.6 %. When correlating the RCPT and the bulk diffusion, the RCPT can be multiplied by a factor of 3.77×10^{-3}, but again

there is a large variation from 2.69 x 10^{-3} to 5.42 x 10^{-3} and a standard deviation of 1.17 x 10^{-3}. The TER 50-2 mixture was not used in this correlation as only one of the three mixtures was tested using the bulk diffusion test.

These results show that there is a correlation between the rapid tests and the bulk diffusion for the materials used in this test program; however, without a much larger sample set it is difficult to draw any definite correlation. Other researchers have also tried to make comparisons, but many of these researchers have been hesitant to publish any factors or best fit equations. The complete comparison can be seen in Appendix H.

5.4 Flexural Strength and Toughness

A summary of the flexural strength and toughness results for the concrete mixtures are given in Table 5.8. All results presented are the average of three specimens tested 28 days after casting. Complete tables of all individual flexural strength and toughness test results as well as the load vs. deflection curves are shown in Appendix I. In this thesis, although the purpose of adding fibers to the concrete mixtures was to control plastic shrinkage cracking and determine the effects on chloride diffusion, the results of the flexural tests showed that macro synthetic fibers can significantly improve the flexural toughness of concrete, even when added at low dosages. The fiber addition could possibly be incorporated into the reinforcement calculation and cause a reduction in reinforcement steel, especially reinforcement placed for shrinkage purposes.

Table 5.8 Summary of Flexural Strength and Toughness Results

Mixture No.	Fiber Volume Fraction (%)	Avg. Flexural Strength (MPa)	Std. Deviation Flexural Strength (MPa)	Avg. Flexural Toughness JSCE (MPa)	Std. Dev. JSCE (MPa)
NC	-	5.96	0.29	-	-
FA	-	5.89	0.34	-	-
TER 50-1	-	4.84	0.20	-	-
TER 50-1 F1	0.20	3.9	0.41	0.39	0.079
TER 50-1 F1	0.33	3.6	0.35	0.83	0.149
TER 50-1 F2	0.20	4.30	0.21	0.67	0.063
TER 50-2	-	4.46	0.55	-	-
TER 50-2 F1	0.20	4.00	0.09	0.44	0.071
TER 50-2 F2	0.16	3.00	0.37	0.49	0.148

The results showed a variation in the strength which can be contributed to some of the samples not being dry before testing, thus giving a low strength reading due to the sensitivity of the test and not the addition of fibers at dosages used in this thesis; however, the fiber addition did significantly improve the flexural toughness (JSCE) of the FRC mixtures. It can be seen that increasing the fiber dosage increases the post crack toughness. It can also be seen that fiber F2 performs better than fiber F1 in terms of toughness, and has similar post crack toughness when added at 0.16 % compared to 0.20 % of fiber F1. Fiber F2 performs better as it has a lower denier compared to fiber F1 thus allowing more fibers to be added for the same volume.

5.5 Freeze Thaw Resistance

A summary of the dynamic moduli obtained from before and after the freeze thaw testing are shown in Table 5.9. All results presented are the average of two specimens tested 56 days after casting and then again after being subjected to 300 freeze thaw cycles, which lasted approximately 63 days. Fiber F2 was not tested due to time constraints; however, it is believed that they would not have any effect on the freeze thaw results. The FA samples both broke apart during removal from the mold; however, it was clear that these samples performed poorly because of the reduced entrained air content. A picture of one of the FA samples prior to removal from the mold can be seen in Figure 5.12. It can be seen that there is a large crack in the sample and it has expanded against the sides of the mold. Complete tables of all individual freeze thaw test results are shown in Appendix J.

Table 5.9 Summary of Freeze Thaw Test Results

Mixture No.	NC	FA	TER 50-1	TER 50-1	TER 50-1	TER 50-2	TER 50-2
Fiber Volume Fraction (%)	-	-	-	0.20	0.33	-	0.20
Avg. Transverse Modulus (GPa)	28.04	30.53	27.92	28.84	29.76	28.67	28.34
Avg. Transverse Modulus – 300 Cycles (GPa)	26.27	-	25.20	24.50	27.60	25.46	26.15
Avg. Transverse Modulus Reduction (%)	6.32	-	9.62	15.04	7.40	11.18	7.68
Std. Dev. Transverse Modulus Reduction (%)	2.10	-	3.48	0.62	3.30	3.75	0.92
Avg. Longitudinal Modulus (GPa)	28.92	30.74	28.71	29.75	30.27	29.06	29.50

Avg. Longitudinal Modulus – 300 Cycles (GPa)	26.25	-	25.47	25.38	27.68	26.62	26.61
Avg. Longitudinal Modulus Reduction(%)	9.19	-	10.95	14.76	8.54	8.34	10.00
Std. Dev. Longitudional Modulus Reduction (%)	2.22	-	6.13	2.11	0.94	2.11	4.81

The results showed that exposure to freeze thaw damage does result in a maximum reduction in transverse and longitudinal dynamic moduli of 15 %, with an average around 10 %. The results also showed that the addition of fiber F1 and F2 has no significant effect on the freeze thaw resistance, as noted by previous researchers. As mentioned before, the FA samples broke during removal from the molds; however, it was clear that the samples performed very poorly, as seen in Figure 5.12, due to the reduced entrained air content. This emphasizes how important it is to ensure the proper entrained air content is achieved, otherwise severe damage may occur which could lead to structural damage and high repair or replacement costs.

Figure 5.12 Broken FA Freeze Thaw Sample

5.6 Service Life Prediction

Version 2 of the Life 365 service life prediction software was used to predict the service lives of the mixtures presented in this thesis. During the course of this thesis, the software was updated from version 1 to version 2 which predicted longer service lives than the previous version. The author attempted to determine the changes that caused the increase in service life predicted by the software. The author was unable to determine the cause, however he believes it may have been caused by a different time step being used in the finite difference model among other things. The results from the software are presented in Table 5.10 and screenshots of the various tabs are presented in Appendix K.

Table 5.10 Predicted Service Lives

Mixture	Diffusion Coefficient (D28) Entered ($x10^{-12}$ m^2/s)	*m Value*	Predicted Service Life (Yrs) 75mm Cover	Predicted Service Life (Yrs) 53mm Cover
NC	30.17	0.2	2.1	1.1
FA	18.97	0.6	19.0	4.3
TER50-1	5.62	0.6	122.0	37.2
TER50-2	4.78	0.6	147.8	48.1

The diffusion coefficients used as the input for the software were the averages determined from the bulk diffusion tests. The TER50-1 and TER50-2 coefficients are the average of all fiber and non-fiber mixtures as fiber did not appear to have a noticeable effect on the diffusion coefficient. The *m* values were chosen based on the research presented in Chapter 3. Halifax, NS was chosen for the location specific data and the service lives are for the tidal zone, which is the harshest environment for chloride

diffusion. The service lives presented are the time to corrosion initiation, after which the propagation phase begins, which usually lasts 6 years before repair is required.

When 75 mm of cover is considered, it is clear that the ternary mixtures provide a much longer service life on average compared to the FA and NC mixtures. It is also clear that the NC has an exceptionally short service life even when the recommended cover depth is achieved. The FA mixture has a reasonable service life of 19 years, which would mean repair at 25 years.

If a 22 mm deep shrinkage crack were introduced into the concrete, resulting in a reduction of the effective cover from 75 mm to 53 mm, then the service lives of all the mixtures would be reduced. It can be seen that the most drastic reduction is in the FA mixture which loses over 75% of its uncracked service life. The TER50 mixtures lose over 66% of their uncracked service lives and the NC mixture loses nearly 50% of its service life albeit was very short to begin with.

It is clear that the TER50 mixtures provide the best service life even when cracked compared to mixtures with just fly ash, or normal concrete mixtures. If a crack occurs, it causes a reduction in the effective cover, thus reducing the service life of the structure drastically; 50% or more in the case of a 22 mm deep shrinkage crack.

CHAPTER 6 SUMMARY OF TEST RESULTS

The results of the research program are summarized as in the following sections.

6.1 Fresh Properties

All of the non-fiber mixtures maintained a slump value between 130 and 160 mm and entrained air content between 5 and 6 %, with the exception of the FA mixture, which performed poorly in the freeze thaw test as a result. The density of the mixtures was between 2330 and 2375 kg/m^3. The mixtures were workable and easy to cast and finish with vibration.

The addition of macro-synthetic fibers resulted in a reduction in slump, thus a greater amount of plasticizer was required to achieve the desired slump. All of these fiber mixtures maintained a slump between 95 and 185 mm, entrained air content between 5 and 6 % and densities between 2300 and 2345 kg/m^3. The mixtures were also workable and easy to cast and finish with vibration.

6.2 Plastic Shrinkage Cracking

The plastic shrinkage resistance of the TER mixtures was significantly enhanced by the addition of macro-synthetic fibers. The addition of two different fibers at dosages up to 0.33 % by volume resulted in significant reduction or elimination of plastic shrinkage cracking caused by settlement around reinforcing bars placed 35 mm from the surface. This fiber addition, most importantly, reduced the ratio of crack length to the length of the center reinforcing bar. In the case of fiber F1, the addition of 0.20 % of fiber reduced the percentage of crack length to bar length from 72.3 % to 43.4 %, and adding another 0.13 % of fiber eliminated the cracking altogether in the TER 50-1 mixture. The TER 50-2 mixture only required 0.20 % of fiber F1 to reduce the percentage from 42 % to zero. Fiber F2 only required dosages of 0.20 % and 0.16 % to eliminate cracking in the TER

50-1 and TER 50-2 mixtures, respectively. This is very important as most shrinkage cracking occurs directly above inclusions such as rebar. Reducing this crack length is very important when considering large structures that have long continuous pieces of steel rebar. Fiber F2 performed better than fiber F1 as less of the fiber was required by volume in both the TER 50-1 and TER 50-2 mixtures to eliminate plastic cracking. This is due to the fact that there are more F2 fibers in the same volume of F1 fibers, as a result of a slightly different cross-section, thus a lesser volume is needed to have the same number of individual fibers.

The TER 50-2 mixture performed better than the TER 50-1 mixture due to the approximately 50/50 ratio of coarse to fine aggregate allowing a lower paste content, which reduced the time to initial set, thus reducing the overall crack area. The NC and FA mixtures did not display any plastic shrinkage cracking due to settlement; however it is believed that these mixtures would display plastic shrinkage cracking caused by capillary stress in structures with a large surface area exposed during curing.

6.3 Hardened Properties

A summary of the hardened properties is in the following sections.

6.3.1 Compressive Strength

All mixtures investigated in this thesis achieved the minimum compressive strength at 28 days of 35 MPa and were all below 40 MPa allowing for an easy comparison while the addition of fibers resulted in no negative effect on the compressive strength of the TER mixtures.

6.3.2 Chloride Penetration

The ability of the TER mixtures to resist the ingress of chlorides was significantly better than both the NC and FA mixtures in all tests despite having the same w/c ratio of 0.4, the recommended maximum in current codes. In the case of the bulk diffusion tests, the TER mixtures were over four times better than the NC mixture and three times better than the FA mixture. This is due to the enhanced properties of the TER mixtures by the relatively high volume of supplementary cementitious materials (7 % silica fume and 25 % fly ash). The silica fume has a very large impact on the early age chloride resistance, while the fly ash decreases the diffusion coefficient over time. The addition of fibers had no effect on the 28 day chloride resistance of uncracked specimens.

The chloride tests demonstrated that the commonly used NC or FA mixture is inadequate in providing long term protection to reinforcement. Whereas a mixture using ternary blended cements, similar to the TER mixtures used in this thesis, shows a significant improvement in the service life and the long term protection of reinforcement when the surface remains uncracked. The cracked samples showed that cracks can lead to a significant increase in the chloride penetration depth when compared to uncracked samples. This clearly indicates that plastic shrinkage cracking can significantly impair the permeability and thus the overall durability of marine structures. This would lead to a shortened service life and costly repairs. This also confirms that concrete with a low permeability cannot be assured by mixture design alone. Plastic shrinkage also needs to be considered when designing concrete mixtures for marine structures.

6.3.3 Flexural Strength and Toughness

Fiber addition has other benefits that include a significant improvement in the flexural toughness. This improvement can be of significant importance to the durability of many

marine structures and a high enough dosage could even lead to a reduction of reinforcing bars or an increase in cover depth as the reinforcement would not be needed near the surface to resist shrinkage cracking, thus increasing the service life even further.

6.3.4 Freeze Thaw Resistance

All mixtures showed some reduction in dynamic modulus in both the transverse and longitudinal directions, but this was expected even with the recommended percentage of entrained air. The reduction varied from 6 to 15 %. However, the reduction is more pronounced in small samples as it is only the outer surface of the concrete that is affected.

The FA mixture only had 3 % entrained air due to an error during air content testing. This caused the two samples to be destroyed by the freeze thaw action. These samples were a good example of the damage that can occur when the entrained air content is inadequate.

6.4 Service Life Prediction

When the service life of a structure is considered, the use of a TER mixture provides a very long service life if it remains uncracked. If shrinkage cracking occurs, it can result in a reduction in the effective cover depth which significantly reduces the service life of the structure, by as much as 66% in a TER mixture with a 22 mm deep shrinkage crack. Therefore, maintaining an uncracked concrete surface is crucial to ensuring a long service life.

6.5 Recommendations

The following research is needed to further characterize the benefit of synthetic fibers to plastic shrinkage cracking and the chloride test methods:

- Large slabs need to be tested with the mixtures in this thesis along with fiber addition to determine if the optimum fiber volume fractions determined in this thesis will eliminate plastic shrinkage cracking caused by capillary stress.

- Additional chloride diffusion samples for comparison of the rapid methods and the bulk diffusion method need to be tested to establish a better relationship between the tests.

- Samples should be tested at different ages to determine if fibers have any effect on the long term diffusion coefficients of concrete.

The researcher recommends that the current design codes and specifications be changed to include recommendations of supplementary materials to be used when designing marine concrete mixtures. The codes or specifications should also recommend considering shrinkage cracking when designing a mixture as it can greatly reduce service life of a structure and could possibly recommend fiber reinforcement as a solution to reduce the shrinkage cracking potential. This could be achieved by introducing a maximum cement content, minimum supplementary cementitious material content depending on the desired level of chloride resistance and a suggestion to optimize the coarse to fine aggregate ratio based on the maximum cement content. It should also be noted that proper curing needs to be ensured especially when ternary mixtures are being used.

CHAPTER 7 CONCLUSIONS

Macro-synthetic fibers and ternary blended cements have been studied by several researchers and it has been demonstrated that each of them are of great benefit to the durability of concrete structures. The compatibility of these two technologies and the overall benefit of fiber addition to marine concrete mixtures were studied with the aim to provide long service lives while maintaining a relatively impermeable surface free from cracking in marine freeze thaw environments. The mixtures designed in this thesis were able to be easily placed even with the addition of up to 0.33 % by volume of macro-synthetic fibers. This required numerous mixture proportioning trials at different fiber dosages and two different fibers to produce FRC mixtures that highlighted the benefits of the synthetic fibers tested. It is believed that the TER mixtures with fiber addition developed in this thesis will be able to address and greatly reduce or eliminate problems caused by plastic shrinkage cracking while maintaining a long service life. The mixtures in this thesis can be an excellent replacement of typical marine concrete mixtures that are proportioned according to current codes and usually have durability problems associated with them.

REFERENCES

AASHTO Committee, (2011), AASHTO M 194 – Standard Specification for Chemical Admixtures for Concrete, Standard Specifications for Transportation Materials and Methods of Sampling and Testing, 31st Ed.

ACI Committee 222, (1985), Corrosion of Metals in Concrete, ACI Journal, January – February, pp. 1 – 30.

ACI Committee 305, (2010), Hot Weather Concreting, ACI 305R-10, American Concrete Institute, Farmington Hills, MI.

ACI Committee 544, (1993), Guide for Specifying, Proportioning, Mixing, Placing and Finishing Steel Fiber Reinforced Concrete, ACI Materials Journal, Vol. 90, January – February, pp. 94 – 101.

Ahmad, S., (2003), Reinforcement corrosion in Concrete Structures, Its Monitoring and Service Life Prediction – A Review, Cement & Concrete Composites, Vol. 25, pp. 459 – 471.

Aldred, J. M., (1988), Admixtures – Effects on Corrosion, Hong Kong Engineer, November, pp. 45 – 51.

Aldred, J. M., (1988), HPI Concrete, Concrete International, November, pp. 52 – 57.

Almussalam, A. A., Maslehuddin, M., Abdul-Waris, M., Dakhil, F. H., and Al-Amoudi, O. S. B., (1999), Plastic Shrinkage Cracking of Blended Cement Concretes in Hot Environments, Magazine of Concrete Research, Vol. 51, No. 4, pp. 241 – 246.

Al-Tayyib, A. J., and Al-Zahrani, M., (1990), Use of Polypropylene Fibers to Enhance Deterioration Resistance of Concrete Sulfate Skin Subjected to Cyclic Wet/Dry Sea Exposure, ACI Materials Journal, Vol. 89, pp. 363 – 370.

Al-Tayyib, A. J., Al-Zahrani, M., Rasheeduzzafar, and Al-Sulaimani, G. J., (1988), Effect of Polypropylene Fiber Reinforcement on the Properties of Fresh and Hardened Concrete in the Arabian Gulf Environment, Cement and Concrete Research, Vol. 18, pp. 561 – 570.

Andrade, C., (1993), Calculation of Chloride Diffusion Coefficients in Concrete from Ionic Migration Measurements, Cement and Concrete Research, Vol. 23, No. 3, pp. 724 – 742.

ASTM International, (2004), ASTM C1556 – Standard Test Method for Determining the Apparent Chloride Diffusion Coefficient of Cementitious Mixtures by Bulk Diffusion, 2011 ASTM Book of Standards.

ASTM International, (2006), ASTM C1579 – Standard Test Method for Evaluating Plastic Shrinkage Cracking of Restrained Fiber Reinforced Concrete (Using a Steel Form Insert), 2011 ASTM Book of Standards.

ASTM International, (2007), ASTM C127 – Standard Test Method for Density, Relative Density (Specific Gravity), and Absorption of Coarse Aggregate, 2011 ASTM Book of Standards.

ASTM International, (2007), ASTM C128 – Standard Test Method for Density, Relative Density (Specific Gravity), and Absorption of Fine Aggregate, 2011 ASTM Book of Standards.

ASTM International, (2008), ASTM C215 – Standard Test Method for Fundamental Transverse, Longitudinal, and Torsional Resonant Frequencies of Concrete Specimens, 2011 ASTM Book of Standards.

ASTM International, (2008), ASTM C403 – Standard Test Method for Time of Setting of Concrete Mixtures by Penetration Resistance, 2011 ASTM Book of Standards.

ASTM International, (2008), ASTM C666 – Standard Test Method for Resistance of Concrete to Rapid Freezing and Thawing, 2011 ASTM Book of Standards.

ASTM International, (2008), ASTM C1218 – Standard Test Method for Water-Soluble Chloride in Mortar and Concrete, 2011 ASTM Book of Standards.

ASTM International, (2009), ASTM C511 – Standard Specification for Mixing Rooms, Moist Cabinets, Moist Rooms, and Water Storage Tanks Used in the Testing of Hydraulic Cements and Concretes, 2011 ASTM Book of Standards.

ASTM International, (2010), ASTM C39 – Standard Test Method for Compressive Strength of Cylindrical Concrete Specimens, 2011 ASTM Book of Standards.

ASTM International, (2010), ASTM C78 – Standard Test Method for Flexural Strength of Concrete (Using Simple Beam with Third-Point Loading), 2011 ASTM Book of Standards.

ASTM International, (2010), ASTM C138 – Standard Test Method for Density (Unit Weight), Yield, and Air Content (Gravimetric) of Concrete, 2011 ASTM Book of Standards.

ASTM International, (2010), ASTM C143 – Standard Test Method for Slump of Hydraulic-Cement Concrete, 2011 ASTM Book of Standards.

ASTM International, (2010), ASTM C231 – Standard Test Method for Air Content of Freshly Mixed Concrete by the Pressure Method, 2011 ASTM Book of Standards.

ASTM International, (2010), ASTM C260 – Standard Specification for Air-Entraining Admixtures for Concrete, 2011 ASTM Book of Standards.

ASTM International, (2010), ASTM C494 – Standard Specification for Chemical Admixtures for Concrete, 2011 ASTM Book of Standards.

ASTM International, (2010), ASTM C617 – Standard Practice for Capping Cylindrical Concrete Specimens, 2011 ASTM Book of Standards.

ASTM International, (2010), ASTM C1202 – Standard Test Method for Electrical Indication of Concrete's Ability to Resist Chloride Ion Penetration, 2011 ASTM Book of Standards.

ASTM International, (2010), ASTM C1609 – Standard Test Method for Flexural Performance of Fiber-Reinforced Concrete (Using Beam With Third-Point Loading), 2011 ASTM Book of Standards.

ASTM International, (2011), ASTM C33 – Standard Specification for Concrete Aggregates, 2011 ASTM Book of Standards.

Audenaert, K., Yuan, Q., and De Schutter, G., (2010), On the Time Dependency of the Chloride Migration Coefficient in Concrete, Construction and Building Materials, Vol. 24, pp. 396 – 402.

Bader, M. A., (2003), Performance of Concrete in a Costal Environment, Cement & Concrete Composites, Vol. 25, pp. 539 – 548.

Baeckmann, W. V., Schwenk, W., and Prinz, W., (1997), Handbook of Cathodic Corrosion Protection: Theory and Practice of Electrochemical Protection Processes, Gulf Publishing Co. Houston, 567 pp.

Bakharev, T., and Struble, L. J., (1995), Microscopical Features of Freeze-Thaw Deterioration of Concrete, Material Research Society Symposium Proceedings, Vol. 370, pp. 83 – 88.

Balaguru, P. N., (1994), Contribution of Fibers to Crack Reduction of Cement Composite During the Initial and Final Setting Period, ACI Material Journal, Vol. 3, May – June, pp. 280 – 288.

Balaguru, P. N., and Ramakrishnan, V., (1986), Freeze-Thaw Durability of Fiber Reinforced Concrete, ACI Journal, Vol. 83, May – June, pp. 374 – 382.

Bamforth, P. B., (1994), Admitting that Chloride is Admitted, Concrete, London, Vol. 28, No. 6, pp. 18 – 21.

Banthia, N., Azzabi, M., and Pigeon, M., (1993), Restrained Shrinkage Cracking in Fiber-Reinforced Cementitious Composites, Materials and Structures, Vol. 26, August – September, pp. 405 – 413.

Banthia, N., Azzabi, M., and Pigeon, M., (1994), Restrained Shrinkage Test on Fiber-Reinforced Cementitious Composites, ACI SP-155-7, Testing of Fiber Reinforced Concrete, pp. 137 – 152.

Banthia, N., and Yan, C., (2000), Shrinkage Cracking in Polyolefin Fiber-Reinforced Concrete, ACI Materials Journal, July – August, pp. 432 – 437.

Banthia, N., Yan, C., and Mindess, S., (1996), Restrained Shrinkage Cracking in Fiber Reinforced Concrete: A Novel Test Technique, Cement and Concrete Research, Vol. 26, January, pp. 9 – 14.

Barnes, C.L., and Trottier, J. F., (2008), Life Cycle Cost Evaluation of the As-Built Cover Layer in Reinforced Concrete Bridge Decks, Proceedings of the 1st International Symposium on Life-Cycle Civil Engineering, pp. 793 – 798.

Bentz, E. C., Thomas, M. D. A., and Ehlen, M. A., (2010), Life 365 Service Life Prediction Model Software (Version 2.0.1). Available from www.life365.org.

Berke, N. S., and Dalliare, M. P., (1994), The Effect of Low Addition Rate of Polypropylene Fibers on Plastic Shrinkage Cracking and Mechanical Properties of Concrete, Fiber Reinforced Concrete: Development and Innovations, ACI SP-142-2, pp. 19 – 41.

Bloom, R., and Bentur, A., (1995), Free and Restrained Shrinkage for Normal and High Strength Concretes, ACI Materials Journal, Vol. 92, No. 2, pp. 211 – 217.

Broomfield, J. P., (1997), Corrosion of Steel in Concrete, Understanding, Investigation, and Repair, E & FN, Spon, London; New York.

Cabrera, J. G., Cusens, A. R., and Wang, B. Y., (1992), Effect of Superplasticizers on the Plastic Shrinkage of Concrete, Magazine of Concrete Research, Vol. 44, No. 160, pp. 149 – 155.

Caijun, S., and Mo, Y. L., (2008), High-Performance Construction Materials: Scienece and Applications, World Scientific, 431 pp.

Clear, K. C., (1996), Effectiveness of Epoxy-coated Reinforcing Steel – Technical Brief, Canadian Strategic Highway Research Program, April, 6 pp.

Cohen, M. D., Olek, J., and Dolch, W. L., (1990), Mechanism of Plastic Shrinkage Cracking in Portland Cement and Portland Cement Silica Fume Paste and Mortar, Cement and Concrete Research, Vol. 20, January, pp. 103 – 119.

Collepardi, M., Marciallis, A., and Turriziani, R., (1972), Penetration of Chloride Ions in Cement Paste and Concretes, Journal of American Ceramic Soc., Vol. 55, No. 10, pp. 1105-1114.

Dante, R. C., Santamaria, D. A., and Gil, J. M., (2009), Crosslinking and Thermal Stability of Thermosets Based on Novolak and Melamine, Journal of Applied Polymer Science, Vol. 114, pp. 4059 – 4065.

Euclid Chemical, (2010), Tuf-Strand SF Synthetic Macro-Fiber Technical Specification, 2 pp., http://www.euclidchemical.com/fileshare/ProductFiles/techdata/Tuf-Strand_SF.pdf.

Forgeron, D. P., (2005), The Combined Effects of Flexural Fatigue Cycles and Freezing and Thawing Cycles on the Flexural Properties of Plain and Fiber Reinforced Concrete, PhD Thesis, Dalhousie University, 378 pp.

Forgeron, D. P., Brown, J. J., and Omer, A. A., (2011), Influence of Self-Fibrillating Macro-Synthetic Fiber Reinforcement on the Chloride Penetration Resistance of Normal and Self-Consolidating Concrete, ACI Advances in FRC Durability and Field Applications, pp. 58 – 70.

Geiker, M., Thaulow, N., and Anderson, P. J., (1990), Assessment of Rapid Chloride Ion Permeability Test of Concrete With and Without Mineral Admixtures, In Durability of Building Materials, E&FN Spon, London, pp. 493 – 502.

Glass, G. K., and Buenfeld, N. R., (1997), The Presentation of the Chloride Threshold Level for Corrosion of Steel in Concrete, Corrosion Science, Vol. 39, No. 5, pp. 1001 – 1013.

Goodwin, P. D., Fantz, G. C., and Stephens, J. E., (2000), Protection of Reinforcement with Corrosion Inhibitors, Phase II Final Report, University of Connecticut, 125 pp.

Hamilton III, H. R., Boyd, A. J., Vivas, E., and Bergin, M., (2007), Permeability of Concrete – Comparison of Conductivity and Diffusion Methods, DOT Report, University of Florida, 238 pp.

Hammer, T. A., (1998), Cracking in High Performance Concrete before Setting, International Symposium on High Performance and Reactive Powder Concretes, August, Sherbrook, Canada, pp. 332 -348.

Hansson, C. M., Strunge, H., Markussen, J. B., and Frolund, T., (1985), The Effect of Cement Type on the Diffusion of Chlorides, Nordic Concrete Research, Vol. 4, pp. 70 – 80.

Hover, K. C., (1998), Concrete Mixture Proportioning with Water-reducing Admixtures to Enhance Durability: A Quantitative Model, Cement and Concrete Composites, Vol. 20, pp. 113 – 119.

Jacobsen, S., Marchand, J., and Boisvert, L., (1996), Effect of Cracking and Healing on Chloride Transport in OPC Concrete, Cement and Concrete Research, Vol. 26, pp. 869 – 881.

Johansen, R., Dahl, P. A., and Skjolvold, O., (1993), Control of Plastic Shrinkage in Concrete at Early Ages, 18th Conference on Our World in Concrete & Structures, August, Singapore, pp. 149 – 154.

Johnston, C. D., (1996), Proportioning, Mixing and Placement of Fiber-Reinforced Cements and Concretes, Production Methods and Workability of Concrete, Edited by Bartos, Marrs and Cleland, E&FN Spon, London, pp. 155 – 179.

Johnston, C. D., (2001), Fiber-Reinforced Cements and Concretes – Advances in Concrete Technology, Gordon and Breach Science Publishers, Amsterdam, pp. 10 – 24.

Kayir, H., and Weiss, W. J., (2002), A Fundamental Look at Settlement in Fresh Systems: Role of Mixing Time and High Range Water Reducers, First North American Conference on the Design and Use of Self-Consolidating Concrete (SCC), November, pp. 27 – 32.

Kosmatka, S. H., Kerkhoff, B., Panarese, W. C., MacLeod, N. F., and McGrath, R. J., (2002), Design and Control of Concrete Mixtures, Seventh Edition, Cement Association of Canada, 355 pp.

Kraai, P. P, (1985), Proposed Test to Determine the Cracking Potential Due to Drying Shrinkage of Concrete, Concrete Construction, Vol. 30, September, pp. 775 – 778.

Malek, R. I. A., and Roy, D. M., (1996), The Permeability of Chloride Ions in Fly Ash-Cement Pastes, Mortars, and Concrete, MRS Symposium, Vol. 113, Pittsburgh, pp. 291 – 300.

Malhotra, V. M., Carette, G. C., and Bilodeau, A., (1994), A Deicer Salt Scaling Resistance of Dry and Wet-Process Shotcrete, ACI Materials Journal, Vol. 91, pp. 478 – 486.

Mangat, P. S., and Molloy, B. T., (1994), Prediction of Long Term Chloride Concentration in Concrete, Materials and Structures, Vol. 27, pp. 338 – 346.

Millero, F. J., Feistel, R., Wright, D. G., and McDougall, T. J., (2008), The Composition of Standard Seawater and the Definition of the Reference-Composition Salinity Scale, Deep-Sea Research I, Vol. 55, pp. 50 – 72.

Naaman, A. E., Wongtanakitcharoen, T., and Hauser, G., (2005), Influence of Different Fibers on Plastic Shrinkage Cracking of Concrete, ACI Material Journal, Vol. 102, January – February, pp. 49 – 58.

Nanni, A., (2005), Guide for the Design and Construction of Concrete Reinforced with FRP Bars (ACI 440.1 R-03), University of Missouri Center for Infrastructure Engineering Studies, 6 pp.

Naani, A., Ludwig, D. A., and Mcgillis, M. T., (1993), Plastic Shrinkage Cracking of Restrained Fiber-Reinforced Concrete, Transportation Research Record, 1382, pp. 69 – 72.

Neville, A., (1995), Chloride Attack of Reinforced Concrete: An Overview, Materials and Structures, Vol. 28, March, pp. 63 – 70.

Nokken, M., Boddy, A., Hooton, R. D., and Thomas, M. D. A., (2006), Time Dependent Diffusion in Concrete – Three Laboratory Studies, Cement and Concrete Research, Vol. 36, pp. 200 – 207.

Nordic Council of Ministers, (2005), NT Build 433 – Cracking Tendency – Exposure to Drying During the First 24 Hours, Downloaded from www.nordtest.info.

Nordic Council of Ministers, (2011), NT Build 492 – Concrete: Mortar and Cement-Based Repair Materials: Concrete : Chloride Migration Coefficient from Non-Steady-State Migration Experiments, Downloaded from www.nordtest.info.

Omer, A. A., (2006), Development of Fiber Reinforced Self-Consolidating Concrete for Marine Structures in Hot Environments, MASc Thesis, Dalhousie University, 188 pp.

Otsuki, N., Nagataki, S., and Nakashita, K., (1992), Evaluation of $AgNO_3$ Solution Spray Method for Measurement of Chloride Penetration into Hardened Cementitious Matrix Materials, ACI Materials Journal, Vol. 89, No. 6, pp. 587 – 592.

Ozyildirim, C., (1994), Rapid Chloride Permeability Testing of Silica-Fume Concrete, Cement, Concrete and Aggregates, CCAGPD, Vol. 16, No. 1, pp. 53 – 56.

Page, C. L., Short, N. R., and El Tattas, A., (1981), Diffusion of Chloride Ions in Hardened Paste, Cement and Concrete Research, Vol. 11, No. 3, pp.395 – 406.

Page, C. L., Short, N. R., and Holden, W. R., (1986), Influence of Different Cements on Chloride-Induced Corrosion of Reinforcing Steel, Cement and Concrete Research, Vol. 16, pp. 79 – 86.

Papadakis, V. G., Fardis, M. N., and Vayenas, C. G., (1992), Hydration and Carbonation of Pozzolanic Cements, ACI Materials Journal, Vol. 89, No. 2, March-April, pp. 119 – 130.

Poulsen, E., and Mejlbro, L., (2006), Diffusion of Chloride in Concrete – Theory and Application, Taylor & Francis Inc., New York, 442 pp.

Powers, T. C., (1968), The Properties of Fresh Concrete, John Wiley & Sons Inc., New York, 664 pp.

Qi, C., (2003), Quantitative Assessment of Plastic Shrinkage Cracking and Its Impact on the Corrosion of Steel Reinforcement, PhD Thesis, Purdue University, 139 pp.

Radocea, A., (1990), A New Method for Studying Bleeding of Cement Paste, Cement and Concrete Research, Vol. 22, No. 5, pp. 855 – 865.

Radocea, A., (1994), A Model of Plastic Shrinkage, Magazine of Concrete Research, Vol. 46, No. 167, June, pp. 125 – 132.

Radocea, A., (1998), Autogenious Volume Change of Concrete at Very Early Age, Magazine of Concrete Research, Vol. 50, No. 2, pp. 107 – 113.

Ravina D., Shalon, R., (1968), Plastic Shrinkage Cracking, Journal of the American Concrete Institute, Vol. 65, No. 22, April, pp. 282 – 291.

Roy, D. M., (1989), Hydration, Microstructure and Chloride Diffusion of Chloride Ions in Hardened Cement Pastes, ACI SP-114, Detroit, Vol. 2, pp. 1265 – 1281.

RSMeans, (2012), RSMeans Heavy Construction Cost Data, 26th Ed., Reed Construction Publishers & Consultants, Norwall, MA.

Sanjuan, M. A., and Toledo Filho, R. D., (1998), Effect of Crack Control at Early Age on the Corrosion of Steel Bars in Low Modulus Sisal and Coconut Fiber Reinforced Mortars, Cement and Concrete Research, Vol. 28, pp. 555 – 565.

Sansone, J. M., and Brown, M. C., (2007), The Effect of Cracking on Reinforcement Corrosion in Concrete Bridge Decks, NACE International Corrosion: Conference & Expo, 2007.

Soroka, I., and Ravina, D., (1998), Hot Weather Concreting with Admixtures, Cement and Concrete Research, Vol. 20, pp. 129 – 136.

Soroushian, P., Mirza, F., and Alhozaimy, A., (1995), Plastic Shrinkage Cracking of Polypropylene Fiber-Reinforced Concrete, ACI Materials Journal, Vol. 92, September – October, pp. 553 – 560.

Stanish, K. D., Hooton, R. D., and Thomas, M. D. A., (1997), Testing the Chloride Penetration Resistance of Concrete: A Literature Review, University of Toronto, Ontario, Canada.

Stanish, K. D., Hooton, R. D., and Thomas, M. D. A., (2000), A Rapid Migration Test for Evaluation of the Chloride Penetration Resistance of High Performance Concrete, International Symposium on High Performance Concrete, Orlando, pp. 358 – 367.

Stanish, K. D., and Thomas, M. D. A., (2003), The Use of Bulk Diffusion Tests to Establish Time-Dependent Concrete Chloride Diffusion Coefficients, Cement and Concrete Research, Vol. 33, pp. 55 – 62.

Tang, L., and Nilsson, L. O., (1992), Chloride Diffusivity in High Strength Concrete, Nordic Concrete Research, Vol. 11, pp. 162 – 170.

Thomas, M. D. A., and Bamforth, P. B., (1999), Modelling Chloride Diffusion in Concrete Effect of Fly Ash and Slag, Cement and Concrete Research 29, pp. 487 – 495.

Thomas, M. D. A., Bremner, T., and Scott, A. C. N., (2011), Actual and Modeled Performance in a Tidal Zone, Concrete International, Vol. 33, November, pp. 23 – 28.

Thomas, M. D. A., Pantazopoulou, S. J., and Martin-Perez, B., (1995), Service Life Modelling of Reinforced Concrete Structures Exposed to Chlorides – A Literature Review, University of Toronto, Ontario, Canada.

Trottier, J. F., and Mahoney, M., (2001), Innovative Synthetic Fibers, Concrete International, Vol. 23, June, pp. 23 – 28.

Trottier, J. F., Mahoney, M., and Forgeron, D. P., (2002), Can Synthetic Fibers Replace Welded-Wire Fabric in Slabs on Ground, Concrete International, November, pp. 59 – 68.

Trottier, J. F., Morgan, D.R., and Forgeron, D., (1997) Fiber Reinforced Concrete for Exterior Slab on Grade Applications. Influence of Fiber Geometry and Type on Mechanical Properties and Durability, Part I., Concrete International, June, pp. 35-39.

Wang, K. J., Jansen, D., and Shah, S. P., (1997), Permeability of Cracked Concrete, Cement and Concrete Research, Vol. 27, pp. 409 – 415.

Wang, K. J., Shah, S. P., and Phuaksuk, P., (2001), Plastic Shrinkage Cracking in Concrete Materials – Influence of Fly Ash and Fibers, ACI Materials Journal, Vol. 98, November – December, pp. 458 – 464.

Weyers, R. E., Conway, J. C., and Cady, P. D., (1982), Photoelastic Analysis of Rigid Inclusions in Fresh Concrete, Cement and Concrete Research, Vol. 12, pp. 475 – 484.

Wittmann, F. H., (1976), On the Action of Capillary Pressure in Fresh Concrete, Cement and Concrete Research, Vol. 6, January, pp. 49 – 56.

Whiting, D., (1981), Rapid Measurement of the Chloride Permeability of Concrete, Public Roads, Vol. 45, No. 3, pp. 101 – 112.

Xi, Y., and Bazant, P., (1999), Modeling Chloride Penetration in Saturated Concrete, Journal of Materials in Civil Engineering, Vol. 11, No. 1, Paper No. 15595.

Zhang, M. H., and Gjorv, O. E., (1991), Permeability of High Strength Lightweight Concrete, ACI Materials Journal, Vol. 88, No. 5, pp. 463 – 469.

Zollo, R., Ilter, J., and Bouchacourt, G., (1986), Plastic Drying Shrinkage in Concrete Containing Collated Fibrillated Polypropylene Fiber, Third International Symposium on Development in Fiber Reinforced Cement and Concrete, RILEM Symposium FRC 86, Vol. 1, July.

APPENDIX A Admixture Data Sheets

PLASTOL 341

MID-RANGE/HIGH RANGE - WATER REDUCING ADMIXTURE

Euclid Concrete Admixtures

MID-RANGE WATER REDUCERS

PLASTOL 341

Master Format #: 03 3000 03 4000 03 7000

DESCRIPTION

PLASTOL 341 is a polycarboxylate based plasticizing admixture for concrete which is flexible enough to use as an ASTM C 494 Type A & Type F water reducer. Plastol 341 is a mid-range/high-range water reducing and plasticizing admixture for concrete. Plastol 341 shows improved finishing characteristics when compared to other commonly used Type A (typically 5 to 6% water reduction) or Type F (typically 12 to 15% water reduction) admixtures. This mid-range approach to water reducing admixtures allows for a wide range of usable dosage rates for a broad application spectrum. PLASTOL 341 does not contain calcium chloride.

PRIMARY APPLICATIONS

- Ready mix concrete
- Precast concrete
- Cast in place
- Self-consolidating concrete
- Concrete mixtures utilizing Fly Ash, Slag or other natural pozzolans

FEATURES/BENEFITS

Plastic Concrete

- Improves finishability
- Improves workability
- Reduces water requirement
- Improves setting times
- Superior slump retention

Hardened Concrete

- Increases early and late age strengths
- Reduces permeability
- Increases durability

TECHNICAL INFORMATION

The following test results were achieved using typical ASTM C 494 mix design requirements, 517 lb/yd³ (307 kg/m³) cement content and similar (± 0.5)% air content.

These results were obtained under laboratory conditions with materials and mixdesigns meeting the specifications of ASTM C 494. Changes in materials and mix designs can affect the dosage response of PLASTOL 341.

Plastol 341 Compressive Strength Data (psi)

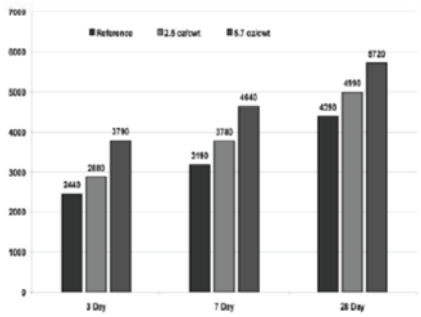

Plastol 341 Set Time Results (psi)

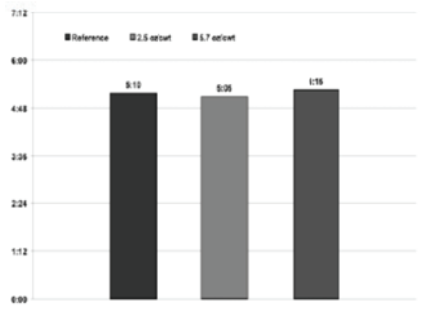

The Euclid Chemical Company
19218 Redwood Rd. • Cleveland, OH 44110
Phone: [216] 531-9222 • Toll-free: [800] 321-7628 • Fax: [216] 531-9596
www.euclidchemical.com

An RPM Company

PACKAGING

PLASTOL 341 is packaged in bulk, 275 gal (1041 L) totes, 55 gal (208 L) drums, and 5 gal (18.9 L) pails.

SHELF LIFE

2 years in original, unopened container.

SPECIFICATIONS/COMPLIANCES

PLASTOL 341 meets or exceeds the requirements of:

- ASTM C 494, Type A and Type F
- AASHTO M 194
- ANSI/NSF STD 61 registered

DIRECTIONS FOR USE

PLASTOl 341 is typically used at dosages of 2 to 10 oz per 100 lbs (130 to 650 mL per 100 kg) of cementitious material. Dosage recommendations depend on the characteristics of the materials being used in the mix design. Higher dosages are acceptable with prior testing and confirmation of the desired performance with specific materials being used.

PLASTOL 341 should be added to the initial batch water when possible. It should not come in contact with dry cement or other admixtures until mixed thoroughly with the concrete batch.

Field testing is strongly recommended to optimize dose range and performance expectations with local materials.

Plastol 341 is compatible with most admixtures including air-entraining agents, accelerators, most water-reducers, retarders, shrinkage reducers, corrosion inhibitors, viscosity modifiers, and microsilica; however, each material should be added to the concrete separately. Please contact a Euclid Sales Professional for any compatibility issues.

PRECAUTIONS/LIMITATIONS

- Care should be taken to maintain PLASTOL 341 above freezing.
- Never agitate with air.
- Add to concrete mix independent of other admixtures.
- In all cases, consult the Material Safety Data Sheet before use.

Rev. 10.10

AIREX-L

Air Entraining Agent For Concrete

Euclid Concrete Admixtures

AIR ENTRAINERS

AIREX-L

Master Format #: 03 3000 03 4000 03 7000

Description

AIREX-L is a liquid solution of hydrocarbons used as an air entraining agent for concrete and complies with ASTM C260. When AIREX-L is added to the concrete mix, it produces a system of microscopic air bubbles that remains very stable in the concrete. The entrainment of air with AIREX-L improves ease of placement, workability and durability of the concrete while minimizing bleeding and segregation.

Features/Benefits

AIREX-L can be used in all normal density concretes as well as low slump concretes where resistance to cycles of freezing and thawing is required. AIREX-L is specifically designed to facilitate air entrainment of low slump and no slump concrete.

Technical Information

Physical Properties

Specific gravity (25º C)	1.007
% of solids by weight	5.0
pH	11.0

Consult your EUCLID representative for additional information or technical assistance.

Packaging

AIREX-L is available in bulk as well as in containers of 1000, 205 or 20 liters.

Shelf Life

2 years in original, unopened package.

Specifications/Compliances

- AIREX-L meets all requirements of ASTM C 260 specifications.
- AIREX-L is approved by the Quebec and Ontario Ministry of Transportation.

Directions for Use

For normal slump concrete use a minimum of 15 mL/100 kg of cementitious material.

For dry concrete (0 to 50 mm slump), use a minimum of 100 mL/100 kg of cementitious material.

For roller compacted concrete (RCC), use 300 to 500 mL/100 kg of cementitious material.

AIREX-L should be added with the mix water or independently of other admixtures. Concrete mixing should ensure adequate dispersion of admixtures.

The quantity of AIREX-L required to obtain the specified air content may be influenced by the following factors:

- Concrete and ambient temperature
- Cement types
- Mineral additives
- Quality of aggregate
- Sand gradation
- Slump of concrete
- Mixing equipment

The Euclid Chemical Company
19218 Redwood Rd. • Cleveland, OH 44110
Phone: [216] 531-9222 • Toll-free: [800] 321-7628 • Fax: [216] 531-9596
www.euclidchemical.com

An RPM Company

PRECAUTIONS/LIMITATIONS

- Keep from freezing
- AIREX-L is not W.H.M.I.S. regulated.
- In all cases, consult Material Safety Data Sheet before use.

AIREX-L can be used and is compatible with the full range of EUCLID admixtures. When EUCON 37, EUCON 537 or PLASTOL 5000 are added to concrete, the use of AIREXTRA in replacement of AIREX-L is recommended for a more stable air void system and enhanced performance of the concrete.

Rev. 05.12

APPENDIX B Plastic Shrinkage Cracking Results

ASTM C1579 Standard Test Method for Evaluating Plastic Shrinkage Cracking of Restrained Fiber Reinforced Concrete

Mixture	Average Crack Width (mm)	Maximum Crack Width (mm)	Crack Length (mm)	Total Crack Area (mm^2)	Fiber Volume Fraction (%)	Reduction in Total Crack Area (%)	Reduction in Average Crack Width (%)	Reduction In Max Crack Width (%)
NC (65mm)	-	-	-	-	-	-	-	-
NC (50mm)	-	-	-	-	-	-	-	-
NC (35mm)	-	-	-	-	-	-	-	-
FA (65mm)	-	-	-	-	-	-	-	-
FA (50mm)	-	-	-	-	-	-	-	-
FA (35mm)	-	-	-	-	-	-	-	-
TER 50-1 (65mm)	-	-	-	-	-	-	-	-
TER 50-1 (50mm)	-	-	-	-	-	-	-	-
TER 50-1 (35mm)	0.34	0.88	256.8	87.3	-	-	-	-
TER 50-1 F1(1.8 kg)	0.15	0.39	154.0	23.1	0.2	73.5	55.9	55.7
TER 50-1 F1(3.0 kg)	-	-	-	-	0.33	100	100	100
TER 50-1 F2 (1.8 kg)	-	-	-	-	0.2	100	100	100
TER 50-2 (50mm)	-	-	-	-	-	-	-	-
TER 50-2 (35mm)	0.19	0.33	149.1	28.3	-	-	-	-
TER 50-2 F1(1.8 kg)	-	-	-	-	0.2	100	100	100
TER 50-2 F2 (1.5 kg)	-	-	-	-	0.16	100	100	100

APPENDIX C Compressive Strength Test Results

ASTM C39 Standard Test Method for Compressive Strength of Cylindrical Concrete Specimens

Date Cast	Date Tested	Sample No	Compressive Strength (MPa)	Average Compressive Strength (MPa)	Std. Deviation (Mpa)
Sept-20-2011	Oct-18-2011	NC 1	38.9	39.6	0.68
		NC 2	40.3		
		NC 3	39.7		
Sept-27-2011	Oct-25-2011	FA 1	40.0	39.8	0.56
		FA 2	39.2		
		FA 3	40.3		
Oct-12-2011	Nov-9-2011	TER50-1 1	36.5	36.2	0.72
		TER50-1 2	36.7		
		TER50-1 3	35.4		
Nov-22-2011	Dec-20-2011	TER50-1 (0.2% F1) 1	35.4	35.0	0.87
		TER50-1 (0.2% F1) 2	34.0		
		TER50-1 (0.2% F1) 3	35.7		
Nov-24-2011	Dec-22-2011	TER50-1 (0.33% F1) 1	34.9	35.2	1.13
		TER50-1 (0.33% F1) 2	34.3		
		TER50-1 (0.33% F1) 3	36.5		
Jan-26-2012	Feb-23-2012	TER50-2 (0.2% F2) 1	38.9	39.0	0.41
		TER50-2 (0.2% F2) 2	39.5		
		TER50-2 (0.2% F2) 3	38.6		
Dec-6-2011	Jan-3-2012	TER50-2 1	37.6	36.8	1.99
		TER50-2 2	34.6		
		TER50-2 3	38.4		
Dec-15-2011	Jan-12-2012	TER50-2 (0.2% F1) 1	37.6	37.9	1.92
		TER50-2 (0.2% F1) 2	40.0		
		TER50-2 (0.2% F1) 3	36.2		
Jan-25-2012	Feb-22-2012	TER50-2 (0.16% F2) 1	35.1	36.4	1.22
		TER50-2 (0.16% F2) 2	37.6		
		TER50-2 (0.16% F2) 3	36.5		

APPENDIX D Rapid Chloride Permeability Test Results

ASTM C1202 Standard Test Method for Electrical Indication of Concrete's Ability to Resist Chloride Ion Penetration

Sample	**NC**

	Cell 1		Cell 2		Cell 3	
Time (min)	Current (mA)	Coulombs	Current (mA)	Coulombs	Current (mA)	Coulombs
1	145	8	149	9	Leak	
30	167	283	162	282		
60	180	598	175	587		
90	192	934	186	913		
120	200	1288	192	1254		
150	206	1653	196	1603		
180	214	2032	201	1961		
210	221	2424	203	2325		
240	226	2827	207	2693		
270	232	3240	208	3066		
300	235	3661	209	3443		
330	239	4089	210	3822		
360	242	4523	213	4205		

Average Charge Passed	4364	Coulombs
Std. Dev. Charge Passed	224.9	Coulombs

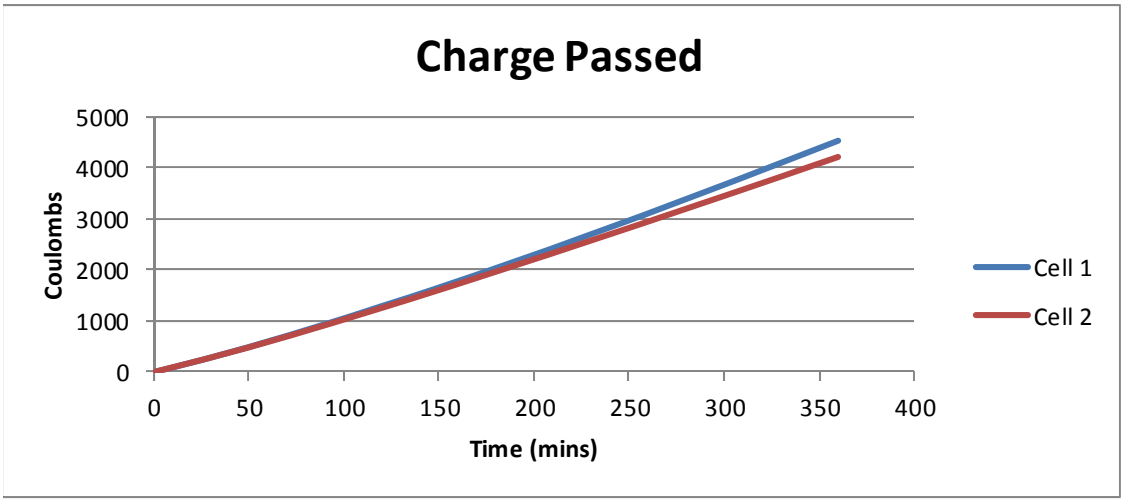

ASTM C1202 Standard Test Method for Electrical Indication of Concrete's Ability to Resist Chloride Ion Penetration

Sample	**FA**

	Cell 1		Cell 2*		Cell 3	
Time (min)	Current (mA)	Coulombs	Current (mA)	Coulombs	Current (mA)	Coulombs
1	116	7	128	7	114	6
30	129	222	145	249	125	218
60	136	462	157	522	133	453
90	144	716	168	815	140	701
120	151	983	177	1126	144	959
150	157	1261	186	1453	148	1224
180	161	1548	193	1795	153	1495
210	164	1843	200	2150	155	1773
240	167	2142	205	2516	157	2053
270	168	2446	211	2891	157	2336
300	170	2752	215	3275	158	2618
330	172	3061	219	3667	158	2903
360	172	3371	221	4063	158	3188

*Invalid due to leak

Average Charge Passed	3280	Coulombs
Std. Dev. Charge Passed	129.4	Coulombs

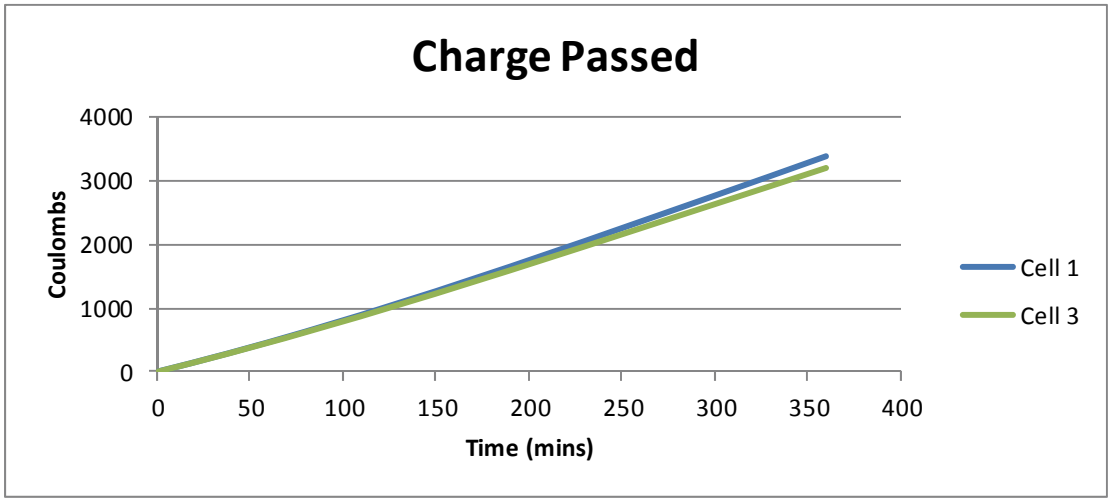

ASTM C1202 Standard Test Method for Electrical Indication of Concrete's Ability to Resist Chloride Ion Penetration

Sample	**TER50-1**

	Cell 1		Cell 2		Cell 3	
Time (min)	Current (mA)	Coulombs	Current (mA)	Coulombs	Current (mA)	Coulombs
1	58	3	59	3	55	3
30	62	110	65	112	60	105
60	65	225	67	232	63	217
90	68	346	71	358	66	334
120	71	472	74	490	69	457
150	73	602	77	626	71	583
180	75	737	80	767	73	715
210	78	875	82	913	75	849
240	79	1017	84	1063	78	988
270	81	1162	86	1216	79	1130
300	82	1309	88	1372	81	1275
330	84	1459	89	1533	82	1423
360	85	1612	91	1696	84	1573

Average Charge Passed	1627	Coulombs
Std. Dev. Charge Passed	62.9	Coulombs

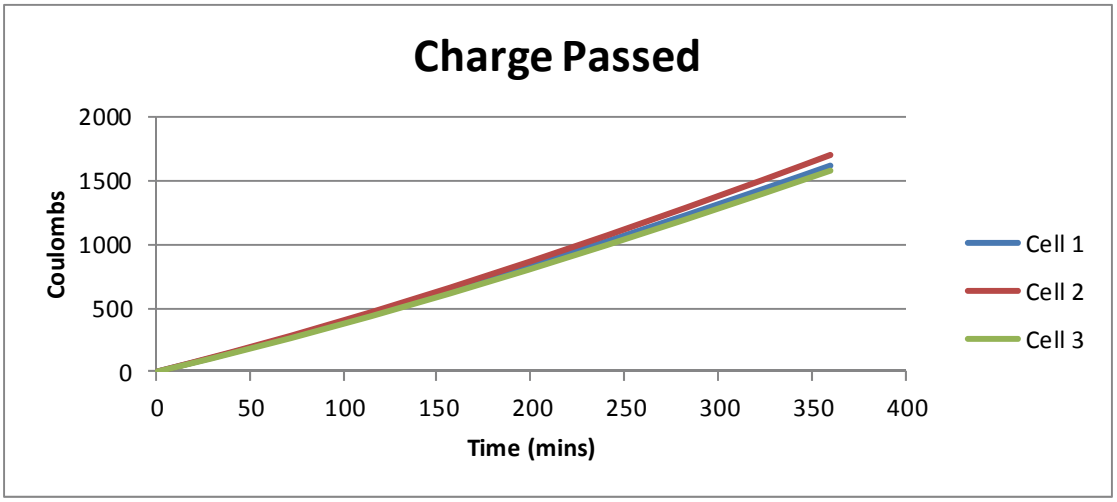

ASTM C1202 Standard Test Method for Electrical Indication of Concrete's Ability to Resist Chloride Ion Penetration

Sample	**TER50-1 (0.2% F1)**

	Cell 1		Cell 2*		Cell 3	
Time (min)	Current (mA)	Coulombs	Current (mA)	Coulombs	Current (mA)	Coulombs
1	45	2	49	3	47	2
30	48	85	54	93	50	88
60	51	175	56	193	53	181
90	52	268	58	297	55	279
120	54	365	61	406	57	382
150	56	465	64	519	59	487
180	57	567	66	636	61	595
210	58	672	68	757	62	706
240	59	778	70	882	63	820
270	60	886	71	1010	64	936
300	61	996	73	1141	66	1054
330	62	1107	75	1275	67	1174
360	62	1219	76	1412	68	1296

*Invalid due to leak

Average Charge Passed	1258	Coulombs
Std. Dev. Charge Passed	54.4	Coulombs

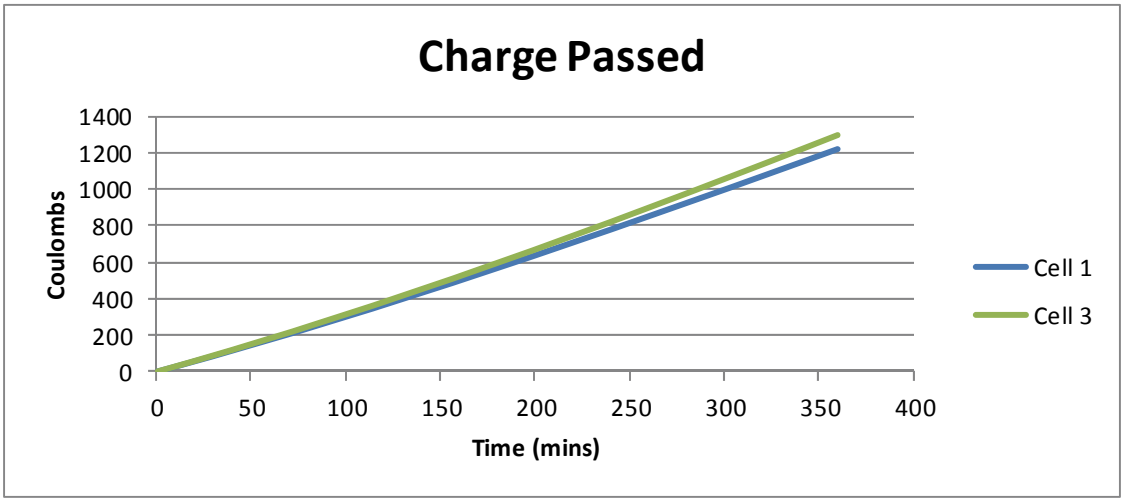

ASTM C1202 Standard Test Method for Electrical Indication of Concrete's Ability to Resist Chloride Ion Penetration

Sample	TER50-1 (0.33% F1)

	Cell 1		Cell 2		Cell 3	
Time (min)	Current (mA)	Coulombs	Current (mA)	Coulombs	Current (mA)	Coulombs
1	45	2	47	2	48	2
30	48	83	50	89	50	89
60	49	172	53	183	53	183
90	51	263	55	281	55	280
120	52	357	56	381	56	381
150	54	453	57	484	57	484
180	55	551	59	589	58	588
210	56	651	59	696	59	695
240	57	754	60	803	60	803
270	58	858	60	912	61	913
300	58	963	61	1023	62	1025
330	59	1069	62	1135	63	1138
360	60	1177	62	1247	63	1252

Average Charge Passed	1225	Coulombs
Std. Dev. Charge Passed	41.9	Coulombs

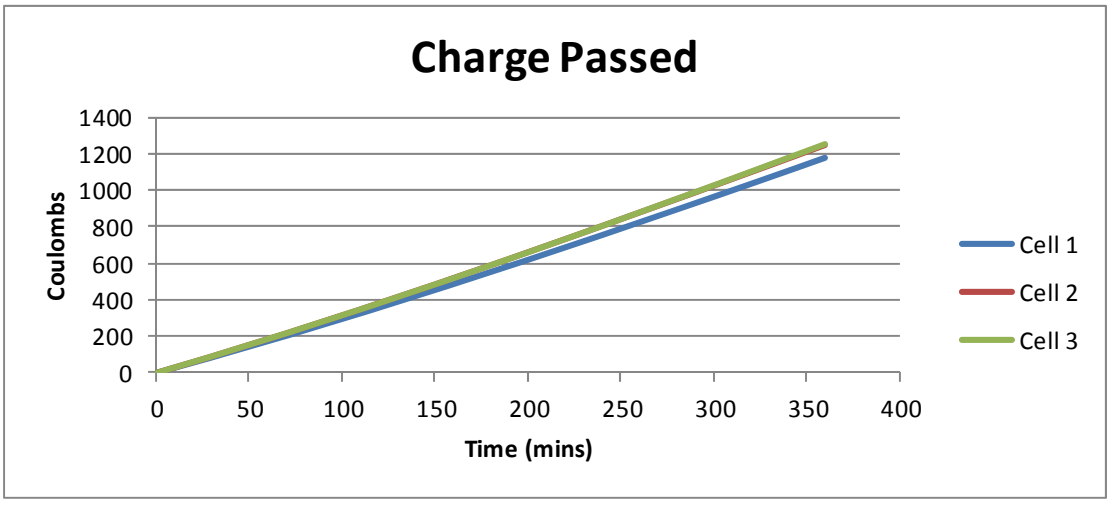

ASTM C1202 Standard Test Method for Electrical Indication of Concrete's Ability to Resist Chloride Ion Penetration

Sample	**TER50-1 (0.2% F2)**

	Cell 1		Cell 2*		Cell 3	
Time (min)	Current (mA)	Coulombs	Current (mA)	Coulombs	Current (mA)	Coulombs
1	52	3	61	3	54	3
30	55	96	66	115	57	101
60	57	197	68	236	59	207
90	59	302	71	362	61	315
120	61	411	73	493	63	427
150	62	522	75	628	64	542
180	64	636	78	766	65	660
210	65	753	79	908	67	780
240	66	871	80	1053	68	903
270	67	991	82	1200	69	1027
300	67	1113	83	1350	70	1152
330	68	1236	84	1501	70	1279
360	69	1360	85	1655	71	1407

*Invalid due to leak

Average Charge Passed	1384	Coulombs
Std. Dev. Charge Passed	33.2	Coulombs

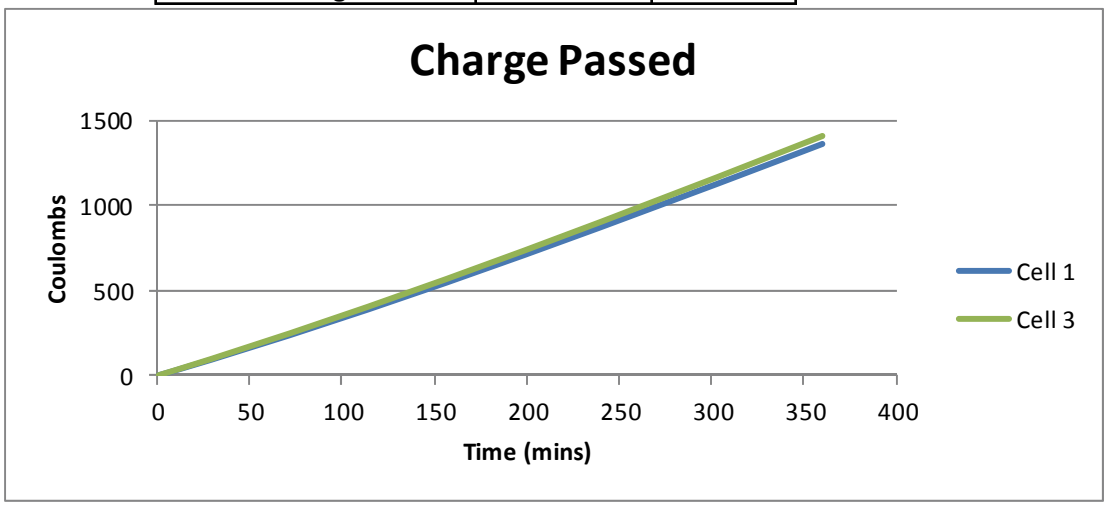

ASTM C1202 Standard Test Method for Electrical Indication of Concrete's Ability to Resist Chloride Ion Penetration

Sample	**TER50-2**

	Cell 1		Cell 2		Cell 3	
Time (min)	Current (mA)	Coulombs	Current (mA)	Coulombs	Current (mA)	Coulombs
1	50	3	49	3	49	3
30	53	93	52	93	52	92
60	55	191	54	189	53	187
90	56	292	56	289	55	286
120	58	396	57	391	57	387
150	59	502	59	496	58	491
180	60	611	60	604	59	597
210	61	721	61	713	60	706
240	62	834	62	825	61	816
270	63	948	63	939	62	928
300	64	1064	64	1054	63	1041
330	65	1182	65	1171	64	1156
360	66	1300	66	1290	64	1272

Average Charge Passed	1286	Coulombs
Std. Dev. Charge Passed	14.2	Coulombs

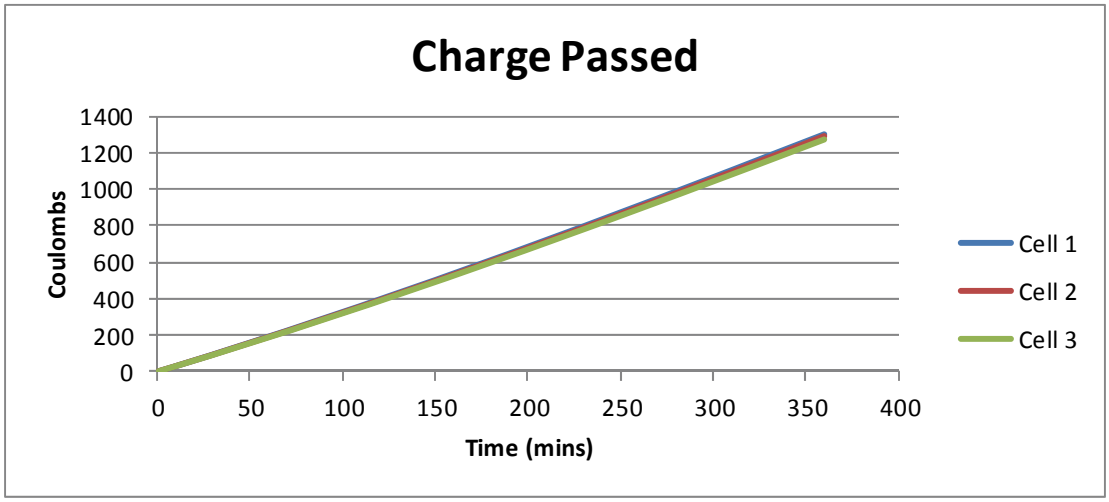

ASTM C1202 Standard Test Method for Electrical Indication of Concrete's Ability to Resist Chloride Ion Penetration

Sample	**TER50-2 (0.2% F1)**

	Cell 1*		Cell 2		Cell 3	
Time (min)	Current (mA)	Coulombs	Current (mA)	Coulombs	Current (mA)	Coulombs
1	55	3	44	2	Leak	
30	60	104	47	82		
60	62	215	48	168		
90	65	330	50	257		
120	68	450	51	348		
150	70	576	53	443		
180	73	705	54	540		
210	75	839	55	639		
240	77	977	56	741		
270	79	1118	57	844		
300	80	1262	58	948		
330	83	1410	59	1054		
360	84	1561	60	1162		

*Invalid due to leak

Average Charge Passed	1162	Coulombs
Std. Dev. Charge Passed	-	Coulombs

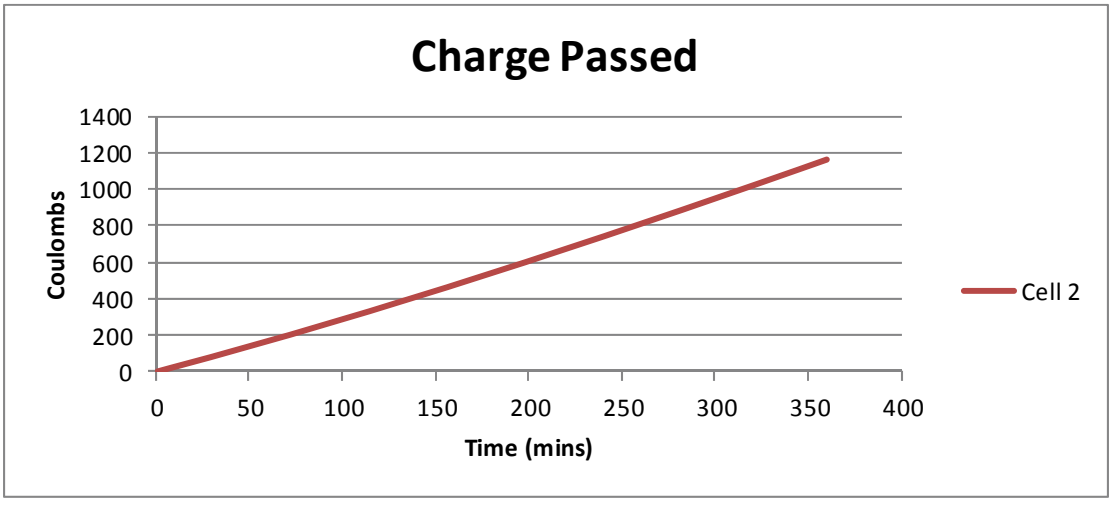

ASTM C1202 Standard Test Method for Electrical Indication of Concrete's Ability to Resist Chloride Ion Penetration

Sample	**TER50-2 (0.16% F2)**

	Cell 1		Cell 2		Cell 3	
Time (min)	Current (mA)	Coulombs	Current (mA)	Coulombs	Current (mA)	Coulombs
1	48	2	44	2	48	2
30	51	89	47	82	51	89
60	53	184	49	169	53	183
90	55	282	50	259	55	280
120	57	383	52	352	57	381
150	59	488	53	447	58	486
180	60	596	54	545	60	593
210	62	707	55	645	61	704
240	63	820	56	747	63	816
270	64	936	57	850	64	931
300	66	1054	58	955	65	1048
330	67	1174	59	1062	66	1167
360	68	1296	60	1170	67	1288

Average Charge Passed	1251	Coulombs
Std. Dev. Charge Passed	70.6	Coulombs

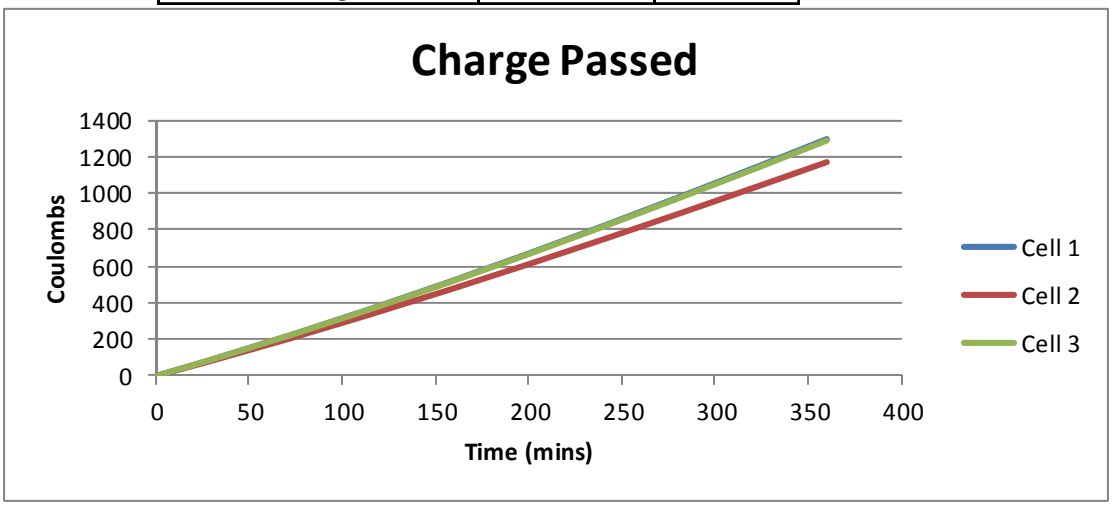

APPENDIX E Rapid Migration Test Results

NORDTEST NT Build 492 Chloride Migration Coefficient from Non-Steady-State Migration Experiments

Mixture	Fiber Volume Fraction	Speciman No.	U (V)	T (°C)	L (mm)	Xd (mm)	t (hrs)	D_{nssm} ($x10^{-12}$ m^2/s)	Average D_{nssm} ($x10^{-12}$ m^2/s)	Std. Deviation D_{nssm} ($x10^{-12}$ m^2/s)
NC	-	1	10.01	22.25	52.0	9.8	24	12.48	13.01	0.48
		2	10.01	21.50	52.0	10.4	24	13.41		
		3	10.01	21.75	53.0	10.1	24	13.13		
FA	-	1	15.02	19.80	53.2	13.3	24	12.27	11.90	0.41
		2	15.02	19.65	51.2	12.9	24	11.46		
		3	15.02	19.10	50.8	13.5	24	11.97		
TER50-1	-	1	20.01	20.20	49.0	11.1	24	7.04	7.79	1.61
		2	20.01	20.00	53.1	13.8	24	9.64		
		3	20.01	20.45	51.0	10.3	24	6.70		
TER50-1 Dry	-	1	20.04	21.80	58.7	8.5	24	6.07	6.07	-
TER50-1	1.8 F1	1	20.05	22.25	50.5	7.7	24	4.77	7.91	2.91
		2	20.05	22.05	50.4	12.73	24	8.44		
		3	20.05	22.10	51.3	15.28	24	10.52		
TER50-1 Dry	1.8 F1	1	30.82	22.40	56.1	16.74	24	8.25	8.25	-
TER50-1	3.0 F1	1	24.99	22.90	51.5	13.14	22.5	7.69	7.49	0.33
		2	24.99	22.85	47.7	13.98	22.5	7.68		
		3	24.99	22.95	49.3	12.68	22.5	7.11		
TER50-1	1.8 F2	1	20.00	22.85	51.8	8.69	24	5.63	6.17	0.54
		2	20.00	22.95	51.8	10.13	24	6.72		
		3	20.00	22.85	50.9	9.51	24	6.15		
TER50-2	-	1	25.02	22.90	51.9	9.87	24	5.27	5.13	0.81
		2	25.02	22.60	52.0	8.17	24	4.26		
		3	25.02	22.90	52.3	10.79	24	5.87		
TER50-2 Dry	-	1	30.81	23.65	54.5	18.85	24	9.16	9.16	-
TER50-2	1.8 F1	1	20.02	22.55	48.5	9.23	24	5.69	6.11	0.72
		2	20.02	23.00	49.7	10.77	24	6.94		
		3	20.02	22.25	50.9	8.89	24	5.68		
TER50-2	1.5 F2	1	20.03	22.80	50.5	8.98	24	5.72	6.23	0.45
		2	20.03	22.85	51.4	9.84	24	6.44		
		3	20.03	23.15	51.9	9.88	24	6.53		

APPENDIX F Bulk Diffusion Test Results

ASTM 1556 Standard Test Method for Determining the Apparent Chloride Diffusion Coefficient of Cementitious Mixtures by Bulk Diffusion

Sample	NC 1

Cs (mass %) =	0.55673	Ci (mass %) =	0.004	Test Duration (d) =	60
Deff (m^2/s) =	2.7078E-11	t (s) =	5184000	Age (d) =	28

	% by weight/mass			
Depth X (m)	Measured	Predicted	Error	Error Squared
0.001	0.538	5.3042E-01	0.008	5.74465E-05
0.0035	0.464	4.6527E-01	-0.001	1.61097E-06
0.0065	0.346	3.8984E-01	-0.044	0.00192177
0.01	0.321	3.0834E-01	0.013	0.000160151
0.014	0.273	2.2697E-01	0.046	0.002118446
0.018	0.170	1.6025E-01	0.010	9.49894E-05
0.022	0.088	1.0856E-01	-0.021	0.000422894
0.0265	0.039	6.6870E-02	-0.028	0.000776737
			SSE =	0.005554046
			MSE =	0.000694256

m =	0.2
D28_t_avg	3.132E-11
D28_t_end	3.405E-11

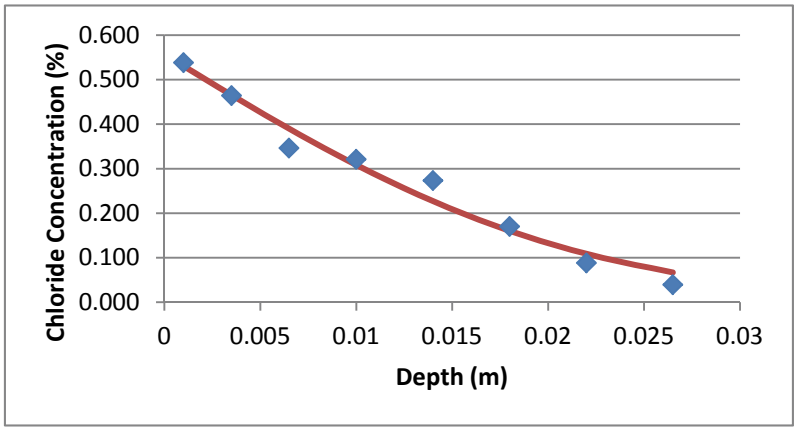

ASTM 1556 Standard Test Method for Determining the Apparent Chloride Diffusion Coefficient of Cementitious Mixtures by Bulk Diffusion

Sample	**NC 2**

Cs (mass %) =	0.93988	Ci (mass %) =	0.016	Test Duration (d) =	60
Deff (m^2/s) =	2.0908E-11	t (s) =	5184000	Age (d) =	28

	% by weight/mass			
Depth X (m)	Measured	Predicted	Error	Error Squared
0.001	1.254	8.8985E-01	0.364	0.132606778
0.0035	0.681	7.6628E-01	-0.085	0.00727237
0.0065	0.586	6.2471E-01	-0.039	0.001498452
0.01	0.453	4.7518E-01	-0.022	0.000491783
0.014	0.336	3.3166E-01	0.004	1.88729E-05
0.018	0.214	2.2063E-01	-0.007	4.40111E-05
0.022	0.138	1.4083E-01	-0.003	7.99172E-06
0.0265	0.084	8.2407E-02	0.002	2.53646E-06
			SSE =	0.141942794
			MSE =	0.017742849

m =	0.2
D28_t_avg	2.419E-11
D28_t_end	2.629E-11

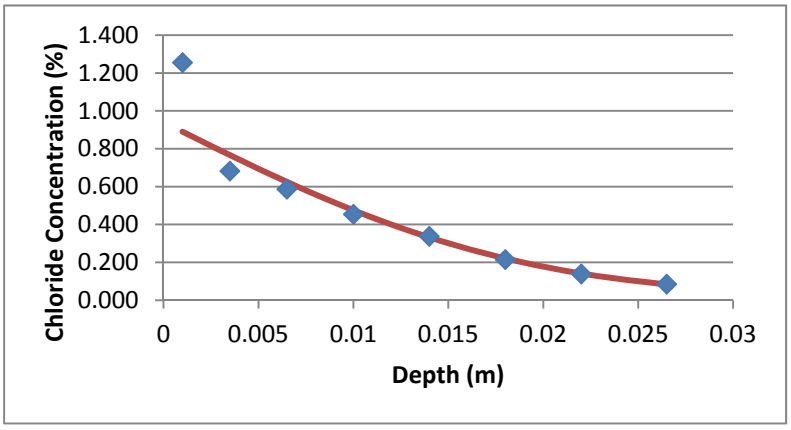

ASTM 1556 Standard Test Method for Determining the Apparent Chloride Diffusion Coefficient of Cementitious Mixtures by Bulk Diffusion

Sample	FA 1

Cs (mass %) =	0.80324	Ci (mass %) =	0.014	Test Duration (d) =	60
Deff (m^2/s) =	9.0940E-12	t (s) =	5184000	Age (d) =	28

	% by weight/mass			
Depth X (m)	Measured	Predicted	Error	Error Squared
0.001	0.768	7.3850E-01	0.029	0.000870241
0.0035	0.558	5.8108E-01	-0.023	0.000532526
0.0065	0.373	4.1117E-01	-0.038	0.001457257
0.0095	0.286	2.7279E-01	0.013	0.000174556
0.0125	0.188	1.7026E-01	0.018	0.000314831
0.0155	0.112	1.0115E-01	0.011	0.000117636
0.0185	0.060	5.8790E-02	0.001	1.46506E-06
0.022	0.044	3.2524E-02	0.011	0.00013169
			SSE =	0.003600202
			MSE =	0.000450025

m =	0.6
D28_t_avg	1.408E-11
D28_t_end	1.808E-11

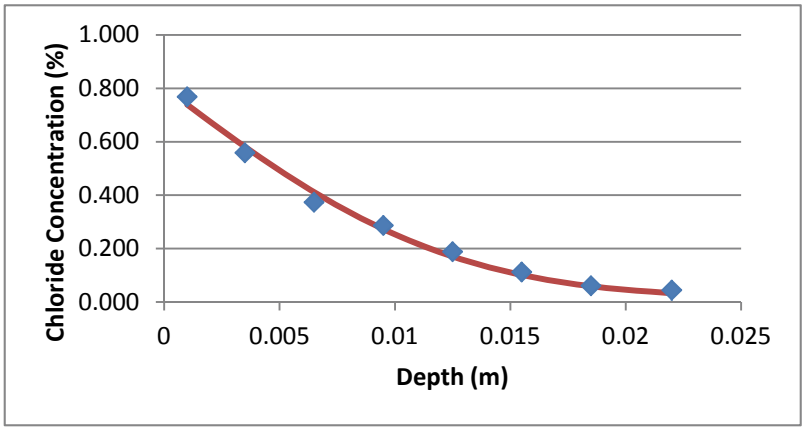

ASTM 1556 Standard Test Method for Determining the Apparent Chloride Diffusion Coefficient of Cementitious Mixtures by Bulk Diffusion

Sample	**FA 2**

Cs (mass %) =	0.70000	Ci (mass %) =	0.013	Test Duration (d) =	60
Deff (m^2/s) =	9.9940E-12	t (s) =	5184000	Age (d) =	28

	% by weight/mass			
Depth X (m)	Measured	Predicted	Error	Error Squared
0.001	0.700	6.4624E-01	0.054	0.002890436
0.0035	0.475	5.1518E-01	-0.040	0.001614132
0.0065	0.398	3.7238E-01	0.026	0.000656407
0.0095	0.286	2.5392E-01	0.032	0.001029247
0.0125	0.206	1.6376E-01	0.042	0.00178388
0.0155	0.107	1.0082E-01	0.006	3.81725E-05
0.0185	0.061	6.0508E-02	0.000	2.41811E-07
0.022	0.028	3.4074E-02	-0.006	3.68967E-05
			SSE =	0.008049414
			MSE =	0.001006177

m =	0.6
D28_t_avg	1.547E-11
D28_t_end	1.987E-11

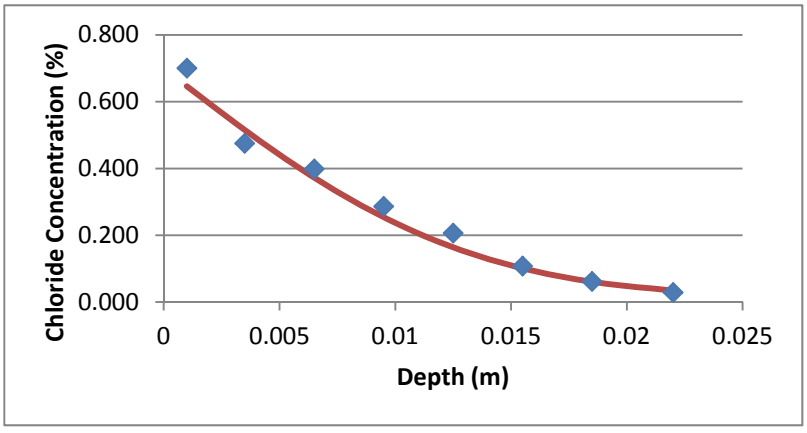

ASTM 1556 Standard Test Method for Determining the Apparent Chloride Diffusion Coefficient of Cementitious Mixtures by Bulk Diffusion

Sample	TER50-1 1

Cs (mass %) =	1.20698	Ci (mass %) =	0.008	Test Duration (d) =	60
Deff (m^2/s) =	2.8653E-12	t (s) =	5184000	Age (d) =	28

	% by weight/mass			
Depth X (m)	Measured	Predicted	Error	Error Squared
0.0005	1.163	1.1193E+00	0.044	0.001905926
0.0015	0.992	9.4699E-01	0.045	0.002026059
0.0025	0.708	7.8310E-01	-0.075	0.005639537
0.004	0.484	5.6315E-01	-0.079	0.006264371
0.006	0.313	3.3289E-01	-0.020	0.0003955
0.008	0.234	1.7845E-01	0.056	0.003085467
0.0105	0.191	7.2802E-02	0.118	0.013970811
0.014	0.105	2.0243E-02	0.085	0.007183828
			SSE =	0.040471499
			MSE =	0.005058937

m =	0.6
D28_t_avg	4.435E-12
D28_t_end	5.696E-12

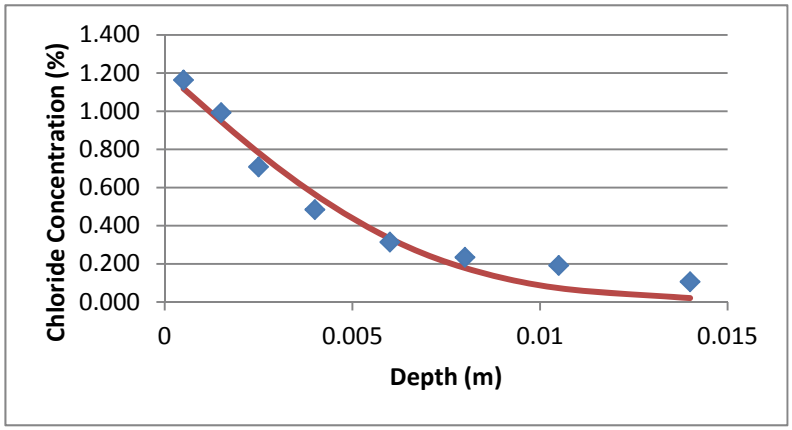

ASTM 1556 Standard Test Method for Determining the Apparent Chloride Diffusion Coefficient of Cementitious Mixtures by Bulk Diffusion

Sample	TER50-1 2

Cs (mass %) =	0.95000	Ci (mass %) =	0.007	Test Duration (d) =	60
Deff (m^2/s) =	3.1296E-12	t (s) =	5184000	Age (d) =	28

	% by weight/mass			
Depth X (m)	Measured	Predicted	Error	Error Squared
0.0005	1.118	8.8404E-01	0.234	0.054736926
0.0015	0.706	7.5413E-01	-0.048	0.002316918
0.0025	0.507	6.3008E-01	-0.123	0.015149184
0.004	0.399	4.6204E-01	-0.063	0.003973903
0.006	0.320	2.8254E-01	0.037	0.001403479
0.008	0.225	1.5806E-01	0.067	0.004481112
0.0105	0.118	6.8561E-02	0.049	0.002444186
0.014	0.059	2.0184E-02	0.039	0.001506698
			SSE =	0.086012406
			MSE =	0.010751551

m =	0.6
D28_t_avg	4.844E-12
D28_t_end	6.221E-12

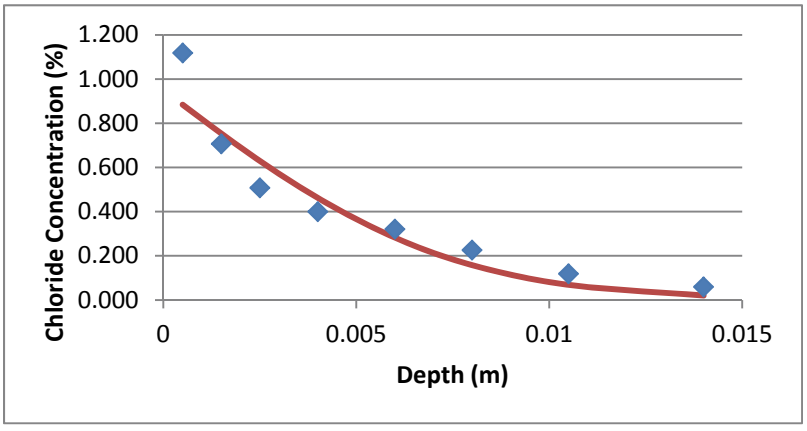

ASTM 1556 Standard Test Method for Determining the Apparent Chloride Diffusion Coefficient of Cementitious Mixtures by Bulk Diffusion

Sample	TER50-1 (0.2% F1) 1

Cs (mass %) =	1.10000	Ci (mass %) =	0.015	Test Duration (d) =	60
Deff (m^2/s) =	3.9714E-12	t (s) =	5184000	Age (d) =	28

	% by weight/mass			
Depth X (m)	Measured	Predicted	Error	Error Squared
0.0005	1.381	1.0326E+00	0.348	0.121374204
0.0015	0.794	8.9946E-01	-0.105	0.011121691
0.0025	0.688	7.7106E-01	-0.083	0.0068991
0.004	0.574	5.9335E-01	-0.019	0.00037457
0.006	0.446	3.9449E-01	0.052	0.002652856
0.008	0.314	2.4556E-01	0.068	0.00468416
0.0105	0.185	1.2542E-01	0.060	0.003549706
0.014	0.077	4.6602E-02	0.030	0.000924051
			SSE =	0.151580337
			MSE =	0.018947542

m =	0.6
D28_t_avg	6.148E-12
D28_t_end	7.895E-12

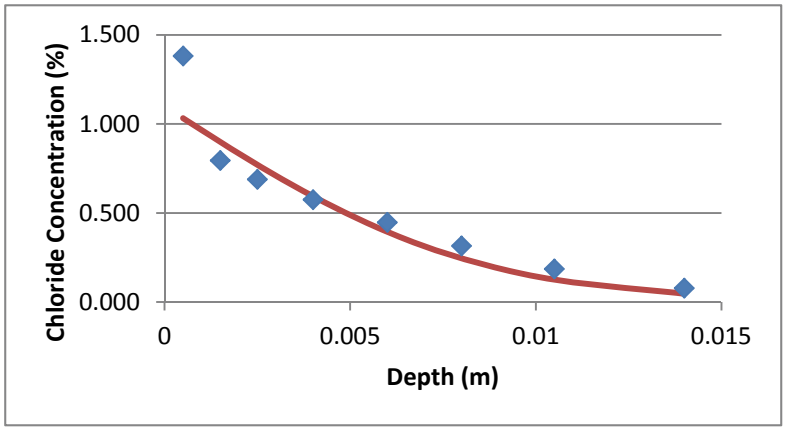

ASTM 1556 Standard Test Method for Determining the Apparent Chloride Diffusion Coefficient of Cementitious Mixtures by Bulk Diffusion

Sample	TER50-1 (0.2% F1) 2

Cs (mass %) =	1.30000	Ci (mass %) =	0.008	Test Duration (d) =	60
Deff (m^2/s) =	2.8885E-12	t (s) =	5184000	Age (d) =	28

	% by weight/mass			
Depth X (m)	Measured	Predicted	Error	Error Squared
0.0005	1.532	1.2059E+00	0.326	0.106312381
0.0015	0.964	1.0209E+00	-0.057	0.003242005
0.0025	0.774	8.4495E-01	-0.071	0.005033427
0.004	0.596	6.0855E-01	-0.013	0.000157464
0.006	0.410	3.6059E-01	0.049	0.002441057
0.008	0.253	1.9376E-01	0.059	0.00350915
0.0105	0.140	7.9089E-02	0.061	0.003710092
0.014	0.065	2.1591E-02	0.043	0.001884302
			SSE =	0.126289878
			MSE =	0.015786235

m =	0.6
D28_t_avg	4.471E-12
D28_t_end	5.742E-12

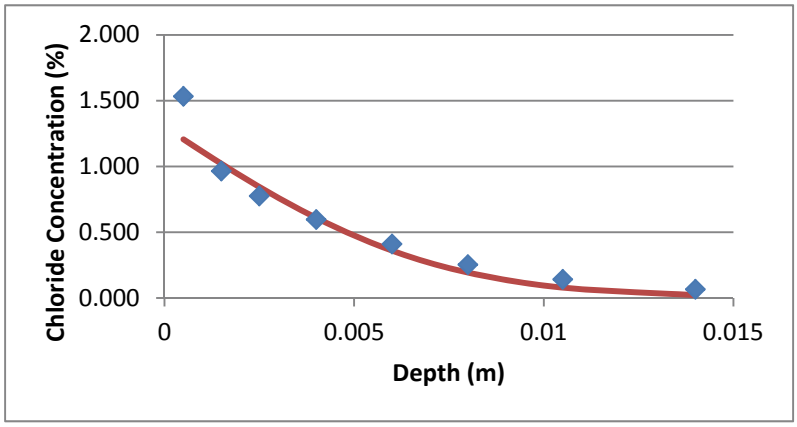

ASTM 1556 Standard Test Method for Determining the Apparent Chloride Diffusion Coefficient of Cementitious Mixtures by Bulk Diffusion

Sample	TER50-1 (0.33% F1) 1

Cs (mass %) =	0.55000	Ci (mass %) =	0.022	Test Duration (d) =	60
Deff (m^2/s) =	1.5198E-12	t (s) =	5184000	Age (d) =	28

	% by weight/mass			
Depth X (m)	Measured	Predicted	Error	Error Squared
0.0005	0.738	4.9708E-01	0.241	0.058044405
0.0015	0.355	3.9452E-01	-0.040	0.001561559
0.0025	0.244	3.0122E-01	-0.057	0.00327447
0.004	0.168	1.8759E-01	-0.020	0.00038372
0.006	0.100	9.0989E-02	0.009	8.11925E-05
0.008	0.064	4.5163E-02	0.019	0.000354819
0.0105	0.043	2.6312E-02	0.017	0.000278498
0.014	0.027	2.2222E-02	0.005	2.28287E-05
			SSE =	0.064001492
			MSE =	0.008000187

m =	0.6
D28_t_avg	2.353E-12
D28_t_end	3.021E-12

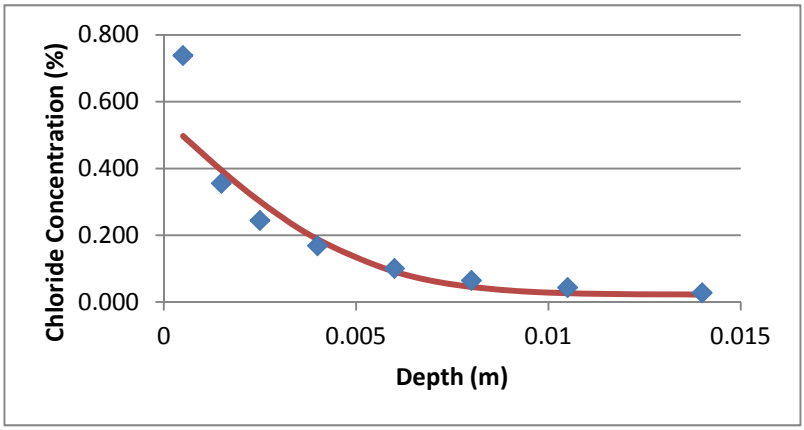

ASTM 1556 Standard Test Method for Determining the Apparent Chloride Diffusion Coefficient of Cementitious Mixtures by Bulk Diffusion

Sample	TER50-1 (0.33% F1) 2

Cs (mass %) =	0.68004	Ci (mass %) =	0.019	Test Duration (d) =	60
Deff (m^2/s) =	2.5855E-12	t (s) =	5184000	Age (d) =	28

	% by weight/mass			
Depth X (m)	Measured	Predicted	Error	Error Squared
0.0005	0.724	6.2918E-01	0.095	0.008990087
0.0015	0.494	5.2935E-01	-0.035	0.00124931
0.0025	0.438	4.3492E-01	0.003	9.46172E-06
0.004	0.279	3.0971E-01	-0.031	0.000943037
0.006	0.170	1.8196E-01	-0.012	0.000142927
0.008	0.113	9.9852E-02	0.070	0.004920686
0.0105	0.074	4.7134E-02	0.066	0.004338365
0.014	0.040	2.3529E-02	0.050	0.00254735
			SSE =	0.023141224
			MSE =	0.002892653

m =	0.6
D28_t_avg	4.002E-12
D28_t_end	5.140E-12

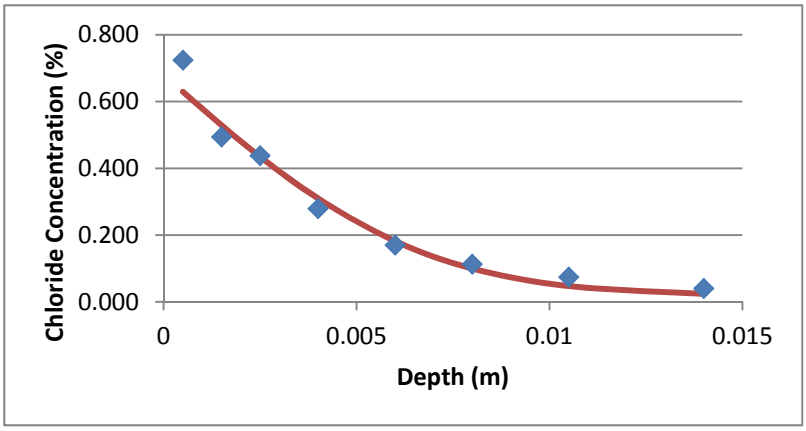

ASTM 1556 Standard Test Method for Determining the Apparent Chloride Diffusion Coefficient of Cementitious Mixtures by Bulk Diffusion

Sample	TER50-2 1

Cs (mass %) =	1.00700	Ci (mass %) =	0.007	Test Duration (d) =	60
Deff (m^2/s) =	1.6573E-12	t (s) =	5184000	Age (d) =	28

	% by weight/mass			
Depth X (m)	Measured	Predicted	Error	Error Squared
0.0005	1.003	9.1099E-01	0.092	0.00846597
0.0015	0.667	7.2445E-01	-0.057	0.003300854
0.0025	0.536	5.5344E-01	-0.017	0.000304084
0.0035	0.390	4.0548E-01	-0.015	0.000239478
0.005	0.243	2.3474E-01	0.008	6.8286E-05
0.007	0.135	9.8278E-02	0.037	0.001348491
0.0095	0.066	2.8917E-02	0.037	0.001375125
0.0125	0.026	9.5654E-03	0.016	0.000270097
			SSE =	0.015372385
			MSE =	0.001921548

m =	0.6
D28_t_avg	2.565E-12
D28_t_end	3.295E-12

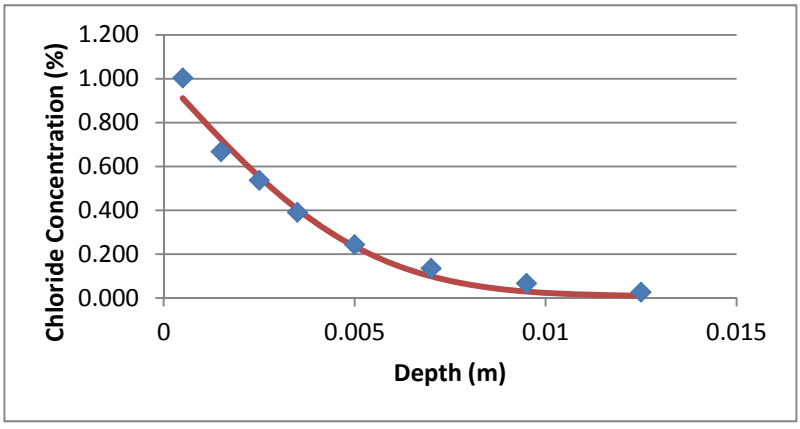

ASTM 1556 Standard Test Method for Determining the Apparent Chloride Diffusion Coefficient of Cementitious Mixtures by Bulk Diffusion

Sample	**TER50-2 2**

Cs (mass %) =	1.00000	Ci (mass %) =	0.006	Test Duration (d) =	60
Deff (m^2/s) =	2.0899E-12	t (s) =	5184000	Age (d) =	28

	% by weight/mass			
Depth X (m)	Measured	Predicted	Error	Error Squared
0.0005	1.404	9.1497E-01	0.489	0.239145807
0.0015	0.700	7.4879E-01	-0.049	0.002380287
0.0025	0.536	5.9368E-01	-0.058	0.00332648
0.0035	0.399	4.5540E-01	-0.056	0.003181438
0.005	0.283	2.8707E-01	-0.004	1.65501E-05
0.007	0.175	1.3784E-01	0.037	0.00138072
0.0095	0.075	4.7019E-02	0.028	0.000782959
0.0125	0.040	1.3202E-02	0.027	0.000718106
			SSE =	0.250932349
			MSE =	0.031366544

m =	0.6
D28_t_avg	3.235E-12
D28_t_end	4.155E-12

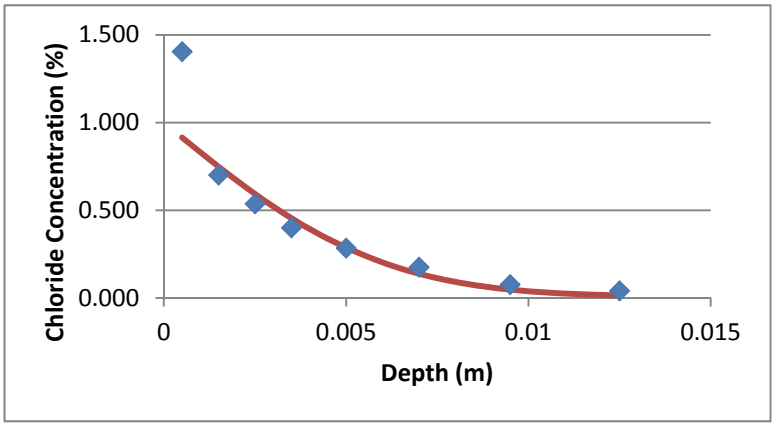

ASTM 1556 Standard Test Method for Determining the Apparent Chloride Diffusion Coefficient of Cementitious Mixtures by Bulk Diffusion

Sample	TER50-2 (0.2% F1) 1

Cs (mass %) =	0.85000	Ci (mass %) =	0.002	Test Duration (d) =	60
Deff (m^2/s) =	2.8885E-12	t (s) =	5184000	Age (d) =	28

	% by weight/mass			
Depth X (m)	Measured	Predicted	Error	Error Squared
0.0005	1.022	7.8827E-01	0.234	0.054631216
0.0015	0.637	6.6684E-01	-0.030	0.000890364
0.0025	0.550	5.5133E-01	-0.001	1.76149E-06
0.0035	0.454	4.4504E-01	0.009	8.02453E-05
0.005	0.320	3.0804E-01	0.012	0.000143107
0.007	0.177	1.7232E-01	0.005	2.18867E-05
0.0095	0.100	7.2020E-02	0.028	0.000782899
0.0125	0.046	2.0963E-02	0.025	0.000626852
			SSE =	0.057178331
			MSE =	0.007147291

m =	0.6
D28_t_avg	4.471E-12
D28_t_end	5.742E-12

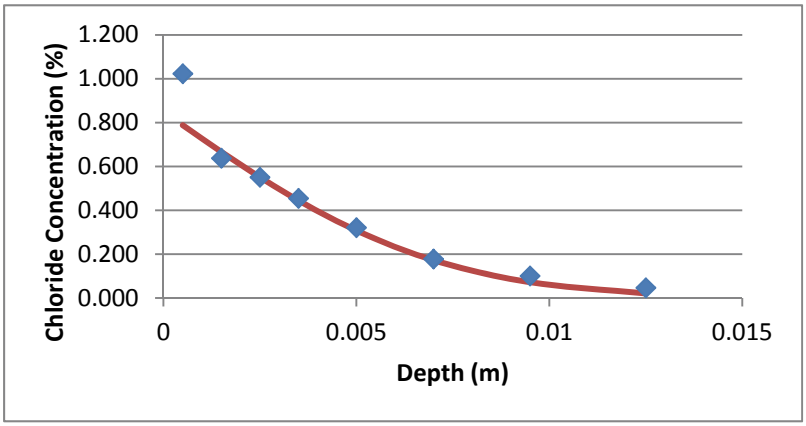

ASTM 1556 Standard Test Method for Determining the Apparent Chloride Diffusion Coefficient of Cementitious Mixtures by Bulk Diffusion

Sample	TER50-2 (0.2% F1) 2

Cs (mass %) =	1.05000	Ci (mass %) =	0.004	Test Duration (d) =	60
Deff (m^2/s) =	2.9885E-12	t (s) =	5184000	Age (d) =	28

	% by weight/mass			
Depth X (m)	Measured	Predicted	Error	Error Squared
0.0005	1.111	9.7513E-01	0.136	0.018459562
0.0015	0.828	8.2779E-01	0.000	4.30426E-08
0.0025	0.671	6.8740E-01	-0.016	0.000268823
0.0035	0.529	5.5785E-01	-0.029	0.000832553
0.005	0.367	3.9003E-01	-0.023	0.000530363
0.007	0.248	2.2215E-01	0.026	0.000668277
0.0095	0.123	9.5926E-02	0.027	0.000733018
0.0125	0.067	2.9866E-02	0.037	0.001378948
			SSE =	0.022871589
			MSE =	0.002858949

m =	0.6
D28_t_avg	4.626E-12
D28_t_end	5.941E-12

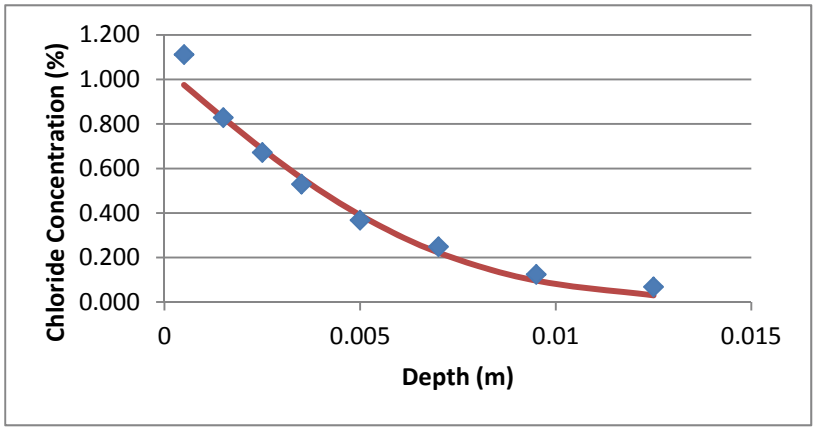

APPENDIX G Cope Wall Diffusion Tests

ASTM 1556 Standard Test Method for Determining the Apparent Chloride Diffusion Coefficient of Cementitious Mixtures by Bulk Diffusion

Sample	Phase 1 Core 1

Cs (mass %) =	0.94443	Ci (mass %) =	0.16	Test Duration (d) =	10950
Deff (m^2/s) =	4.2195E-13	t (s) =	946080000	Age (d) =	7

	% by weight/mass			
Depth X (m)	Measured	Predicted	Error	Error Squared
0.001	0.949	9.2228E-01	0.027	0.000713754
0.011	0.700	7.0679E-01	-0.007	4.61261E-05
0.021	0.459	5.1877E-01	-0.060	0.003571903
0.031	0.359	3.7383E-01	-0.015	0.000219933
0.041	0.320	2.7513E-01	0.045	0.00201289
0.051	0.248	2.1576E-01	0.032	0.001039259
0.061	0.214	1.8421E-01	0.030	0.000887437
0.071	0.201	1.6940E-01	0.032	0.000998727
0.075	0.172	1.6623E-01	0.006	3.32454E-05
0.081	0.146	1.6325E-01	-0.017	0.000297708
			SSE =	0.009820981
			MSE =	0.000982098
m =	0.5	0.4	0.3	0.2
D28_t_avg	5.904E-12	3.483E-12	2.055E-12	1.212E-12
D28_t_end	8.347E-12	4.595E-12	2.529E-12	1.392E-12

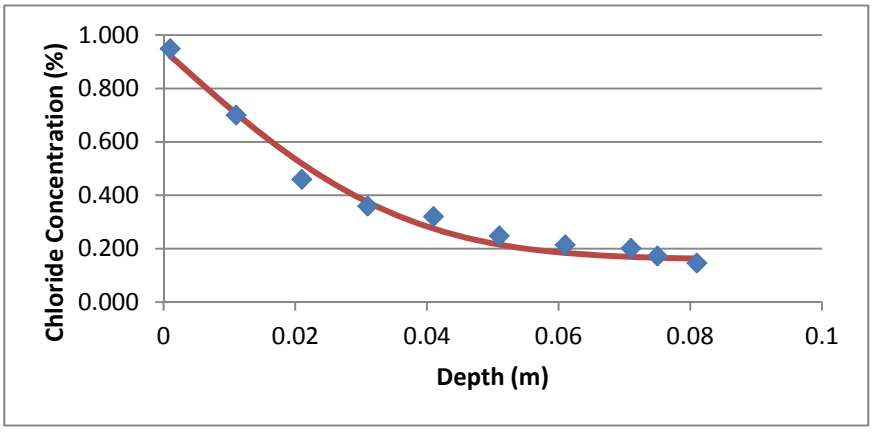

ASTM 1556 Standard Test Method for Determining the Apparent Chloride Diffusion Coefficient of Cementitious Mixtures by Bulk Diffusion

Sample	**Phase 1 Core 2**

Cs (mass %) =	0.33251	Ci (mass %) =	0.08	Test Duration (d) =	10950
Deff (m^2/s) =	1.2220E-12	t (s) =	946080000	Age (d) =	7

	% by weight/mass			
Depth X (m)	Measured	Predicted	Error	Error Squared
0.001	0.225	3.2832E-01	-0.103	0.010674846
0.011	0.356	2.8682E-01	0.069	0.00478614
0.021	0.271	2.4724E-01	0.024	0.000564614
0.031	0.229	2.1108E-01	0.018	0.000321007
0.041	0.185	1.7945E-01	0.006	3.08069E-05
0.051	0.183	1.5294E-01	0.030	0.00090365
0.061	0.159	1.3166E-01	0.027	0.000747502
0.071	0.130	1.1530E-01	0.015	0.000216122
0.075	0.121	1.1000E-01	0.011	0.000120937
0.081	0.108	1.0325E-01	0.005	2.25545E-05
0.091	0.094	9.4753E-02	-0.001	5.66696E-07
0.099	0.082	8.9976E-02	-0.008	6.36133E-05
			SSE =	0.01845236
			MSE =	0.001537697

m =	0.5	0.4	0.3	0.2
D28_t_avg	1.710E-11	1.009E-11	5.951E-12	3.511E-12
D28_t_end	2.417E-11	1.331E-11	7.325E-12	4.032E-12

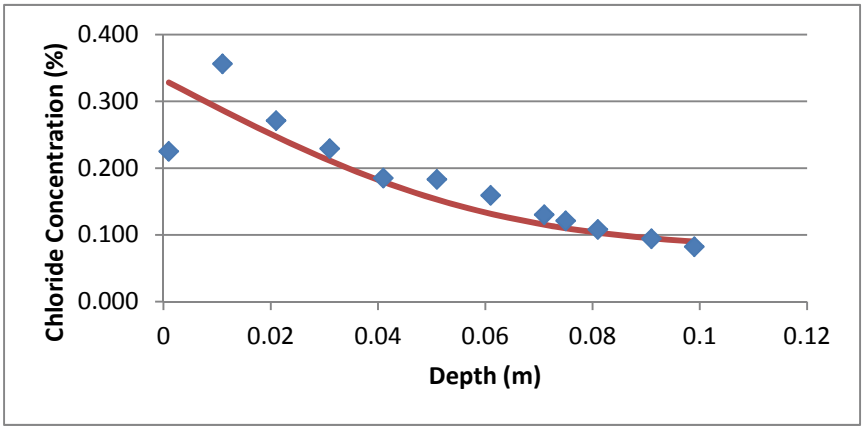

ASTM 1556 Standard Test Method for Determining the Apparent Chloride Diffusion Coefficient of Cementitious Mixtures by Bulk Diffusion

Sample	Phase 2 Core 2

Cs (mass %) =	0.20141	Ci (mass %) =	0.03	Test Duration (d) =	9125
Deff (m^2/s) =	1.5220E-12	t (s) =	788400000	Age (d) =	7

	% by weight/mass			
Depth X (m)	Measured	Predicted	Error	Error Squared
0.001	0.196	1.9862E-01	-0.003	6.84817E-06
0.011	0.143	1.7095E-01	-0.028	0.000781476
0.021	0.148	1.4453E-01	0.003	1.20548E-05
0.031	0.137	1.2031E-01	0.017	0.000278623
0.041	0.108	9.9013E-02	0.009	8.07576E-05
0.051	0.095	8.1053E-02	0.014	0.00019453
0.061	0.081	6.6520E-02	0.014	0.000209679
0.071	0.066	5.5239E-02	0.011	0.000115803
0.075	0.065	5.1558E-02	0.013	0.000180677
0.081	0.048	4.6838E-02	0.001	1.34931E-06
0.091	0.045	4.0837E-02	0.004	1.7327E-05
0.099	0.036	3.7420E-02	-0.001	2.01692E-06
			SSE =	0.001881142
			MSE =	0.000156762

m =	0.5	0.4	0.3	0.2
D28_t_avg	1.944E-11	1.168E-11	7.018E-12	4.216E-12
D28_t_end	2.749E-11	1.541E-11	8.638E-12	4.843E-12

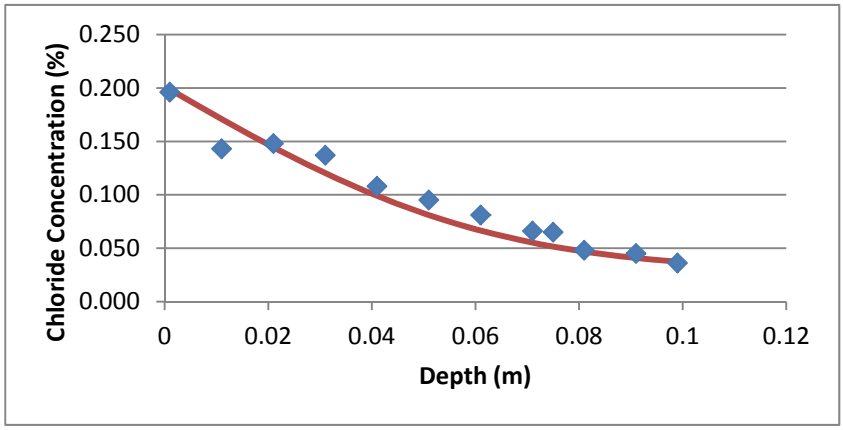

ASTM 1556 Standard Test Method for Determining the Apparent Chloride Diffusion Coefficient of Cementitious Mixtures by Bulk Diffusion

Sample	Phase 2 Core 1

Cs (mass %) =	0.19936	Ci (mass %) =	0.07	Test Duration (d) =	9125
Deff (m^2/s) =	1.5220E-12	t (s) =	788400000	Age (d) =	7

	% by weight/mass			
Depth X (m)	Measured	Predicted	Error	Error Squared
0.001	0.184	1.9725E-01	-0.013	0.000175544
0.011	0.182	1.7637E-01	0.006	3.16546E-05
0.021	0.167	1.5643E-01	0.011	0.000111718
0.031	0.137	1.3815E-01	-0.001	1.32782E-06
0.041	0.121	1.2208E-01	-0.001	1.17088E-06
0.051	0.106	1.0853E-01	-0.003	6.38889E-06
0.061	0.102	9.7560E-02	0.004	1.97124E-05
0.071	0.085	8.9047E-02	-0.004	1.63769E-05
0.075	0.098	8.6269E-02	0.012	0.000137608
0.081	0.090	8.2707E-02	0.007	5.31827E-05
0.091	0.086	7.8179E-02	0.008	6.11738E-05
0.099	0.078	7.5600E-02	0.002	5.76118E-06
			SSE =	0.00062162
			MSE =	5.18016E-05

m =	0.5	0.4	0.3	0.2
D28_t_avg	1.944E-11	1.168E-11	7.018E-12	4.216E-12
D28_t_end	2.749E-11	1.541E-11	8.638E-12	4.843E-12

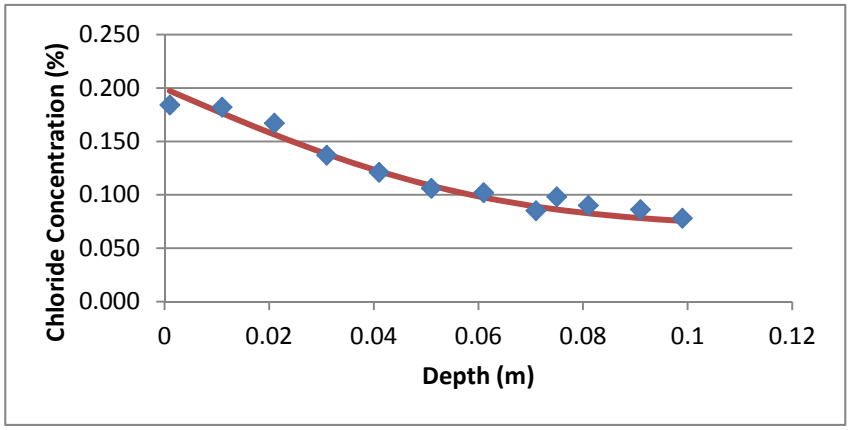

APPENDIX H Chloride Test Comparison

Chloride Test Comparison

VALUES				
Mix	**Fiber**	**Bulk ($x10^{-12}$ m^2/s)**	**RMT ($x\ 10^{-12}$ m^2/s)**	**RCPT (coulombs)**
NC	-	30.17	13.01	4364
FA	-	18.98	11.9	3279.5
TER 50-1	-	5.96	7.79	1627
TER 50-1	0.2	6.82	7.91	1257.5
TER 50-1	0.33	4.08	7.49	1225.3
TER 50-1	0.2	3.72	6.17	1383.5
TER 50-2	-	5.84	5.13	1287.3
TER 50-2	0.2	-	6.11	1162
TER 50-2	0.16	-	6.23	1251.3

RELATIONSHIP			
Mix	**RCPT to RMT**	**RMT to Bulk**	**RCPT to Bulk**
NC	0.30%	231.90%	0.69%
FA	0.36%	159.45%	0.58%
TER 50-1	0.48%	76.51%	0.37%
TER 50-1	0.63%	86.20%	0.54%
TER 50-1	0.61%	54.48%	0.33%
TER 50-1	0.45%	60.37%	0.27%
TER 50-2	0.40%	113.87%	0.45%
TER 50-2	0.53%	-	-
TER 50-2	0.50%	-	-

TER AVG	0.51%	78.29%	0.39%
TER 50-1 AVG	0.54%	69.39%	0.38%
TER 50-2 AVG	0.47%	-	-
TER SDEV	0.08%	23.56%	0.11%
TER 50-1 SDEV	0.09%	14.57%	0.12%
TER 50-2 SDEV	0.07%	-	-

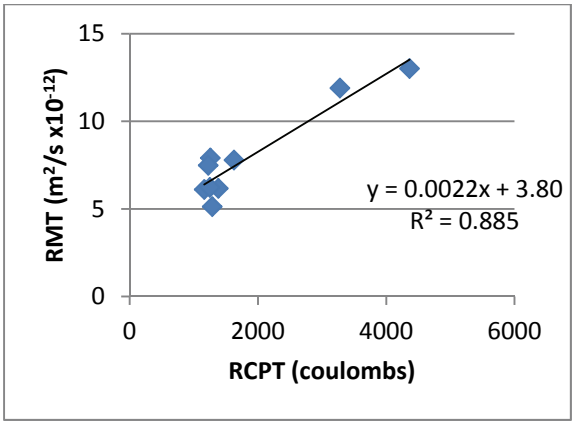
15
10
5
0
0
2000
4000
6000
RMT (m²/s x10⁻¹²)
RCPT (coulombs)
y = 0.0022x + 3.80
R² = 0.885

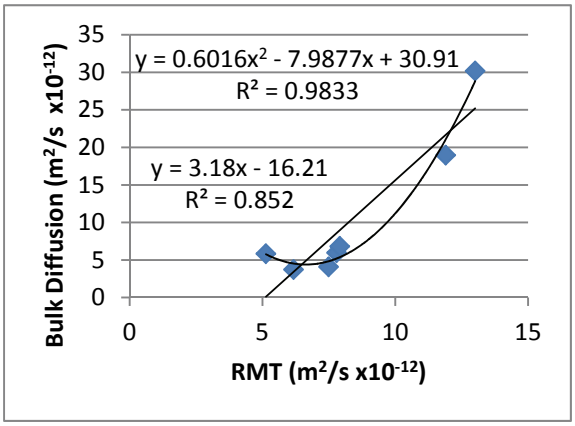
35
30
25
20
15
10
5
0
0
5
10
15
Bulk Diffusion (m²/s x10⁻¹²)
RMT (m²/s x10⁻¹²)
y = 0.6016x² - 7.9877x + 30.91
R² = 0.9833
y = 3.18x - 16.21
R² = 0.852

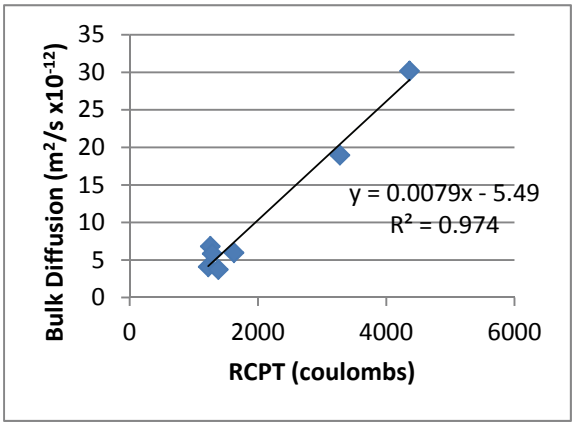
35
30
25
20
15
10
5
0
0
2000
4000
6000
Bulk Diffusion (m²/s x10⁻¹²)
RCPT (coulombs)
y = 0.0079x - 5.49
R² = 0.974

APPENDIX I Flexural Strength and Toughness Results

ASTM C78 Standard Test Method for Flexural Strength of Concrete

Beam Type:	**NC**
Date Tested:	**October 20, 2011**

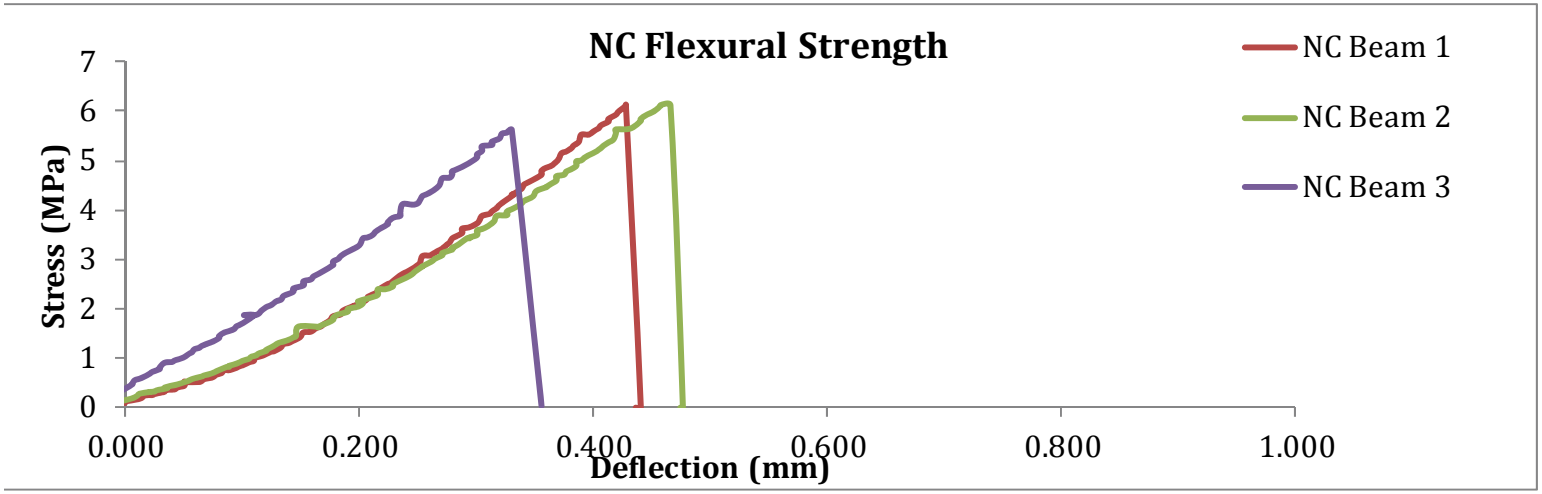

Sample No.	Width (mm)	Height (mm)	First Peak Strength (MPa)
NC Beam 1	153.0	151.0	6.13
NC Beam 2	153.0	152.0	6.12
NC Beam 3	154.0	152.0	5.62
Average (Metric)	**153.3**	**151.7**	**5.96**
Std. Dev.			**0.29**

ASTM C78 Standard Test Method for Flexural Strength of Concrete

Beam Type:	**FA**
Date Tested:	**October 27, 2011**

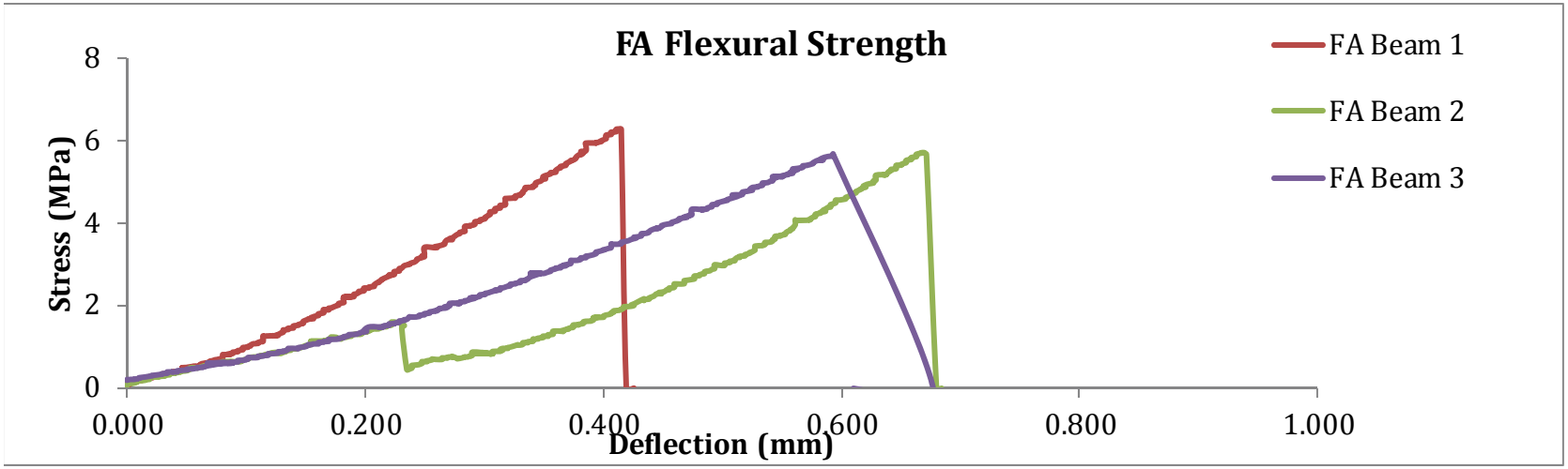

Sample No.	Width (mm)	Height (mm)	First Peak Strength (MPa)
FA Beam 1	152.0	149.0	6.28
FA Beam 2	153.0	152.0	5.71
FA Beam 3	151.0	151.0	5.68
Average (Metric)	**152.0**	**150.7**	**5.89**
Std. Dev.			**0.34**

Beam Type:	TER50-1
Date Tested:	October 27, 2011

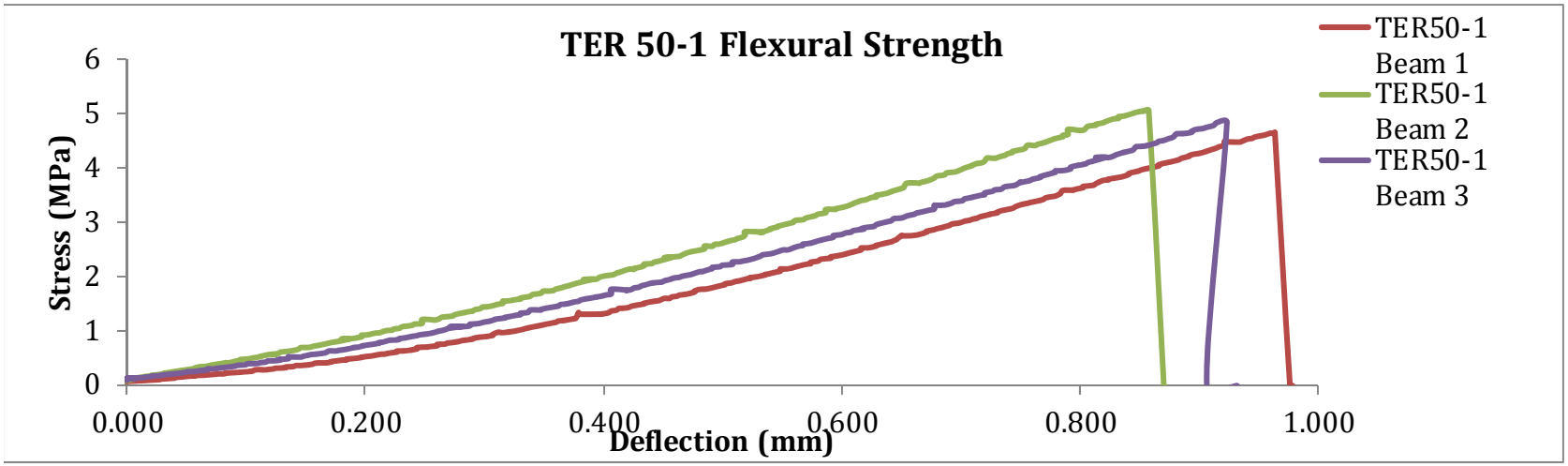

Sample No.	Width (mm)	Height (mm)	First Peak Strength (MPa)
TER50-1 Beam 1	153.0	155.0	4.65
TER50-1 Beam 2	151.0	152.0	5.05
TER50-1 Beam 3	154.0	153.0	4.83
Average (Metric)	**152.7**	**153.3**	**4.84**
Std. Dev.			**0.20**

ASTM C1609 Standard Test Method for Flexural Toughness and First-Crack Strength of Fiber-Reinforced Concrete

Beam Type:	**TER50-1 (1.8 kg F1)**
Date Tested:	**December 20, 2011**

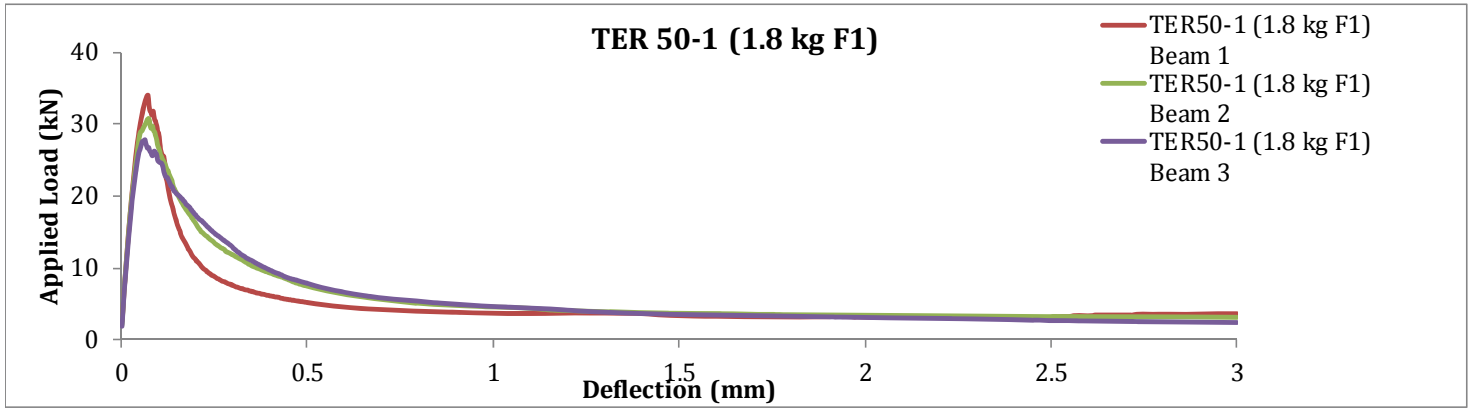

Sample No.	Width (mm)	Height (mm)	First Peak Strength (MPa)	P^{150}_{900} (kN)	f^{150}_{900} (MPa)	P^{150}_{600} (kN)	f^{150}_{600} (MPa)	P^{150}_{400} (kN)	f^{150}_{400} (MPa)	P^{150}_{150} (kN)	f^{150}_{150} (MPa)	T^{150}_{150} (Joules)	JSCE (Mpa)
TER50-1 (1.8 kg F1) Beam 1	152.0	155.0	4.19	7.04	0.87	5.22	0.64	4.10	0.50	3.19	0.39	14.93	0.45
TER50-1 (1.8 kg F1) Beam 2	151.0	151.0	4.02	10.96	1.43	7.49	0.98	5.36	0.70	3.47	0.45	17.41	0.41
TER50-1 (1.8 kg F1) Beam 3	151.0	156.0	3.41	11.66	1.43	7.90	0.97	5.61	0.69	3.14	0.38	17.03	0.30
Average (Metric)	**151.3**	**154.0**	**3.9**	**9.9**	**1.2**	**6.9**	**0.9**	**5.0**	**0.6**	**3.3**	**0.4**	**16.5**	**0.39**
Std. Dev.			**0.41**	**2.49**	**0.32**	**1.44**	**0.19**	**0.81**	**0.11**	**0.18**	**0.04**	**1.33**	**0.0792**

ASTM C1609 Standard Test Method for Flexural Toughness and First-Crack Strength of Fiber-Reinforced Concrete

Beam Type:	**TER50-1 (3.0 kg F1)**
Date Tested:	**December 22, 2011**

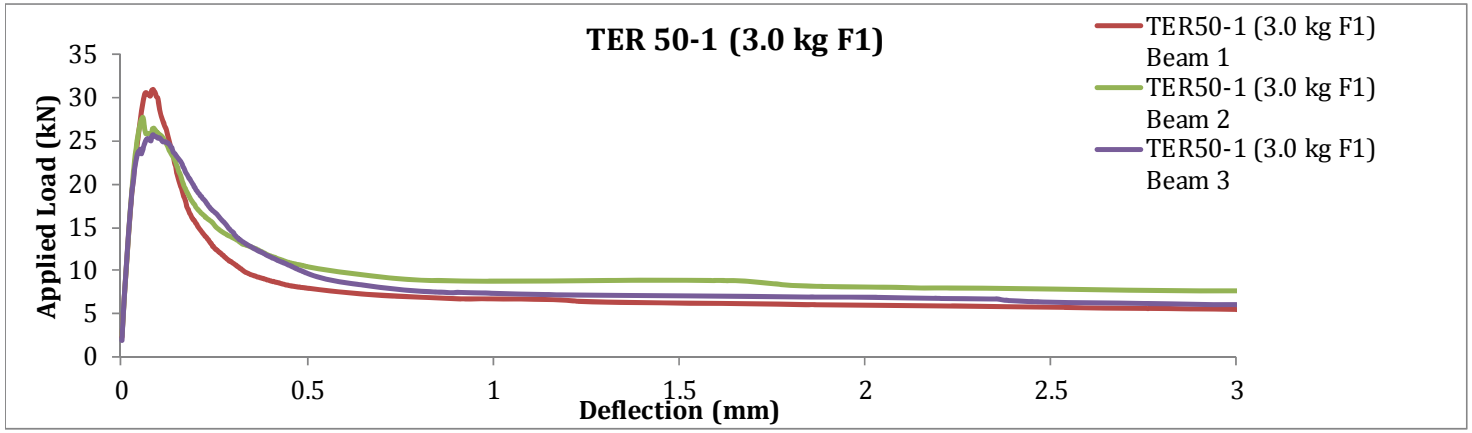

Sample No.	Width (mm)	Height (mm)	First Peak Strength (MPa)	P^{150}_{900} (kN)	f^{150}_{900} (MPa)	P^{150}_{600} (kN)	f^{150}_{600} (MPa)	P^{150}_{400} (kN)	f^{150}_{400} (MPa)	P^{150}_{150} (kN)	f^{150}_{150} (MPa)	T^{150}_{150} (Joules)	JSCE (Mpa)
TER50-1 (3.0 kg F1) Beam 1	151.0	152.0	3.99	9.94	1.28	7.97	1.03	7.02	0.91	6.01	0.77	23.20	0.71
TER50-1 (3.0 kg F1) Beam 2	152.0	151.0	3.60	13.04	1.69	10.47	1.36	9.06	1.18	8.11	1.05	28.45	1.00
TER50-1 (3.0 kg F1) Beam 3	152.0	152.0	3.29	13.25	1.70	9.70	1.24	7.82	1.00	6.94	0.89	25.92	0.78
Average (Metric)	**151.7**	**151.7**	**3.6**	**12.1**	**1.6**	**9.4**	**1.2**	**8.0**	**1.0**	**7.0**	**0.9**	**25.9**	**0.83**
Std. Dev.			**0.35**	**1.85**	**0.24**	**1.28**	**0.17**	**1.03**	**0.14**	**1.05**	**0.14**	**2.62**	**0.149**

ASTM C1609 Standard Test Method for Flexural Toughness and First-Crack Strength of Fiber-Reinforced Concrete

Beam Type:	**TER50-1 (1.8 kg F2)**
Date Tested:	**February 22, 2012**

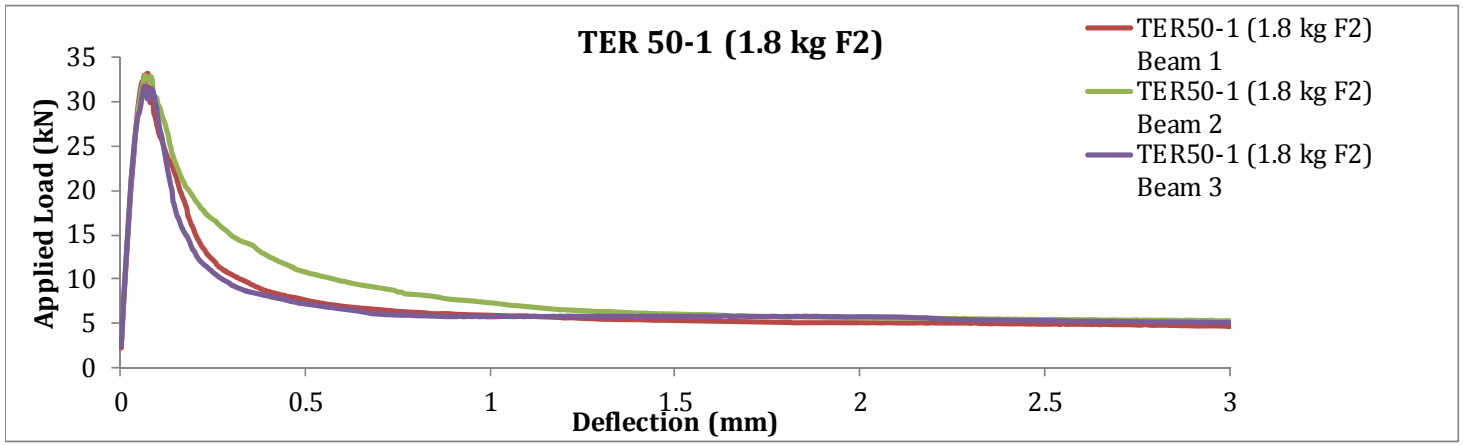

Sample No.	Width (mm)	Height (mm)	First Peak Strength (MPa)	P^{150}_{900} (kN)	f^{150}_{900} (MPa)	P^{150}_{600} (kN)	f^{150}_{600} (MPa)	P^{150}_{400} (kN)	f^{150}_{400} (MPa)	P^{150}_{150} (kN)	f^{150}_{150} (MPa)	T^{150}_{150} (Joules)	JSCE (Mpa)
TER50-1 (1.8 kg F2) Beam 1	150.0	152.0	4.31	9.92	1.29	7.65	0.99	6.38	0.83	5.11	0.66	21.12	0.61
TER50-1 (1.8 kg F2) Beam 2	151.0	147.0	4.55	14.22	1.96	10.82	1.49	8.57	1.18	5.63	0.78	24.84	0.73
TER50-1 (1.8 kg F2) Beam 3	150.0	152.0	4.13	8.82	1.15	7.21	0.94	5.95	0.77	5.77	0.75	21.30	0.66
Average (Metric)	**150.3**	**150.3**	**4.3**	**11.0**	**1.5**	**8.6**	**1.1**	**7.0**	**0.9**	**5.5**	**0.7**	**22.4**	**0.67**
Std. Dev.			**0.21**	**2.86**	**0.44**	**1.97**	**0.31**	**1.41**	**0.22**	**0.35**	**0.06**	**2.10**	**0.0632**

ASTM C78 Standard Test Method for Flexural Strength of Concrete

Beam Type:	**TER 50-2**
Date Tested:	**January 4, 2012**

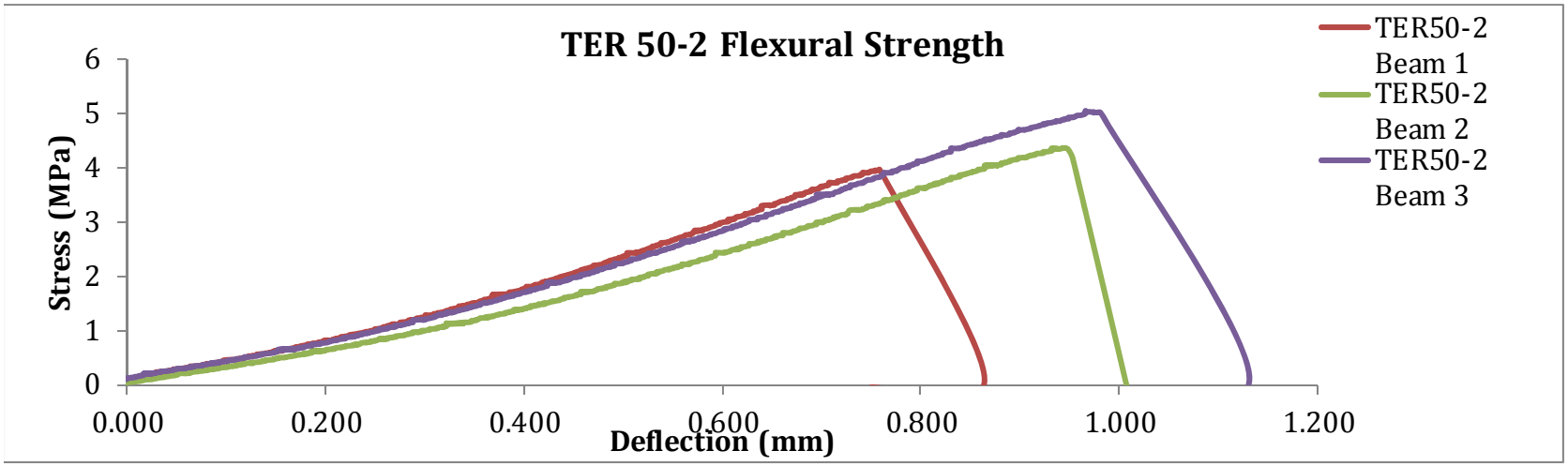

Sample No.	Width (mm)	Height (mm)	First Peak Strength (MPa)
TER50-2 Beam 1	152.0	154.0	3.97
TER50-2 Beam 2	151.0	154.0	4.36
TER50-2 Beam 3	151.0	153.0	5.05
Average (Metric)	**151.3**	**153.7**	**4.46**
Std. Dev.			**0.55**

ASTM C1609 Standard Test Method for Flexural Toughness and First-Crack Strength of Fiber-Reinforced Concrete

Beam Type:	**TER50-2 (1.8 kg F1)**
Date Tested:	**January 11, 2012**

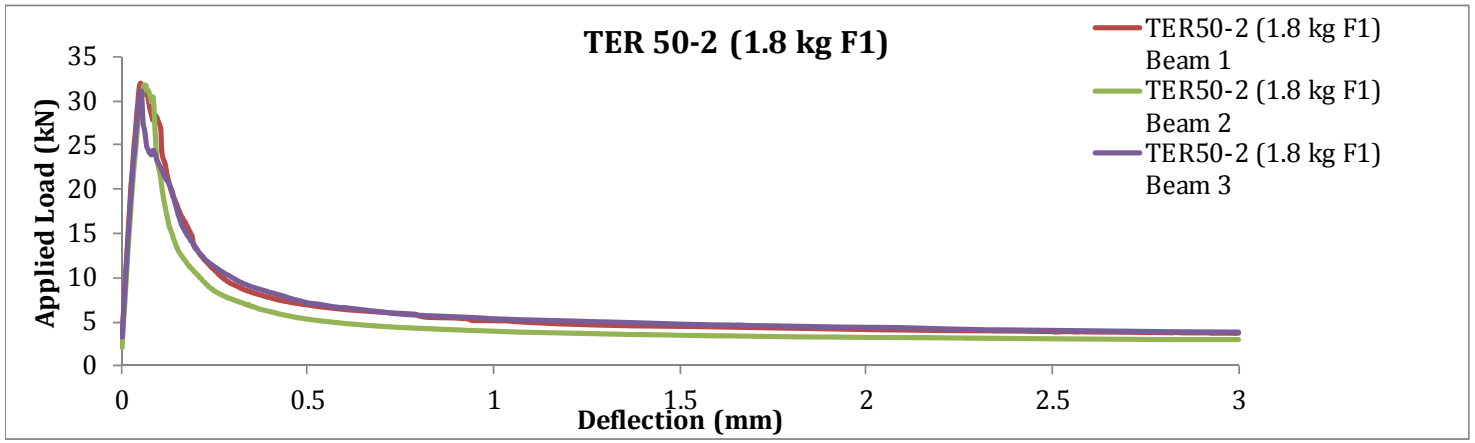

Sample No.	Width (mm)	Height (mm)	First Peak Strength (MPa)	P^{150}_{900} (kN)	f^{150}_{900} (MPa)	P^{150}_{600} (kN)	f^{150}_{600} (MPa)	P^{150}_{400} (kN)	f^{150}_{400} (MPa)	P^{150}_{150} (kN)	f^{150}_{150} (MPa)	T^{150}_{150} (Joules)	JSCE (Mpa)
TER50-2 (1.8 kg F1) Beam 1	151.0	154.0	4.03	8.65	1.09	6.89	0.87	5.95	0.75	4.11	0.52	18.30	0.46
TER50-2 (1.8 kg F1) Beam 2	151.0	156.0	3.90	7.04	0.86	5.30	0.65	4.34	0.53	3.20	0.39	14.08	0.36
TER50-2 (1.8 kg F1) Beam 3	151.0	151.0	4.08	9.27	1.21	7.13	0.93	5.87	0.77	4.37	0.57	18.60	0.50
Average (Metric)	**151.0**	**153.7**	**4.0**	**8.3**	**1.1**	**6.4**	**0.8**	**5.4**	**0.7**	**3.9**	**0.5**	**17.0**	**0.44**
Std. Dev.			**0.09**	**1.15**	**0.18**	**1.00**	**0.15**	**0.91**	**0.13**	**0.61**	**0.09**	**2.53**	**0.0708**

ASTM C1609 Standard Test Method for Flexural Toughness and First-Crack Strength of Fiber-Reinforced Concrete

Beam Type:	**TER50-2 (1.5 kg F2)**
Date Tested:	**February 21, 2012**

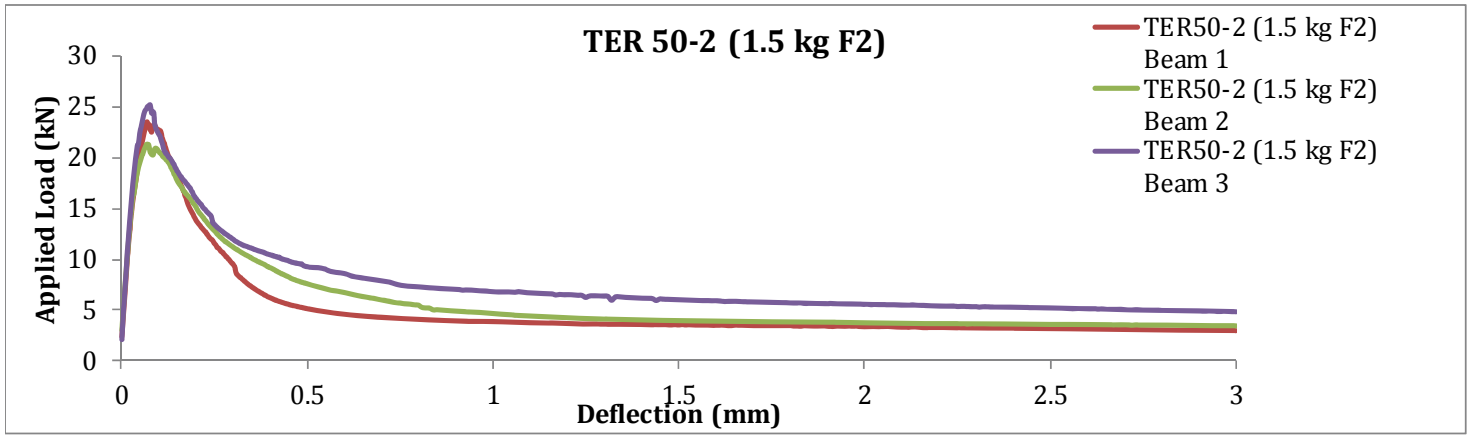

Sample No.	Width (mm)	Height (mm)	First Peak Strength (MPa)	P^{150}_{900} (kN)	f^{150}_{900} (MPa)	P^{150}_{600} (kN)	f^{150}_{600} (MPa)	P^{150}_{400} (kN)	f^{150}_{400} (MPa)	P^{150}_{150} (kN)	f^{150}_{150} (MPa)	T^{150}_{150} (Joules)	JSCE (Mpa)
TER50-2 (1.5 kg F2) Beam 1	150.0	154.0	2.98	7.91	1.00	5.14	0.65	4.17	0.53	3.37	0.43	14.93	0.38
TER50-2 (1.5 kg F2) Beam 2	150.0	154.0	2.70	10.53	1.33	7.60	0.96	5.69	0.72	3.76	0.48	17.14	0.44
TER50-2 (1.5 kg F2) Beam 3	151.0	148.0	3.43	11.34	1.54	9.28	1.26	7.47	1.02	5.56	0.76	22.41	0.66
Average (Metric)	**150.3**	**152.0**	**3.0**	**9.9**	**1.3**	**7.3**	**1.0**	**5.8**	**0.8**	**4.2**	**0.6**	**18.2**	**0.49**
Std. Dev.			**0.37**	**1.79**	**0.27**	**2.08**	**0.31**	**1.65**	**0.25**	**1.17**	**0.18**	**3.84**	**0.1483**

APPENDIX J Freeze Thaw Test Results

ASTM C215 Standard Test Method for Fundamental Transverse, Longitudinal and Torsional Resonant Frequencies of Concrete Specimens

Before Freeze Thaw Exposure								
Sample	**Length (mm)**	**Width (mm)**	**Depth (mm)**	**Mass (g)**	**Transverse Dynamic Modulus (GPa)**	**Longitudinal Dynamic Modulus (GPa)**	**Transverse Modulus AVG (GPa)**	**Longitudinal Modulus AVG (GPa)**
NC 1	349	109	109	6379	27.75	28.37	28.04	28.92
NC 2	354	109	111	6511	28.33	29.47		
FA 1	352	110	107	6689	31.23	31.56	30.53	30.74
FA 2	350	111	107	6462	29.83	29.93		
TER50-1 1	349	109	111	7380	29.40	30.90	27.92	28.71
TER50-1 2	350	109	109	6163	26.45	26.51		
TER50-1 (1.8)	341	105	107	6594	29.84	31.39	28.84	29.75
TER50-1 (1.8)	345	105	107	5938	27.83	28.10		
TER50-1 (3.0)	343	106	106	6724	31.69	31.20	29.76	30.27
TER50-1 (3.0)	347	106	109	6416	27.83	29.34		
TER50-2 1	345	106	107	6315	28.15	28.51	28.67	29.06
TER50-2 2	344	105	106	6493	29.20	29.61		
TER50-2 (1.8)	346	105	107	6855	30.23	31.21	28.34	29.50
TER50-2 (1.8)	338	105	108	6062	26.45	27.79		

ASTM C215 Standard Test Method for Fundamental Transverse, Longitudinal and Torsional Resonant Frequencies of Concrete Specimens

After Freeze Thaw Exposure

Sample	Length (mm)	Width (mm)	Depth (mm)	Mass (g)	Transverse Dynamic Modulus (Gpa)	Transverse Dynamic Modulus Reduction (%)	Longitudinal Dynamic Modulus (Gpa)	Longitudinal Dynamic Modulus Reduction (%)	Transverse Modulus AVG (GPa)	Trans. AVG Reduction	Std. Dev. Trans. Modulus Reduction	Longitudinal Modulus AVG (GPa)	Long. AVG Reduction	Std. Dev. Long. Modulus Reduction
NC 1	346	104	106	5718	25.58	7.81	26.21	7.62	26.27	6.32	2.10	26.25	9.19	2.22
NC 2	344	104	102	5401	26.96	4.84	26.30	10.76						
FA 1*	-	-	-	-	-	-	-	-	-	-	-	-	-	-
FA 2*	-	-	-	-	-	-	-	-						
TER50 1	343	105	105	6002	25.85	12.08	26.18	15.29	25.20	9.62	3.48	25.47	10.95	6.13
TER50 2	343	105	105	5606	24.55	7.16	24.76	6.62						
TER50 (1.8) 1	341	104	106	6162	25.48	14.60	27.23	13.26	24.50	15.04	0.62	25.38	14.76	2.11
TER50 (1.8) 2	345	105	105	5028	23.52	15.48	23.53	16.25						
TER50 (3.0) 1	342	105	105	6228	30.08	5.07	28.32	9.21	27.60	7.40	3.30	27.68	8.54	0.94
TER50 (3.0) 2	343	105	106	5918	25.12	9.73	27.03	7.88						
TER75 1	345	105	107	5910	25.75	8.52	26.55	6.85	25.46	11.18	3.75	26.62	8.34	2.11
TER75 2	343	105	105	5882	25.16	13.83	26.70	9.83						
TER75 (1.8) 1	345	105	104	6280	27.71	8.32	29.14	6.60	26.15	7.68	0.92	26.61	10.00	4.81
TER75 (1.8) 2	337	105	106	5418	24.59	7.03	24.07	13.40						

APPENDIX K Life 365 Screenshots

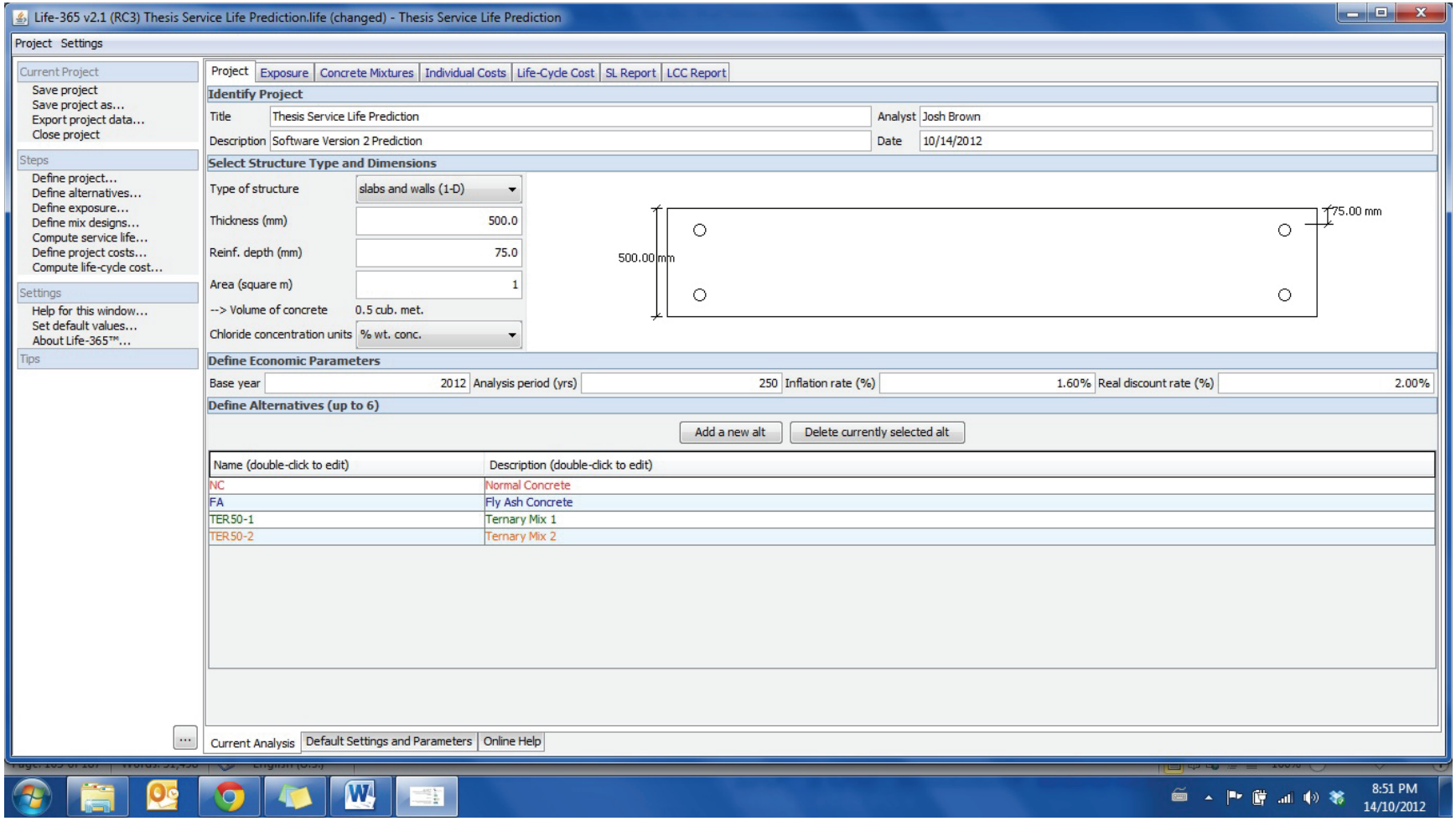
Life-365 v2.1 (RC3) Thesis Service Life Prediction.life (changed) - Thesis Service Life Prediction
Project Settings
Current Project
Save project
Save project as...
Export project data...
Close project
Steps
Define project...
Define alternatives...
Define exposure...
Define mix designs...
Compute service life...
Define project costs...
Compute life-cycle cost...
Settings
Help for this window...
Set default values...
About Life-365™...
Tips
Project
Exposure
Concrete Mixtures
Individual Costs
Life-Cycle Cost
SL Report
LCC Report
Identify Project
Title
Thesis Service Life Prediction
Analyst
Josh Brown
Description
Software Version 2 Prediction
Date
10/14/2012
Select Structure Type and Dimensions
Type of structure
slabs and walls (1-D)
Thickness (mm)
500.0
Reinf. depth (mm)
75.0
Area (square m)
1
--> Volume of concrete
0.5 cub. met.
Chloride concentration units
% wt. conc.
500.00 mm
75.00 mm
Define Economic Parameters
Base year
2012
Analysis period (yrs)
250
Inflation rate (%)
1.60%
Real discount rate (%)
2.00%
Define Alternatives (up to 6)
Add a new alt
Delete currently selected alt
Name (double-click to edit)
Description (double-click to edit)
NC
Normal Concrete
FA
Fly Ash Concrete
TER50-1
Ternary Mix 1
TER50-2
Ternary Mix 2
Current Analysis
Default Settings and Parameters
Online Help
8:51 PM
14/10/2012

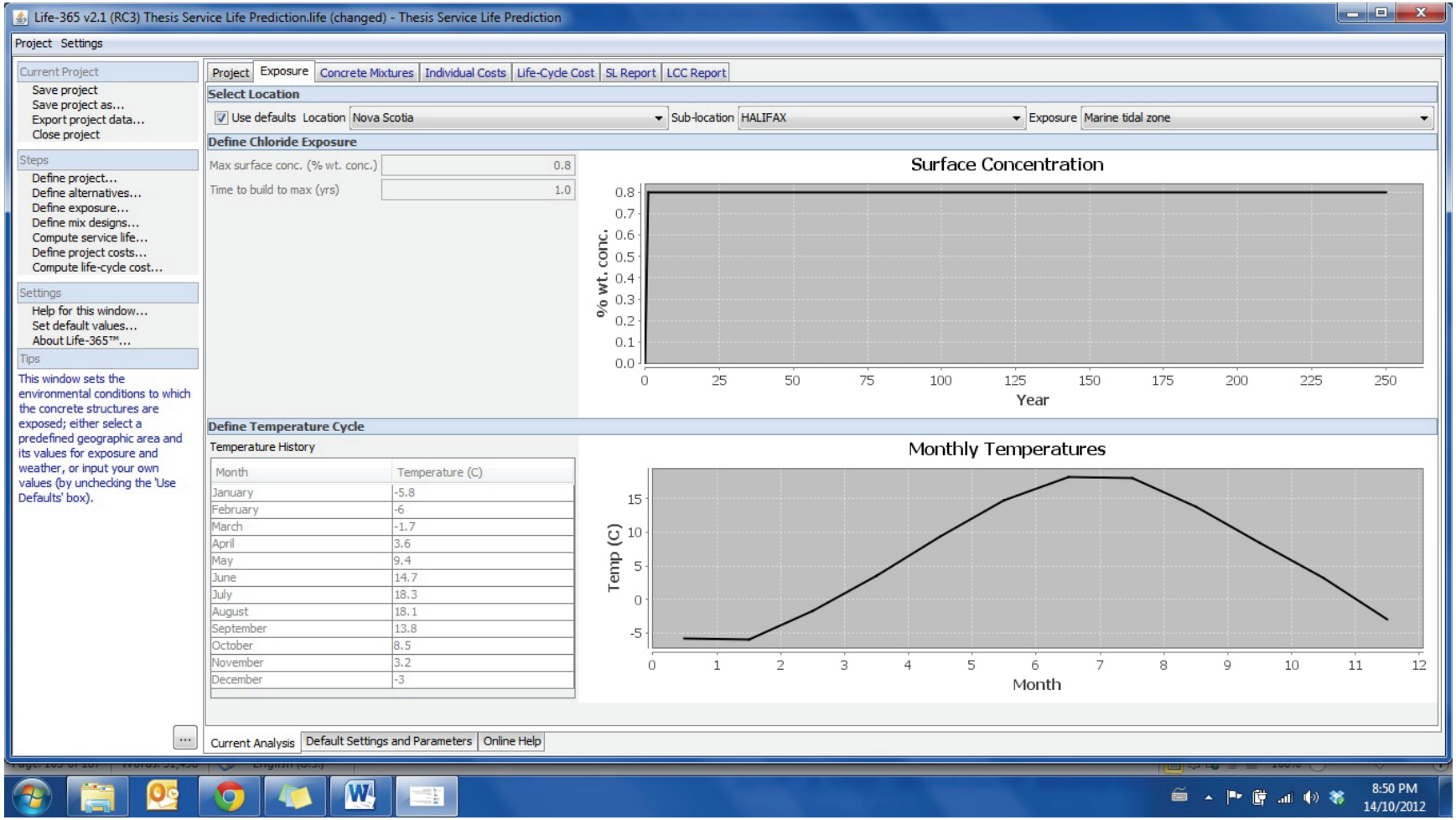
Life-365 v2.1 (RC3) Thesis Service Life Prediction.life (changed) - Thesis Service Life Prediction
Project Settings
Current Project
Save project
Save project as...
Export project data...
Close project
Steps
Define project...
Define alternatives...
Define exposure...
Define mix designs...
Compute service life...
Define project costs...
Compute life-cycle cost...
Settings
Help for this window...
Set default values...
About Life-365™...
Tips
This window sets the environmental conditions to which the concrete structures are exposed; either select a predefined geographic area and its values for exposure and weather, or input your own values (by unchecking the 'Use Defaults' box).
Project
Exposure
Concrete Mixtures
Individual Costs
Life-Cycle Cost
SL Report
LCC Report
Select Location
Use defaults
Location
Nova Scotia
Sub-location
HALIFAX
Exposure
Marine tidal zone
Define Chloride Exposure
Max surface conc. (% wt. conc.)
0.8
Time to build to max (yrs)
1.0
Surface Concentration
% wt. conc.
Year
Define Temperature Cycle
Temperature History
Month
Temperature (C)
January -5.8
February -6
March -1.7
April 3.6
May 9.4
June 14.7
July 18.3
August 18.1
September 13.8
October 8.5
November 3.2
December -3
Monthly Temperatures
Temp (C)
Month
Current Analysis
Default Settings and Parameters
Online Help
8:50 PM
14/10/2012

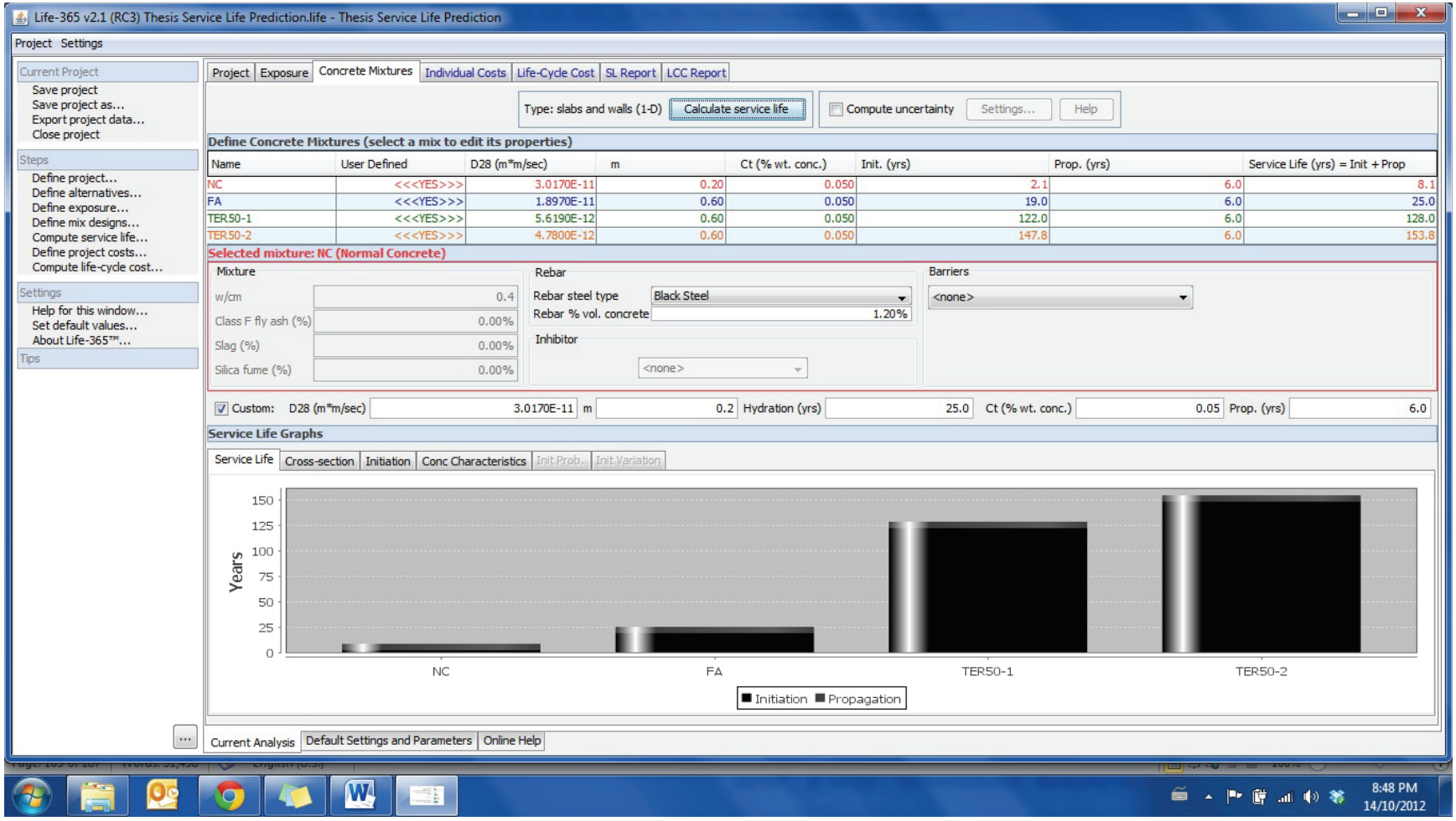
Life-365 v2.1 (RC3) Thesis Service Life Prediction.life - Thesis Service Life Prediction
Project Settings
Current Project
Save project
Save project as...
Export project data...
Close project
Steps
Define project...
Define alternatives...
Define exposure...
Define mix designs...
Compute service life...
Define project costs...
Compute life-cycle cost...
Settings
Help for this window...
Set default values...
About Life-365™...
Tips
Project Exposure Concrete Mixtures Individual Costs Life-Cycle Cost SL Report LCC Report
Type: slabs and walls (1-D) Calculate service life
Compute uncertainty Settings... Help
Define Concrete Mixtures (select a mix to edit its properties)
Name | User Defined | D28 (m*m/sec) | m | Ct (% wt. conc.) | Init. (yrs) | Prop. (yrs) | Service Life (yrs) = Init + Prop
NC | <<<YES>>> | 3.0170E-11 | 0.20 | 0.050 | 2.1 | 6.0 | 8.1
FA | <<<YES>>> | 1.8970E-11 | 0.60 | 0.050 | 19.0 | 6.0 | 25.0
TER50-1 | <<<YES>>> | 5.6190E-12 | 0.60 | 0.050 | 122.0 | 6.0 | 128.0
TER50-2 | <<<YES>>> | 4.7800E-12 | 0.60 | 0.050 | 147.8 | 6.0 | 153.8
Selected mixture: NC (Normal Concrete)
Mixture
w/cm 0.4
Class F fly ash (%) 0.00%
Slag (%) 0.00%
Silica fume (%) 0.00%
Rebar
Rebar steel type Black Steel
Rebar % vol. concrete 1.20%
Inhibitor
<none>
Barriers
<none>
Custom: D28 (m*m/sec) 3.0170E-11 m 0.2 Hydration (yrs) 25.0 Ct (% wt. conc.) 0.05 Prop. (yrs) 6.0
Service Life Graphs
Service Life Cross-section Initiation Conc Characteristics Init Prob. Init Variation
Years
150
125
100
75
50
25
0
NC
FA
TER50-1
TER50-2
Initiation Propagation
Current Analysis Default Settings and Parameters Online Help
8:48 PM
14/10/2012